Universidad Autónoma de Madrid

Programa de Doctorado en Biociencias Moleculares

Tesis doctoral

Regulation of ATPase dimer formation and optogenetic control of metabolism

Rocío Nieto Arellano

Madrid 2018

Facultad de Ciencias

Universidad Autónoma de Madrid

Regulation of ATPase dimer formation and optogenetic control of metabolism

Doctorando:

Rocío Nieto Arellano

Licenciada en Biología

Madrid 2018

Director de tesis:

José Antonio Enríquez Domínguez

El Doctor José Antonio Enríquez Domínguez, líder del grupo de investigación “Genética Funcional del Sistema de Fosforilación oxidativa” del Centro Nacional de Investigaciones Cardiovasculares (CNIC),

CERTIFICA

Que la Tesis Doctoral “Regulation of ATPase dimer formation and Optogenetic control of metabolism” ha sido realizada en la Fundación Centro Nacional de Investigaciones Cardiovasculares Carlos III, bajo su tutela, y que reúne las condiciones para optar al grado de Doctor.

Madrid, enero 2018

Fdo. José Antonio Enríquez

Abstract

ABSTRACT

The oxidative phosphorylation system comprises three fundamental processes: electron transport, proton pumping and ATP synthesis. Electron transport is required for both anabolic and catabolic processes, which require the delivery of electrons to the mitochondrial electron chain. This flux of electrons drives proton pumping and generates an electrochemical gradient across the mitochondrial inner membrane. This gradient is used by ATP synthase (ATPase, complex V) to generate ATP. Electron transport and proton pumping can be detached in many non-mammalian eukaryotes because they have non-proton-pumping oxidases. Mitochondrial ATPase is structured in two domains, the F_O domain, hydrophobic and embedded in the mitochondrial inner membrane, and the F_1 domain, hydrophilic, which protrudes through the mitochondrial matrix and is responsible for the ATP synthesis from ADP and Pi. In recent years, new ATPase subunits have been discovered: DAPIT and 6.8kDa protein (MP68). Very little is known about them, but DAPIT has been related with glucose metabolism and diabetes. They have been recently reported to form an ATPase subdomain called the intermembrane space domain (IMD), formed by only these two proteins. In this thesis, the functional role of DAPIT and MP68 was evaluated by generating knockout mouse models. An opposite role for each one was demonstrated: while DAPIT promotes ATPase dimerisation, MP68 prevents it. In the absence of DAPIT, an ATPase subcomplex is dissociated, which indicates that DAPIT promotes ATPase structure maintenance.

Next we focused on developing cellular tools where mitochondrial ATP synthesis capacity could be studied separately from electron transport. For this purpose, we designed optogenetic tools to generate an electrochemical gradient in mitochondria. Optogenetic tools were initially used in the neural field to modify and control the channel flux in neurons to alter their activity. Here we transformed light energy into an energy, that cells can use to grow. By expressing deltarhodopsin in mammalian cells, we were able to rescue energy deficiencies using light as a source of energy.

Resumen

RESUMEN

El sistema de fosforilación oxidativa concentra tres funciones principales: el transporte de electrones, el bombeo de protones y la síntesis de ATP. El transporte de electrones es requerido para procesos anabólicos y catabólicos en los que participan las reacciones de oxidación–reducción que se llevan a cabo en la mitocondria. El bombeo de protones está impulsado por el flujo de electrones, y genera un gradiente electroquímico en la membrana interna mitocondrial. Este gradiente es utilizado por la ATP sintasa (ATPasa o complejo V) para la síntesis de ATP. Los procesos de transporte de electrones y el bombeo de protones solo pueden desacoplarse en organismos eucariotas no mamíferos, ya que presentan oxidasas que no bombean protones. La ATPasa mitocondrial está formada por dos dominios, el dominio F_O, hidrofóbico, embebido en la membrana interna; y el dominio F_1, hidrofílico, localizado hacia la matriz mitocondrial, y que contiene la estructura responsable de la síntesis de ATP a partir de ADP y fosfato inorgánico. En los últimos años, se han descubierto nuevas subunidades, DAPIT y la proteína 6.8kDa (MP68). La función de mabas es poco conocida, pero DAPIT ha sido relacionada con el metabolismo de la glucosa y diabetes. Recientemente, se ha descrito un nuevo subdominio de la ATPasa llamado “dominio del espacio intermembrana” (IMD) que está formado únicamente por ambas proteínas. En esta tesis, se ha evaluado la función de DAPIT y MP68 generando ratones con falta de función para cada una de ellas, demostrando su función opuesta entre ellas. Mientras que DAPIT promueve la formación de dímeros de ATPasa, MP68 promuve su disociación. Además, en ausencia de DAPIT se genera un subcomplejo de ATPasa, indicando que DAPIT promueve el mantenimiento de la estructura de este complejo.

Por otro lado, en esta tesis se han desarrollado herramientas celulares para estudiar la capacidad de síntesis de ATP de forma independiente al transporte de electrones. Para ello, se han utilizado herramientas optogenéticas. Estas técnicas se han utilizado tradicionalmente en estudios neurales, para modificar y controlar el flujo a través de canales modificando su actividad. En esta tesis, se han desarrollado células capaces de transformar la energía de la luz en energía aprovechable para crecer. Gracias a la expresión de una deltarodopsina en células de mamífero, éstas son capaces de rescatar deficiencias energéticas usando la luz como fuente de energía.

Index

Abbreviations

Å	Ångström
A/BA	Acrylamide/bis-acrylamide
ADP	Adenosine diphosphate
ATP	Adenosine triphosphate
ATPase	ATP synthase
BN	Blue native
bp	(DNA) base pairs
BSA	Bovine serum albumin
CaCl2	Calcium chloride
CoQ	Ubiquinone
CsA	Cyclosporine A
Cyt c	Cytochrome c
DDM	n-Dodecyl--D-Maltoside
DNA	Deoxyribonucleic acid
DP5	Maltopentose
MgAMP-PNP	Adenosine 5´-[β, γ-imido]triphosphate magnesium
MgADP	Adenosin 5´(Trihydrogen Pyrophosphate)
EDTA	Ethylenediaminetetraacetic acid
EMMA	European Mouse Mutant Archive
ES	Embryonic stem
EuMMCR	European Mouse Mutant Cell Repository
FBS	Foetal bovine serum
FCCP	Carbonyl cyanide-4-(trifluoromethoxy)phenylhydrazone
FRT	Flippase recognition target
GTT	Glucose tolerance test
IF_1	Inhibitor factor 1
kDa	kilo Dalton
IMM	Inner mitochondrial membrane
IMS	Intermembrane space
ITT	Insulin tolerance test
IVF	*In vitro* fertilisation
IMS	Intermembrane space
nDNA	Nuclear DNA
mETC	mitochondrial electron transport chain
MOI	Multiplicity of infection
MOPS	(3-(N-morpholino)propanesulfonic acid)
mPTP	Mitochondrial permeability transition pore

MRI	Magentic resonance iamging
mtDNA	Mitochondrial DNA
NADH	Reduced nicotinamide adenine nucleotide
ORF	Open reading frame
OXPHOS	Oxidative phosphorylation system
o/n	Overnight
PBS	Phosphate-buffered saline
Pi	Inorganic phosphate
rev/s	Revolutions per second
ROS	Reactive oxygen species
RT	Room temperature (25ºC)
SDS	Sodium dodecyl sulphate
STZ	Streptozotocin
TCA	Tricarboxylic acid cycle
Tris	Tris(hydroxymethyl)aminomethane
µm	micro Molar
V	Vol

Introduction

I. MITOCHONDRIA BIOLOGY

I.1 Mitochondrial function

Mitochondria are endosymbiotic organelles that harbour different critical functions, provide energy to cells in the form of ATP, and also harbour the TCA cycle and beta oxidation of fatty acids and the metabolism of certain amino acids. They also generate reactive oxygen species (ROS), buffer calcium from the cytosol and regulate cell death. Mitochondria have their own genetic information in mitochondrial DNA (mtDNA), discovered in the 1960s (Nass and Nass, 1963; Schatz, Haslbrunner and Tuppy, 1964; Sagan, 1967; Schwartz and Dayhoff, 1978). mtDNA not only provides genetic information, but is also important for cell viability. Mitochondria are not only important for their role in energy production, but other roles, such as controlling stem cell function and fate are being progressively recognised for mitochondria (Folmes *et al.*, 2012). In addition, a metabolic change from glycolytic to oxidative, as well as the regulation of the mitochondria permeability transition pore (mPTP), are both necessary to achieve embryonic cardiomyocyte maturation (Hom *et al.*, 2011). It has been shown that mutation in mtDNA causes diseases (Holt, Harding and Morgan-Hughes, 1988; Wallace *et al.*, 1988), triggers carcinogenesis (Carew and Huang, 2002; Petros *et al.*, 2005) and is related with the apoptosis process (Kroemer and Reed, 2000). The accumulation of these mutations results in premature aging in mice (Trifunovic *et al.*, 2004).

In mitochondria, energy is produced through mitochondrial oxidative phosphorylation (OXPHOS). Glucose is converted into two pyruvates and thus reduces two cytosolic NAD^+ to NADH and produces two ATP molecules. Next pyruvate enters mitochondria and is transformed into Acetyl-CoA and CO_2 to produce $NADH+H^+$ and $FADH_2$. Fatty acids are also oxidised by beta oxidation to produce acetyl-CoA, $NADH+H^+$ and $FADH_2$. In both cases, acetyl-CoA enters the tricarboxylic acid cycle (TCA) and generates more $NADH+H^+$. Both $NADH+H^+$ and $FADH_2$ are oxidised by the mitochondrial electron transport chain (mETC). NADH releases electrons to complex I by reducing ubiquinone (CoQ) to ubiquinol. The different enzymes that use FAD as a cofactor (like Complex II) release electrons directly to CoQ to form ubiquinol. Ubiquinol is reoxidised by complex III, which sends electrons downhill to cytochrome c (cyt c) and complex IV, and finally to oxygen to produce H_2O (Fig. 1) (Wallace, Fan and Procaccio, 2010; Enríquez, 2016).

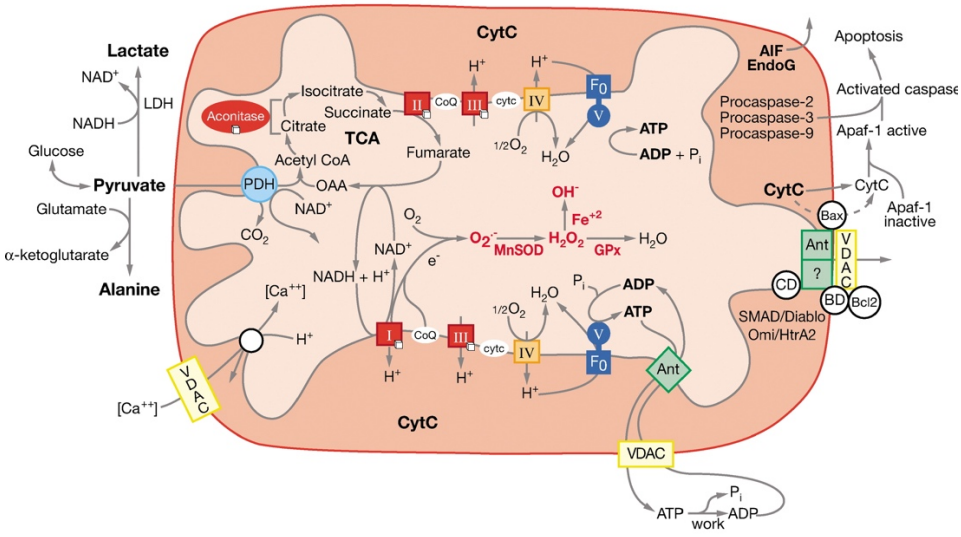

Figure 1. Mitochondrial oxidative phosphorylation diagram (adapted from Wallace, 2005). Glucose is converted into pyruvates which enter into the mitochondria and is transformed into Acetyl-CoA producing $NADH+H^+$ and $FADH_2$. These two molecules are oxidised by the mitochondrial electron transport chain.

Complexes I, III and IV use the energy released by the electron flux to translocate protons (H^+) from the inner mitochondrial matrix to the intermembrane space (IS). In this way they generate an electrochemical gradient, which is also known as proton motive force (p.m.f.) and drives ATP synthesis form ADP and Pi by H^+-ATPase.

I.2 Mitochondrial morphology

Mitochondria are delimited by two membranes: the inner (IMM) and the outer (OMM). The space between both membranes is known as the inner mitochondrial space (IMS), while the matrix is located inside the IMM. This morphology was observed for the first time by electron microscopy (Palade, 1952; Sjostrand, 1953). The IMM and OMM form different sub-compartments that perform specific functions. Thus the OMM forms specialised structures that interact with the endoplasmic reticulum (ER), named mitochondria-associated membranes (MAMs) (Vance, 2014) whose composition differs from other OMM areas (Giorgi *et al.*, 2015). In this way there are defined specialised regions in the IMM very much enriched in OXPHOS components located in the cristae edge.

Mitochondrial morphology can switch from an elongated form to a more fragmented status due to fusion and fission events and, as a result, the cristae structures in the IMM change. These cristae-remodelling processes occur during apoptosis, for example, when cytochrome c is released from mitochondria (Scorrano et al., 2002). The morphology of these cristae also changes under physiological conditions, in different organs and

developmental stages. Mitochondrial fission occurs during the process of eliminating non-functional mitochondria by mitophagy (Twig et al., 2008), or in the G2/M phase of the cell cycle to secure mitochondria segregation during cell division (Smirnova et al., 2001). The opposite phenomenon, the fusion process, increases in a different cell cycle phase, G1/S, (Mitra et al., 2009), during a starvation period (Rambold et al., 2011) or during embryonic development (Chen et al., 2000).

During development, mitochondria take a simple structure with fragmented cristae and a small mtDNA copy number (Folmes *et al.*, 2012; Folmes and Terzic, 2016). Cardiomyocytes from E9.5 embryos have fragmented and perinuclear mitochondria, but on day E13.5 they extend more into the cytoplasm, and become organised and filamentous (Hom *et al.*, 2011). Taken together, all these changes facilitate energy production.

The morphology of mitochondrial cristae is important from a bioenergetic point of view (Cogliati *et al.*, 2013). Cristae increase the IMM surface and the amount of mETC (Scheffler, 1999), and it has been proposed that this increases ATP production capacity by oxidative phosphorylation (Palade, 1953). Apart from this incremented surface, it is believed that cristae also provide a benefit in energy production terms (Cogliati, Enriquez and Scorrano, 2016), based on mathematical models (Demongeot *et al.*, 2007), by minimising the distance between ADP/ATP translocation and the ATP synthesis site.

Cardiolipin is an important lipid that determines mitochondrial shape. It is an acidic phospholipid found in mitochondrial membranes and its reduction in the IMM has been shown to severely alter the mitochondria ultrastructure, as in Barth syndrome (Xu *et al.*, 2006; Chicco and Sparagna, 2007). Cardiolipin has also been described to estabilish the supercomplexes of mETC (Pfeiffer *et al.*, 2003; McKenzie *et al.*, 2006), and the III_2+IV_2 association is unstable in its absence (Mileykovskaya and Dowhan, 2014).

Another protein involved in cristae remodelling is Opa1, optic atrophy type 1 protein, a dynamic-like GTPase whose mutations are associated with autosomal dominant optic atrophy type I disease (Alexander *et al.*, 2000; Delettre *et al.*, 2000). Processing large Opa1 isoforms is essential for mitochondrial fusion (Duvezin-Caubet *et al.*, 2006). There are different proteases that control Opa1 cleavage, including Yme1L or Oma1 (MacVicar and Langer, 2016).

The ATPase complex is an important modulator of cristae formation. In *Paramecium multimicronucleatum* mitochondria, ATPase is on the edge of cristae (Allen, Schroeder and Fok, 1989). In yeast, ATPase subunits e and g have been reported as non-essential for ATP synthesis, but their absence confers a characteristic structure to cristae in the form of concentric circles (Paumard *et al.*, 2002). Other subunits, such as ATP6, have been described as modulators of ATPase conformation, but are not absolutely necessary for cristae formation (Rak *et al.*, 2007; Habersetzer *et al.*, 2013). Another hypothesis that could

explain the role of ATPase is that it forms a pH gradient that could lead to a membrane curvature that gives rise to cristae formation (Rieger, Junge and Busch, 2014).

I.3 Electron transport chain complexes and their organisation

The OXPHOS system constitutes the most important pathway to produce energy in the cell. It is formed by ATPase and four complexes: complexes I, II, III and IV.

Complex I

The NADH dehydrogenase complex transfers two electrons from NADH to ubiquinone, and is coupled with the translocation of four protons from the matrix to the IMS. It is composed of 44 proteins with a weight of 960kDa, of which seven are codified by mtDNA. Recently, its structure has been resolved by cryoelectronmicroscopy with a resolution of 4.2 Å in bovine mitochondria (Fiedorczuk *et al.*, 2016; Zhu, Vinothkumar and Hirst, 2016). Complex I is formed by three different modules: N, that links NADH and oxidises it; Q, that transfers electrons to CoQ; and P, the hydrophobic module in the IMM involved in proton pumping (Fig. 2A).

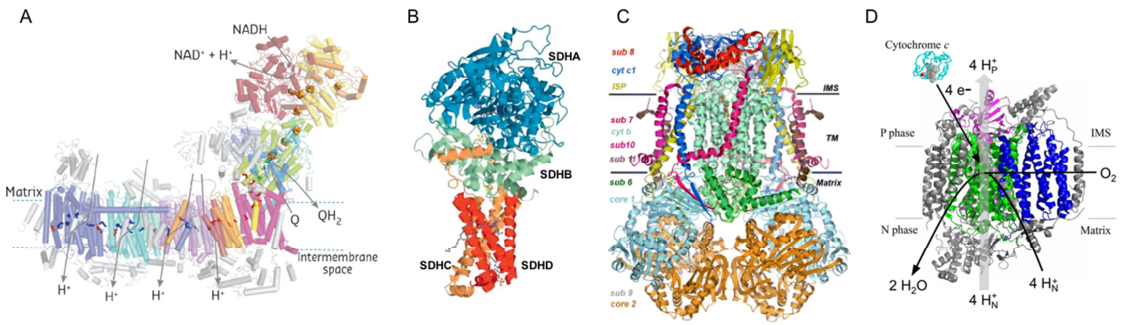

Figure 2. Complexes from the mitochondrial electron transport chain. A. Mammalian complex I structure. **B.** Complex II structure (modified from (Bezawork-Geleta *et al.*, 2017). subunits of SDH: SDHA (blue), SDHB (green), SDHC (brown), and SDHD (red). **C.** Complex II structure, modified from (Xia *et al.*, 2007). **D.** Structure and cofactor of mammalian cytochrome c oxidase. The three subunits codified in mtDNA are in green (Cox1), pink (Cox2) and blue (Cox3) (modified from: Rich, 2017).

Complex II

Complex II, or succinate dehydrogenase, is also an enzyme of the tricarboxylic acid cycle that catalyses the oxidation of succinate to fumarate. It transfers electrons from $FADH_2$ to ubiquinone. It is located in the IMM, faces the intermembrane space and is composed of four subunits: SDHA, SDHB (both make up the catalytic site), SDHC and SDHD (allow its location in the IMM) (Hägerhäll, 1997) (Fig. 2B). It is a special complex as it does not pump protons, and is the only complex that does not contain any subunits codified by mtDNA.

Complex III

Complex III, or cytochrome c reductase, transfers electrons from ubiquinone to cytochrome c (Fig. 2C). This process is coupled with the pumping of four protons to the IMS. It is composed of 11 subunits, of which only one, mtCytb, is codified by mtDNA (Iwata, 1998).

Complex IV

Complex IV, or cytochrome c oxidase, is the last of the complexes of the mETC. Its function is to transfer electrons from cytochrome c to molecular oxygen by generating H_2O. Four protons are translocated during this reaction. This complex is formed by 14 subunits, three of which form the catalytic core, and are encoded by mtDNA, Cox1, Cox2 and Cox3 (Fig. 2D).

Complexes organisation

The organisation of the mETC in the IMM has been a matter of debate for decades. In the 1950s the "solid model" was proposed by Keilin and Hartree to explain the organisation of mitochondrial complexes (Keilin and Hartree, 1947). This model described the complexes joined as one to act as static entities to secure communication among them (Slater, 2003). The "solid model" was questioned after the isolation of active individual complexes took place (Hatefi *et al.*, 1962). Moreover, the description of the mobility of coenzyme Q between CII and CIII went against the proposed "solid model".

A new model, namely the "fluid model", was described in 1986 by Hackenbrock and colleagues (Hackenbrock, Chazotte and Gupte, 1986). This model stated that complexes could diffuse into the IMM in an aleatory manner. Electron transport was described as a random collision between complexes that depended on the velocity of coenzyme Q and of cytochrome c diffusion

In 2000, the "supercomplexes" structures were discovered by native electrophoresis, Blue Native gel (BN-PAGE) (Schägger and Pfeiffer, 2000). BN-PAGE allowed the discovery of the stable associations among OXPHOS complexes. The largest form of supercomplexes is formed by the I+III_2+IV association, known as the respirasome. Other frequent associations are the I+III_2 supercomplex and III_2+IV. Although these associations also exist in plants, they can vary in the stoichiometry (Eubel, Heinemeyer and Braun, 2004). As example, in *Saccharomyces cerevisiae,* since they lack complex I, the only supercomplex observed was III_2+IV_2 (Schägger and Pfeiffer, 2000). The largest amounts of these supercomplexes are found in mammals such as mouse, bovine or human.

Based on evidence that favours the two previous models, (Boekema and Braun, 2007; Lenaz and Genova, 2007), a new model was proposed, known as the "plasticity model"

(Acín-Pérez *et al.*, 2008), which combines the possibility of finding complexes, and not only those associated among them, but also individually.

The I+III_2 supercomplex from *Arabidopsis thaliana* was the first to be investigated by cryoelectronmicroscopy techniques (Dudkina *et al.*, 2005). In 2016, three independent groups simultaneously provided respirasome structures with significantly improved resolution (Gu *et al.*, 2016; Letts, Fiedorczuk and Sazanov, 2016; Wu *et al.*, 2016). Sazanov (Letts, Fiedorczuk and Sazanov, 2016), and the Kühlbrandt groups (Sousa *et al.*, 2016) provided a resolution of 5.8 Å or 9 Å, respectively, from bovine heart. The Yang group provided a resolution of up to 4 Å from porcine mitochondria and human mitochondria. These groups also provided details of two different respirasome conformations, “tight” and “loose”. In a tight conformation, complex IV comes into contact with both complex I and III, whereas in a loose conformation complex IV comes into contact only with complex I (Letts, Fiedorczuk and Sazanov, 2016).

The stability of supercomplexes is influenced by different proteins, and also by other non-protein factors. The first proposed proteins were Rcf1 and Rfc2 in *S. cerevisiae* (Chen *et al.*, 2012). The deletion of these proteins suppresses supercomplexes formation because it impairs the association between CIII and CIV. Currently, it seems that these factors are in fact directly involved in the assembly of CIV, and indirectly impact supercomplex formation through CIV assembly alterations (Garlich *et al.*, 2017). Therefore, they cannot be considered specific factors for supercomplex assembly.

The only *bona fide* assembly factor described to date is COX7A2L, or SACF1, which denotes the name of “Supercomplex Assembly factor 1”. SCAF1 is a protein of 113 amino acids, including the mitochondrial import sequence. A mutated version of SCAF1 has been described in a subset of inbred mouse strains, notably all investigated C57B/L6-derived substrains (Lapuente-Brun *et al.*, 2013). This mutated form of 111 amino acids has an intramolecular microdeletion which causes the loss of two amino acids that render it unable to interact with complex IV (Cogliati et al. 2016). The mechanism of interaction between CIII and CIV is determined by the interchange of the structural subunits of CIV that determine if this complex associates with $CIII_2$, dimerise-forming CIV_2 or remains as monomer CIV. These proteins are COX7A1, which favours CIV dimmer formation, COX7A2 that favours CIV monomers, and COX7A2L or SCAF1 that allows the physical superassembly between complexes III_2 and IV. Additional tissue-specific isoforms modulate CIV dimerisation: COX6A2 or COX6A1 (Cogliati *et al.*, 2016).

Apart from these protein factors, other components, such as cardiolipin, also regulate the supercomplexes assembly (Pfeiffer *et al.*, 2003). This phospholipid is important for membrane potential maintenance (Gohil *et al.*, 2004). Cardiolipin-deficient cells show the instability of the III_2+IV_2 supercomplex (Pfeiffer *et al.*, 2003).

The regulation of supercomplexes formation and their plasticity is important to substrate adaptation and optimised mitochondria metabolism. The assembly of CIII and CI generates two independent pools of coenzyme Q for the electrons from both NADH and $FADH_2$ by avoiding substrate competition in the mETC (Lapuente-Brun et al, 2003; Guaras et al, 2006).

The organisation of complexes in supercomplexes is an important issue during embryo development in mice. The assembly of supercomplexes around stage E11.5 of embryo development has been shown to correspond to a cardiac development step (Beutner, Eliseev and Porter, 2014), which indicates that mitochondrial regulation is also important during cardiac maturity (Menendez-Montes *et al.*, 2016).

II. ATP SYNTHASE

II.1 F_1F_O-ATPase structure

The F_1F_O-ATPase complex is formed by 16 proteins (Collinson *et al.*, 1994) and is located in the membranes of different structures, including mitochondria, chloroplasts or eubacteria. The general shape of the complex is similar in all three. F_1F_O-ATPase is composed of three domains, the F_1, F_O and the slender stalk that links all the domains together. The F_1 domain is extrinsic to the membrane, which is where ATP is produced and hydrolysed. The F_O domain is embedded in the membrane and forms the channel that allows protons to pass through the membrane and to couple it with ATP synthesis. Initially the slender stalk was considered an artifact, until it was defined by electron microscopy in *Escherichia coli* (Gogol, Lücken and Capaldi, 1987) (Fig. 3). Later, it was demonstrated that if this stalk was disrupted, the F_1 domain would be released as a globular complex.

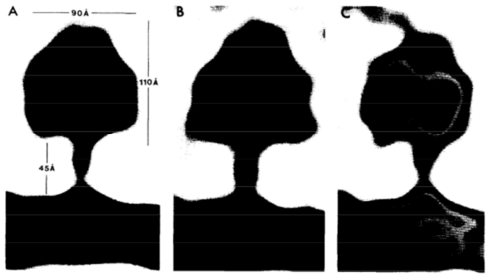

Figure 3. Analysis of the electron microscopy images of ATPase from *Escherichia coli*. The average of the different side views of F_1 and F_O computed from (**A**) 30 particles aligned by correlation methods; (**B**) 10 particles with a cleft in the F_1 domain; (**C**) 10 particles with a solid F_1 domain.

The F_1 domain is comprised of five globular proteins, α, β, γ, δ and ε in a specific stoichiometry $\alpha_3\beta_3\gamma_1\delta_1\varepsilon_1$ with a weight of 350kDa (J.E.Walker *et al.*, 1985; Abrahams *et al.*, 1994; Collinson *et al.*, 1994). Subunits α and β are arranged in an alternating conformation, which generates a spherical structure with a diameter of 100 Å. This structure envelops subunits γ that are localised in the central block by fixing these subunits to the F_O domain. Subunits δ and ε contribute to this association by binding to the end of the cylinder form by c subunits (Fig. 4).

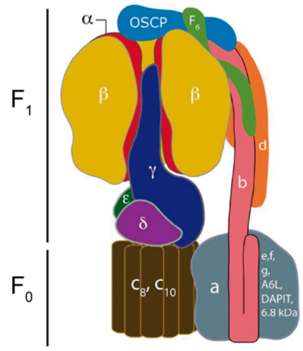

Figure 4. Organisation of protein subunits in mitochondria ATP synthase (from (Walker, 2013)).

The F_O domain´s name is attributed to oligomycin because is the domain that confers sensitivity to this antibiotic (Racker, 1963; J. Symersky *et al.*, 2012). F_O is composed of subunits a, b, c, d, e, f, g, and A6L in the membrane domain. The c-subunits form a ring with different numbers of subunits depending on the species. In bovine mitochondria, the number of c-subunits is 8, and is 10 in yeast (Jindrich Symersky *et al.*, 2012).

Other ATPase subunits form the central stalk, or stator, whose function is to fix F_1 during rotation in order to provide structural sustenance. It is composed of the oligomycin-sensitive conferring protein (OCP), and subunits b, d and F6. The structure of these proteins is of low-degree conservation between species, but their function is very well conserved.

There are other subunits that form part of ATPase, but their role is not yet well-defined. The f subunit, essential for ATP synthesis, produces the phenotype of uncoupled ATP synthase when it is lost (Spannagel *et al.*, 1997). Subunit i has been described only in yeast ATPase, and it produces the dissociation of the ATPase complex when it is absent. Although subunits e, k, and g are involved in dimer formation, the only essential subunit for this process is e (no protein homologous to subunit k in yeast has been described in mammals).

Two new peptides have been recently discovered, proteins MLQ and AGP. MLQ is a 6.8kDa mitochondrial proteolipid, MP68 (Terzi *et al.*, 1990; Chen *et al.*, 2007; Meyer *et al.*,

2007), and AGP is a diabetes-associated protein found in insulin-sensitive tissue (DAPIT) (Päivärinne and Kainulainen, 2001) (see Section II.6).

There are some particular situations, such as Rho0 cells, whose lack of mtDNA causes distinct ATPase organisation. These cells do not have subunits a and A6L encoded by mtDNA, and when the ATPase is resolved in a BN gel, the ATPase complex is not observed even though a subcomplex formed by F_1-c is detected. Furthermore, peptides DAPIT and 6.8kDa protein (MP68) have not been detected by mass spectrometry in these cells, which indicates the possibility that these proteins may be involved in the ATPase complex assembly.

II.2 ATPase dimerisation

ATPase was first isolated in a monomeric form with 16 proteins. Next the dimeric and oligomeric forms of ATPase were described by using different detergents, such as digitonine (Krause *et al.*, 2005). With a detergent at a low concentration, after resolving in a gel under native conditions, ATPase is observed in different conformations, e.g., monomeric, dimeric, tetrameric and hexameric.

ATP synthase dimers were first identified in yeast (Arnold *et al.*, 1998). The protein composition in monomeric and dimeric ATPase forms do not appear to be the same as there are three dimer specific subunits, e, g and k, which are not essential for ATPase enzymatic activity. The deletion of the g gene is not essential for ATPase dimerisation, but the morphology of cristae dramatically changes and mitochondria become enlarged (Giraud *et al.*, 2002; Paumard *et al.*, 2002). More recently, the dimeric F_1F_O-ATPase structure has been observed in yeast and is necessary to cause membrane bending to form cristae (Hahn *et al.*, 2016) (Fig. 5). Moreover, larger ATPase assemblies have been identified by the BN-PAGE technique (Krause *et al.*, 2005; Wittig and Schägger, 2005).

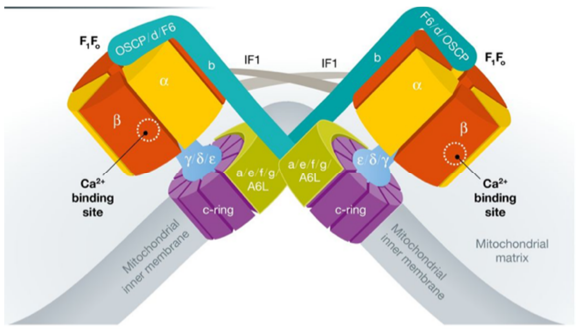

Figure 5. Schematic representation of ATPase dimerisation. ATPase dimers determine the curvature of the inner mitochondrial membrane (modified from (Chinopoulos, 2017)).

In physiological contexts, ATPase dimerisation is also important during ageing. In mature cells, the proportion of dysfunctional mitochondria is higher than in young cells. These mitochondria also display a vesicular morphology that lacks cristae, and ATPase dimers dissociate into monomers (Daum et al., 2013).

As described in Section I.2, ATPase plays an important role in cristae formation, promoting cristae morphology maturation. In line with this, ATPase is important during germ cell differentiation in *Drosophila*, and not because of its role in energy production, but because of the function it performs in cristae formation (Teixeira *et al.*, 2015).

II.3 ATP synthesis

The catalytic ATPase site has been described based on X-ray images from bovine (Abrahams *et al.*, 1994) and yeast F_1F_O-ATPase. As the γ subunit assembly takes place asymmetrically, ATPase takes an asymmetric structure and can be observed in different conformations. While the central stalk rotates, ATPase can be found in three varying conformations of the β-subunit, which confers different catalytic properties (Fig. 6). Although conformations β_{TP} and β_{DP} take similar structures, they exhibit differential preference in binding nucleotides. While β_{TP} can bind MgAMP-PNP (a non-hydrolysable analogue of ATP), β_{DP} binds MgADP. Conformation β_E, also known as “open” or “empty”, takes a different structure due to the γ-subunit, and is unable to bind any nucleotide. This latter conformation is the active one, which releases the ATP molecule.

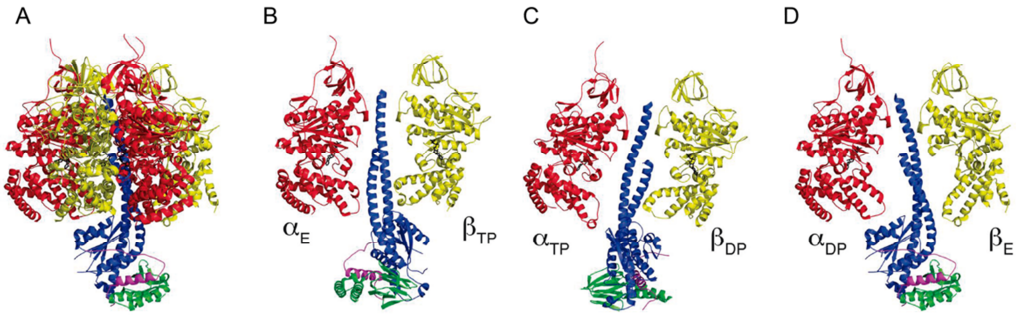

Figure 6. Structure of the F_1 domain of bovine ATPase (modified from (Walker, 2013)). **A.** Catalytic F_1 with the three different conformations. After each rotation of 120º, a conformation change occurs. **B.** State represented by conformation β_{TP} with affinity to Mg-AMP-PNP. **C.** Conformation represented by the presence of β_{DP}, with affinity to Mg-ADP. **D.** State without any affinity to nucleotides, characterised by β_E. It is the active conformation.

During ATP synthesis, the direction of c-ring cylinder movement is right-handed and this rotation is generated by a p.m.f. at a speed of 100-150 rev/s. During ATP hydrolysis,

however, the rotation direction reverses. This rotation is produced by the interaction with protein a, and the 360º rotation prompts the synthesis of the 3 ATP molecules.

II.4 F_1F_O-ATPase regulation

F_1F_O-ATPase activity depends on the energy available in cells. When the proton gradient is low, the β-subunit binds MgADP by assuming a conformation that render the complex inactive. Other molecules inhibit ATP synthesis, such as ATPase inhibitory factor 1 (IF_1). At a pH of 6.7, it forms a complex with ATPase that both inhibits ATP synthesis and prevents ATP hydrolysis. IF_1 is also regulated by post-translational modifications, specifically by phosphorylation, which controls the ATPase function in different contexts depending on substrate availability or the energy demanded by the cell (García-Bermúdez, Cuezva and Bernardi, 2016; Esparza-Moltó, Nuevo-Tapioles and Cuezva, 2017).

II.5 Role of ATP synthase in apoptosis

The apoptosis process occurs when cells die in a programmed manner. It is an energy-consuming process that takes place in events like cell turnover, embryo development or cell death caused by toxic agents (Elmore, 2007). During apoptosis, the permeabilisation of the IMM occurs and apoptotic factors are released from the mitochondria to the cytoplasm. The structure that would lead to the release of these factors is known as the mitochondrial permeability transition pore (mPTP) (Rasola and Bernardi, 2007; Kwong and Molkentin, 2015). The mPTP is a structure located in the IMM and is permeable to solutes and ions and, specifically, the release of calcium and cytochrome c triggers the apoptosis process (Eskes *et al.*, 1998).

The “permeability transition” concept was proposed for the first time by Haworth and Hunter (Hunter and Haworth, 1979), but its physiological role and composition have been debated for some time. Initially it was suggested that the adenine nucleotide translocator (ANT) is involved in mPTP formation because of the inhibition of the mPTP by adenine nucleotides. The use of genetic tools to knockout ANT has demonstrated that this hypothesis is incorrect, and that ANT is not essential for mPTP formation. A similar situation occurs with the Vdac complex; nor does it participate in mPTP regulation (Halestrap, 2009).

It is believed that ATP synthase is required for mPTP formation (Giorgio *et al.*, 2013) and ATPase dimers have been proposed as the mPTP. The purification of these dimers retains mPTP activity (Giorgio *et al.*, 2013). Moreover, their role in calcium release in *Drosophila* (Von Stockum *et al.*, 2015) has been demonstrated and suggests that the process is not exclusively mammalian (Azzolin *et al.*, 2010). Alternatively, it has been proposed other

mPTP identity independently of ATPase dimerisation. In this hioptesis, it is describd the c-ring subunit of ATPAse as the mPTP (Alavian *et al.*, 2014).

Currently, the composition of the mPTP remains unclear. Different studies have raised doubts about the proposed models. The idea that c-ring forms the mPTP has been ruled out using atom molecular dynamic simulations (Zhou *et al.*, 2017). More recently, the belief that the peripheral stalk and c-subunits are required to retain mPTP activity has been excluded (He, Carroll, *et al.*, 2017; He, Ford, *et al.*, 2017).

II.6 New peptides associated with ATPase

DAPIT and MP68 have remained undetected for a long time. Experimental conditions were important to detect them. When exogenous phospholipids are absent, the small proteins are lost during chromatography, but if the preparation includes some phospholipids, DAPIT and MP68 are found in the purified ATPase complex. Peptides DAPIT and MP68 have been identified with sequences AGPEADAQFHFTGIKKYFN and MLQSLIKKVWIPMKPYYTQAYQEI, respectively (Fig. 6). Both have been detected in mass spectrometry experiments (Rexroth *et al.*, 2004; Chen *et al.*, 2007), in the monomeric and dimeric forms of the bovine ATPase complex (Meyer *et al.*, 2007; Nůsková *et al.*, 2015), and as individual proteins. The same study found no differences in the hydrolysis capacity of ATPase when MP68 was dissociated. Both share a common transmembrane region (Fig. 7) and several phosphorylation sites which have not been confirmed by a proteomic analysis (Carroll, Fearnley and Walker, 2006).

Figure 7. Alignment and structural analysis of proteins MLQ and AGP. The transmembrane region is marked in red, phosphorylation sites are marked in blue, and green and yellow denote the unmarked amino acids, which are identical, similar and non-similar. **A.** Alignment of the DAPIT sequence from *R. norvegicus* (R.n.), *Bos taurus* (B.t.) (gi91207977), *Homo sapiens* (H.s.) (gi 14249376), and *S. bullata* (S.b.) (gi23505740). **B.** Alignment of the MP68 sequence from *R. norvegicus* (R.n.), *Bos taurus* (B.t.) (gi91207977) and *S. bullata* (S.b.) (gi23505740) (modified from (Meyer *et al.*, 2007).

These two peptides were initially attributed to peripheral functions, but then more important roles were ascribed to them when they appeared in a screening of regulators of oxidative phosphorylation (Baughman *et al.*, 2009). In the screening, for which shRNAs were used, more than 85% of mRNA levels were depleted and the oxygen consumption rate (OCR) was measured. No alterations in the OCR were observed in either the shRNA of the *Dapit* and *Mp68* cells, or in the expression levels of other proteins of the mETC, including NDUFB8, SDHB or ATP5a. Although DAPIT and MP68 were proposed as the principal candidates to interact with mETC genes, changis in the oxidative phenotype in these mutants was not observed.

The interactions between the subunits of the ATPase complex, more specifically those involving DAPIT and MP68 have been analysed in covalent cross-linking assays. DAPIT and MP68 protein, as well as other peptides including ATP8, e, f, or g, have been described as supernumerary subunits. Nonetheless, this has not been confirmed by gel staining intensity where all the ATPase subunits have been resolved (Lee *et al.*, 2015). Lysine K49, in the carboxyl terminal of MP68, is linked to the same region of DAPIT K55, and also to different lysines of supernumerary subunits e, f or g (Fig. 8).

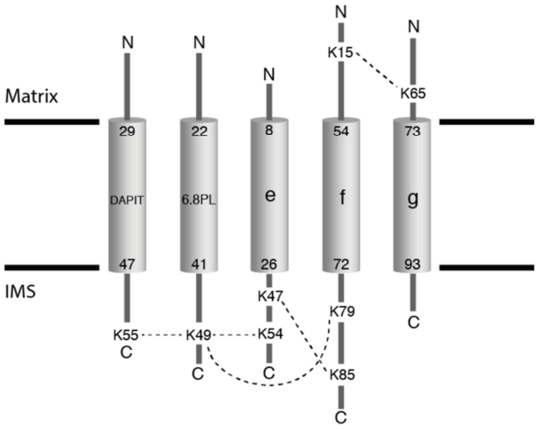

Figure 8. The cross-links detected between some ATPase subunits. The residues that cross-link between the supernumerary subunits of ATPase are shown in the figure (from (Lee *et al.*, 2015)).

Recently, the three-dimensional structure of a new ATPase domain has been observed in cryo-electron microscopy (cryo-EM) images and by a computational analysis (Fischer *et al.*, 2017). It is named the intermembrane space domain (IMD), and is described as a new domain associated with the traditional F_O ATPase complex, but is clearly separated.

The presence or absence of the IMD determines state 1 or state 2 of the ATPase structure, respectively (Fig. 9A). The IMD was identified in individual particles associated with ATPase that come into contact with the rotor region (Fig. 9B), and its structure is divided

into a tubular domain, SD1, and a globular domain, SD2 (Fig. 9C). In the particle where the IMD is absent, the transmembrane region remains unaffected, which indicates that the IMD does not play a role in membrane bending (Fig. 9D).

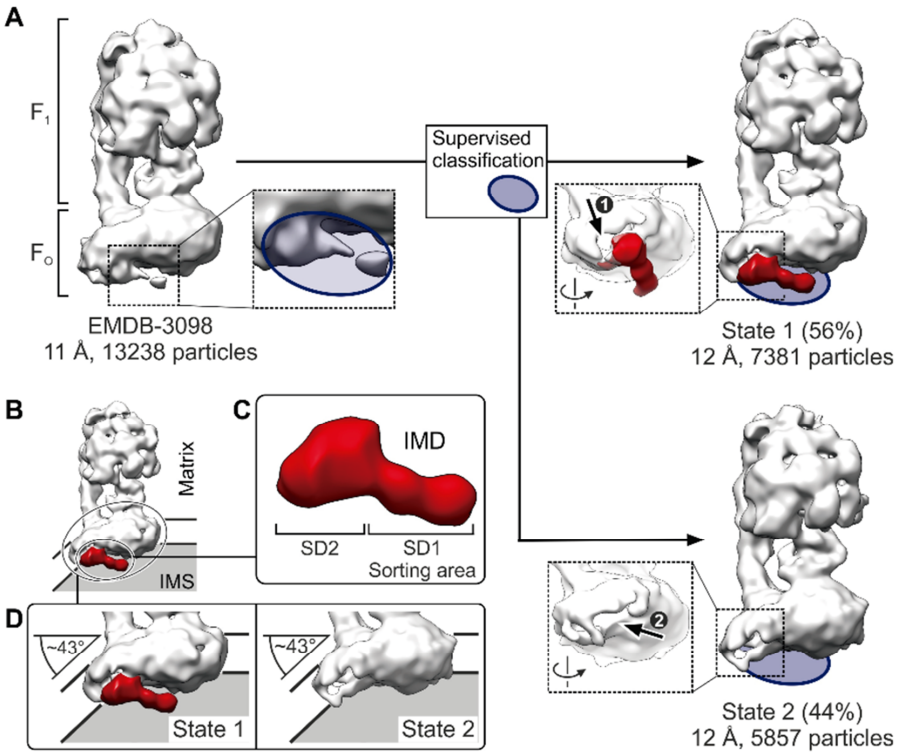

Figure 9. Description of FoF1 ATP synthase with and without an intermembrane space domain (IMD). A. After a computational analysis of the cryo-EM images, an IMD was described to be slightly associated with bovine ATPase. Two groups of structures are separated, state 1 where an IMD is present, and state 2 where an IMD is absent. **B.** The IMD is located in the inner mitochondrial space (IMS). **C.** The IMD structure with two domains: SD1 (tubular) and SD2 (globular). **D.** The IMD is not essential for membrane bending. From (Fischer *et al.*, 2017).

The absence of DAPIT and MP68 in stage 2 led to the conclusion that the IMD is formed by them, supported by the fact that strong interactions with other ATPase components were lacking, and also by their absence in preparations with small amounts of phospholipids. Furthermore, different structural models were proposed using the IMD structure and the previous cross-linking analysis, which concluded that these two proteins are the only candidates that occupy the IMD space (Fig. 10A-C).

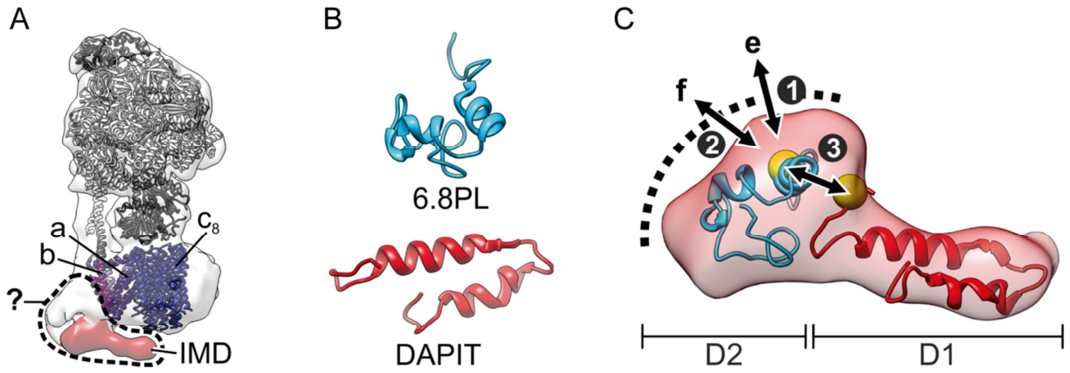

Figure 10. Structural composition of the mammalian IMD. A. Representation of state 1 of the IMD. The F_1 domain is depicted in grey, the c-ring rotor of ATPase is shown in blue, subunit a in purple and subunit b in magenta. **B.** Model of subunits DAPIT MP68 obtained by iTasser. **C.** Modelling DAPIT and MP68 in the IMD. Yellow spheres indicate the residues involved in cross-linking. From (Fischer *et al.*, 2017).

Similar IMD structures were found in other ATP synthases from yeast or ciliates, but their shape differed. The common aspect of these three cases was that the IMD always came into contact with the rotor region, which indicates its importance in regulating its function or its structure. The interaction between the IMD and the c subunits could affect the function of ATPase; in this scenario, the IMD would act as an inhibitor of F_O (similarly to IF1 in F_1). Nonetheless, the function performed by the IMD did not come over very clearly, and one suggestion is that it may be involved in the regulation of the mPTP opening monitored by either a lipid plug or dimer formation.

DAPIT (AGP)

DAPIT (diabetes-associated protein in insulin-sensitive tissue) is a basic hydrophobic protein that is 58 amino acids long with a single transmembrane helix. Its C-terminal domain is located in the intermembrane space (IMS) (Lee *et al.*, 2015) (Fig. 11).

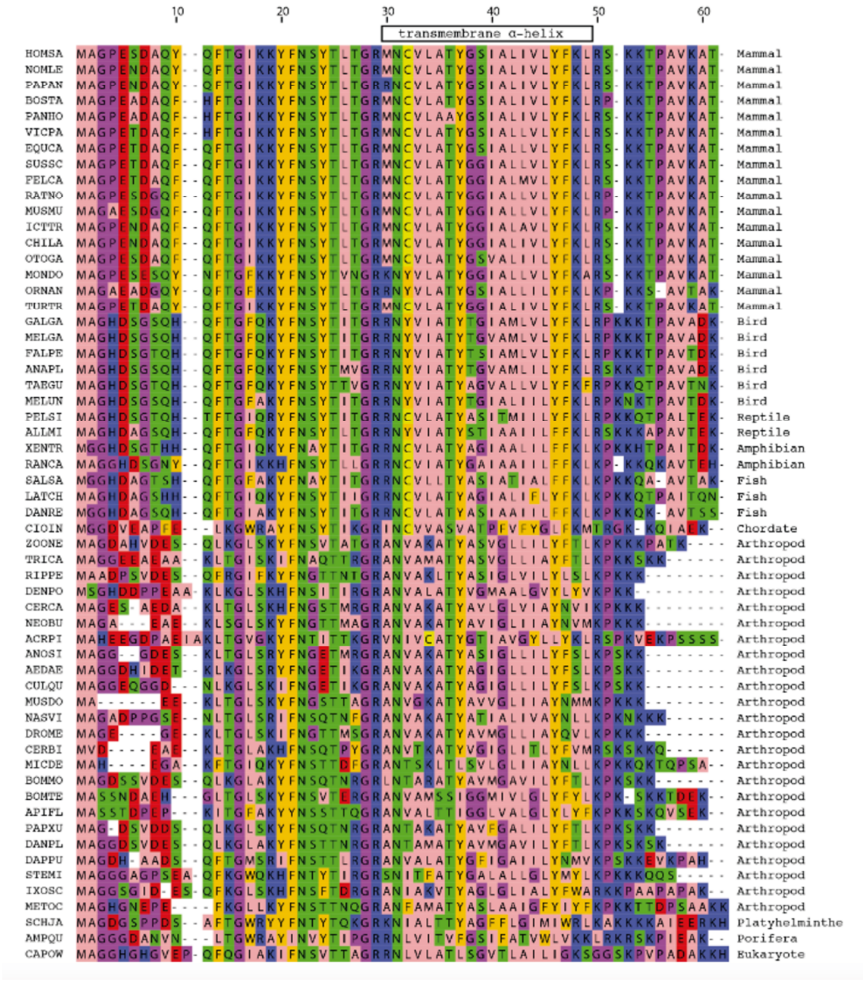

Figure 11. Conservation of the DAPIT protein sequence in metazoans. The sequence of DAPIT proteins of several organisms appears with this colour code: pink, hydrophobic; orange, aromatic; blue, basic; red, acidic; green, hydrophilic; magenta, proline and glycine. Yellow denotes cysteine residues. From (Lee *et al.*, 2015).

This peptide has been described in a streptozotocin-induced diabetes rat model (Päivärinne and Kainulainen, 2001). Streptozotocin (STZ) is an antibiotic, an analogue of glucose molecules that induces diabetes type I. STZ enters the beta cells of the pancreas by specific transporter GLUT2, which is enriched in this cell type. Therefore in this model, a high DAPIT mRNA expression was detected in tissues such as the brain, skeletal or cardiac muscle, but levels were lower in other tissues like the lung, liver or kidney. Following STZ treatment, Dapit mRNA decreased in the diabetic rat compared to the control ones. For this reason, the detected ORF was called DAPIT, diabetes-associated protein in insulin tissues. The DAPIT protein has been highly conserved during evolution. The human protein has a 58-98% similarity to proteins *Fugu* and *Xenopus*, and shares 40% identity with *Drosophila melanogaster* homologous protein Neb-cGP. In all these species, it is noteworthy that 13 amino acids are conserved, which indicates their potential importance in the DAPIT structure or function (Päivärinne and Kainulainen, 2001).

Given its general expression pattern, it was initially considered to perform a general function. In particular, insect homologue Neb-cGP has been described as a stimulator of cAMP. According to these data, DAPIT may be involved in this process under diabetic conditions (Päivärinne and Kainulainen, 2001).

HeLa cells with low DAPIT levels, by shRNAs, show loss of the ATPase population in mitochondria at the protein level, but not mRNA (Ohsakaya *et al.*, 2011). They also present impaired ATP synthesis and cell growth. In these cells, these authors did not observe any disassembly of ATPase or supercomplexes.

With the human cells that overexpress the DAPIT protein, glucose metabolism modulation has been observed (Kontro *et al.*, 2015). In these cells, the mtDNA content and mitochondrial mass lower, while the mitochondrial membrane potential increases. A tendency towards glycolytic metabolism has been detected, which promotes the activation of HIF1alpha in Wnt/beta catenin signalling.

6.8kDa protein (MP68)

This protein has been described simultaneously to the DAPIT protein (Terzi *et al.*, 1990; Chen *et al.*, 2007; Meyer *et al.*, 2007). Although the interference of the *Mp68* gene in cells reduces both the ATPase population and ATP production (Fujikawa *et al.*, 2014), the mRNA levels of the main ATPase subunits remain unaffected.

III. METABOLIC CONTROL BY OPTOGENETICS

III.1 Optogenetics systems

Optogenetic tools were traditionally used to modulate signalling in cells, whereby light induces conformational changes to proteins by triggering a cellular response. Initially, light-sensitive channels were developed to modulate the polarity of neurons to thus initiate a signalling pathway (Zemelman *et al.*, 2002). Beyond the neuroscience field, optogenetic applications are broader, and optogenetics is also used to manipulate gene expression (Yazawa *et al.*, 2009; Kennedy *et al.*, 2010) and to modulate the behavior of individual cells for example, by modifying cell polarity. The commonest method to do this is by modulating protein dimerisation with light (Levskaya *et al.*, 2009; Guglielmi, Falk and De Renzis, 2016). By way of example, changing the conformational status of proteins to produce an active protein is used to photoactivate Rac and to control cell motility (Wu *et al.*, 2009).

III.2 Optogenetics in metabolism

These tools have also been used In the metabolism field to modulate gene expression and to modify and study metabolism (Idevall-Hagren *et al.*, 2012; Inglés-Prieto *et al.*, 2015). All these examples use light as a trigger to induce conformational change. However, the possibility of using optogenetic systems to convert light energy into energy that can be used by cells to grow has been explored only minimally.

III.3 Deltarhodopsin

The first described microbial rhodopsine was in *Halobacterium salinarun* (Grote and O'Malley, 2011), but later others were found in several species. They all share a structure determined by seven transmembrane helices and they perform different functions as light-driven protons, ions or photosensors (Lanyi, 1998) (Fig. 12).

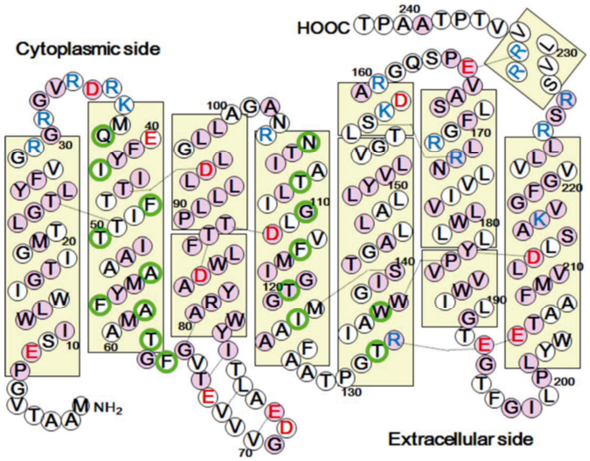

Figure 12. Diagram of the rhodopsin structure of *Haloterrigena thermotolerans.* Transmembrane helices are represented in rectangles, the amino acids with a positive and negative charge are depicted in blue and red, respectively. The green circles include the amino acids that interact between helices, and the pink circles show the most conserved residues between rhodopsins (from (Zhang *et al.*, 2013)

More specifically, Deltarhodopsin (HtdR) is a light-driven proton (H+) pump present in the membrane of *Haloterrigena turkmenica* (Kamo *et al.*, 2006) and others species. Its structure in different organisms is similar.

The functionality of HtdR has been demonstrated in artificial vesicles, which expresses HtdR together with F_oF_1-ATP synthase. HtdR translocates H^+ into vesicles and ATP synthase can use the H^+ gradient to generate ATP from ADP in the extra-vesicle medium. This protein has also been used in cells to partially rescue membrane damage following neurotoxin 1-methyl-4-phenyl-1,2,3,6-tetrahydropyridine (MPTP) treatment (Hara *et al.*, 2013).

III.4 Detaching ATP synthesis from the mitochondrial electron transport chain by optogenetics

Deltarhodopsin expression in cells is a way to separate ATP synthesis from electron transport in the mETC. Previously, this effect was achieved by the expression of other proteins, such as Ndi1 from *Saccharomyces cerevisiae* and Aox from fungi (Perales-Clemente et al., 2008). Ndi1 is a NADH dehydrogenase with NADH DH/CoQ reductase activity that can substitute the function of complex I in yeast, but without H+ pumping. Aox is an alternative oxidase present in plants and fungi that is able to oxidase the CoQ. With the expression of both these proteins in mitochondrial-deficient cells, it is possible to restore the capacity of these mutant cells so they can grow in the absence of pyruvate and uridine because they are able to restore the electron flux. Although these two proteins can

restore the electron flux, they cannot restore proton pumping, which means that these cells are unable to grow in galactose. Expressing deltarhodopsin in these cells would allow the ETC function to be fully restored.

Objectives

The role attributed to ATP synthase as the main energy producer of the cell has been maintained for years. Nonetheless, new functions have been defined, such as a regulator, apoptosis or as a determinant of mitochondrial cristae morphology. For this reason, the structure of this complex has been studied in detail, which led to the discovery of new subunits associated with it. We are interested in characterising these new subunits and their role in the ATPase function.

Optogenetics is a technique that has been traditionally used in the neural field to modulate cell behavior. We aim to extend its applications to the metabolism field.

Taken together, the specific objectives of this doctoral thesis are the:

1. Characterisation of proteins DAPIT and MP68 at the structural and functional levels.

2. Modulation of survival in the absence of the functional mETC.

Methods

I. CELL CULTURE

III.1 Mammalian cells

The following cells were used in this work (Table 1)

Table 1. The cells used in this work.

Line	nDNA	mtDNA	Mutation	ETC	Origin	Reference
L929^{mtC57}	L929	C57BL/6	-	All complexes are stable	Cybrids generated by transferring the platelet of cells C57BL/6 to $\rho^0$929	Moreno-Loshuertos *et al*. 2006
ND4^{KO}	L929	3T3	Mt-nd4 10227delA (homoplastic)	Complex I absent	Random mutation in 3T3 cells and transfer to L929 cells	Perales-Clemente *et al*. 2010
Cox10^{KO}	129/SvJ	C57BL/6	Cox10 knockout (homozygosis)	Complexes I and IV absent	Cre protein expression in the Cox10$^{flox/flox}$ fibroblasts	Diaz et al. 2006
F3T3	L929	3T3	-	All complexes are stable	Cybrids generated by the fusion of mitochondria from 3T3 cells with $\rho^0$929 cells	R. Moreno

III.2 Culture medium

The culture medium used to grow the cell lines was DMEM medium that contained L-glutamine and glucose at a concentration of 25 mM. The following were also added: 5% of FBS, 1mM sodium pyruvate, 100 units/mL penicillin and 100 ug/mL streptomycin. For the culture of some mutant cells with deficiencies in the ETC, uridine was added at a concentration of 50 ug/mL.

The medium used in the growth curve (Section I.5) was modified to ensure that other components did not interfere with growth, only with the carbon source of glucose or galactose. This prepared medium consisted of DMEM (Sigma D5030) in water supplemented with 2 mM L-glutamine, 1 mM sodium pyruvate, 5% dialysed FBS, 100 units/mL penicillin, 100 ug/mL streptomycin and phenol red. Then depending on the experiment, the medium was supplemented with 5 mM or 25 mM of glucose or galactose.

III.3 Culture conditions

Cells were grown at 37ºC at a constant level of 5% CO_2. The medium was frequently changed every 48 h, except in the growth curve experiment where the medium was changed daily.

III.4 Ectopic gene expression in mammalian cells

To get a stable expression of an exogenous protein a lentiviral infection was used.

To obtain viral particles, 293T cells were used and transfected with transfection reagent X-treme-GENE-HO (Roche) following the manufacturer's instructions. Firstly cells were placed in a medium that contained 25 µM chloroquine to avoid degrading exogenous DNA. Next 7 µg of the DNA that coded the viral capsid (the psPAX2 vector), 3 µg of the DNA that coded the viral envelope (pMD2G) and 10 µg of plasmid pWXLD with the sequence of interest were added to the FBS-free medium (Table 2).

Table 2 . Plasmids used to express exogenous proteins in mammalian cells.

Plasmid	Bacterial resistance	Eukaryotes promotor	Eukaryotes selection	Origin	Use
pWXLD	ampicillin	EF1 alpha	puromycin	TronoLab (with some modifications)	Lentiviral vector to expression in eukaryotes
psPAX2	ampicillin	CMVeh	-	TronoLab	Lentiviral packaging vector (2nd generation)
pMD2G	ampicillin	CMV	-	TonoLab	Lentiviral envelop vector

The produced viral particles were released to the medium and were collected 48 h and 72 h post-transfection. The medium was filtered with a 0.45 µM filter to eliminate cell debris before storing it at -80ºC. A small portion of it was kept to quantify the number of viral particles by qPCR (Scherr *et al.*, 2001). After determining the concentration, a particular MOI (multiplicity of infection) was selected (1, 5 or 10) as well as the infected cell line. Cells were incubated with viral particles for 6 h and were then cultured in normal medium. The antibiotic was added to the medium to select the infected cells after 48 h, which allowed enough time for the selection gene to be expressed, specifically the puromycin resistance gene.

III.5 Growth curve

To determine the ability of the different cell types to grow, a growth curve in the presence of glucose or galactose as a carbon source was performed. The cells with mutations in the ETC protein cannot survive in galactose medium because its conversion into energy is very slow, and glycolysis does not suffice to produce all the ATP required for cells to grow.

Cells were cultured in p96 plates at a density of around 2000 cells/well (depending on cell type). Cell growth was monitored daily by the CyQUANT™ NF Cell Proliferation Assay Kit (Thermo Fisher C35006) to measure DNA content. The number of plates depended on the experiment time. Typically, 5 days sufficed to evaluate the growth changes in different substrates.

In some experiments, different inhibitors, such as Antimycin a (inhibit complex III), were used to examine cell growth in its presence.

III.6 Cell growth in light conditions

To HtdR-expressing cell been an active protein which translocates protons, it is needed a source of light. Here, a standard cell incubation was transformed in an illuminated incubator thanks to the position of torch into it (Fig. 13). The torch used contains several LEDs that provides a whit light without warm up the place.

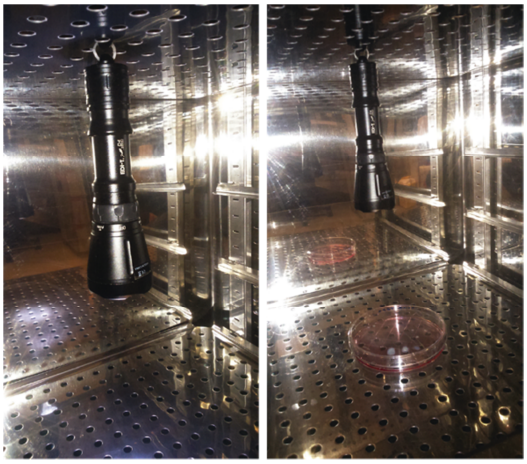

Figure 13. Photography of the illuminated incubator assembly. The torch was ubicated at the top of the incubator and the light illuminates the plates.

III.7 Immunofluorescence

Immunofluorescence was completed to detect the presence of some proteins. Cells were grown in p12 plates on glass covers. Firstly, they were fixed with 4% paraformaldehyde in culture medium for 15 minutes at 37ºC. Next they were washed several times with PBS. To permeabilise cells, covers were treated with PBS with triton X-100 for 5 min in the same plate. A blocking step was used by adding PBS with triton X-100 and 2% BSA for 10 min. Finally, the primary antibody was added to the blocking solution to detect the protein of interest (Table 3).

Table 3. Antibodies used for immunofluorescence

Detected antigen	Species	Catalogue number	Company
HA epitope	Rat IgG1	11867423001	Sigma
Tom20	Rabbit IgG	sc-11415	Santa Cruz
DAPIT	Rabbit IgG	17716-1-AP	Proteintech
Ndufa9	Mouse IgG	ab14713	Abcam

IV. ANIMAL MODELS

IV.1 Mouse strains

Two mouse strains were generated during this thesis. The first was a knockout for the DAPIT protein. The frozen sperm of a *Dapit* transgenic mouse C57BL/6N-Usmg5$^{tm1a(EUCOMM)Wtsi/}$H was obtained from the European Mouse Mutant Archive (EMMA) with ID EM:07834 and the following construct (Fig. 14).

Figure 14. Scheme of the construction of transgenic mice. The lacZ- and neomycin-resistant genes lie between the FRT sites, and the main exons, 2 and 3, lie between the loxP sites (From EMMA).

This is a very versatile construct. Firstly, *Dapit* expression could be followed because of lacZ expression and its subsequent detection via X-gal staining. Secondly, since it is a conditional transgenic mouse, the DAPIT protein could be specifically deleted in different tissues depending on the particular cre line used.

In vitro fertilisation (IVF) of the C57BL/6 female mice was performed at the Transgenesis Unit of the CNIC. Descendants were genotyped to select the transgenic line of interest. Transgenic mice were then crossed with a flippase mouse line to thus eliminate the neo and lacZ cassettes found between the FRT sites. Lastly, in order to achieve full knockout, mice were crossed with the Sox2:cre mouse line (Hayashi, Tenzen and McMahon, 2003), which expresses cre recombinase under the control of the Sox2 promotor during early development.

The second mouse strain generated was a knock-out of *Mp68*. In this case, embryonic stem (ES) cells were obtained from the European Mouse Mutant Cell Repository (EuMMCR). The transgenic ES for the 2010107E04Rik gene (*Mp68*) was performed in the JM8A1.N3 cell line. The basis of the structure of the used construct was the same as the transgenic *Dapit* one, the lacZ cassette, and the codifying exons placed between the loxP sites.

IV.2 PCR for genotyping

To genotype mice, a piece of tail was cut from mice during weaning, and DNA was extracted using the REDExtract-N-Amp™ Tissue PCR Kit following the datasheet indications. Taq DNA polymerase was used to genotype.

The primers used to genotype the different mouse lines are specified (Tables 4 and 5).

Table 4. Primers to genotype the *Dapit* transgenic mice

To genotype the DAPIT mice	Sequence
Wild-type allele	TGCCAGTTCTTGGCTTACACT
	AAGGCCAGCTAAAGTTGGAG
Transgenic allele	TGCCAGTTCTTGGCTTACACT
	GAACTTCGGAATAGGAACTTCG
Floxed allele	AAGGCGCATAACGATACCAC
	CCGCCTACTGCGACTATAGAGA
Knockout allele	AAGGCGCATAACGATACCAC
	TGGGAAAGCACTTAACCCCA

Table 5. Primers to genotype the *Mp68* transgenic mice

To genotype the *Mp68* mice	Sequence
Wild-type allele	GGGAATGTGGGTATCTAGTTTGGT
	AATGAAGACGGAGGCCTGTT
Transgenic allele	GGGAATGTGGGTATCTAGTTTGGT
	ACTTCGGAATAGGAACTTCGGT
Floxed allele	AAGGCGCATAACGATACCAC
	CCGCCTACTGCGACTATAGAGA
Knockout allele	AAGGCGCATAACGATACCAC
	TAGACAGACAGCCAGTCCCG

V. PROTEIN RESOLVING AND ANALYSIS

V.1 Protein extraction and quantification

Proteins were extracted from cells with RIPA buffer (50 mM TrisHCl pH7.4, 50 mM NaCl, 1%Triton x-100, 0.5% sodium deoxycholate, 5 mM EDTA, and a protease inhibitor cocktail (11697498001 Sigma). Cells from a p100 plate were pelleted and washed with cold PBS twice. The pellet was then resuspended in 200 µL of RIPA buffer, incubated at 4ºC for 15 min and placed on a rotating wheel. Lastly, cells were centrifuged at 15,000g for 15 min at 4ºC and the supernatant was collected.

The Bradford method was used to quantify the protein concentration in the samples (Bio-Rad 5000006) (Bradford, 1976). Next 1 µL of sample was added to each well, which

already contained 200 µL of water, and were quantified by triplicate readings. A standard protein curve using 0, 1, 2, 3, 4, 5, 10 and 15 µL of 1 mg/mL stock of BSA was used to measure the absorbance of the samples. Finally, 50 µL of Bradford reagent were added, mixed well and measured in a spectrophotometer at 595 nm.

V.2 SDS-PAGE electrophoresis

Standard denaturing (SDS-PAGE) conditions were used to resolve proteins. A 30% percentage of acrylamide/bis-acrylamide (29:1 ratio) (A/BA) was used and they were run in gel with stacking and resolving parts (Table 6).

Table 6. SDS-PAGE gel composition

	Resolving 12.5%	Resolving 7%	Stacking
Tris HCl 1M pH 8.8	1.87 mL	1.87 mL	-
Tris HCl 1M pH 6.8	-	-	0.25 mL
A/AB 30%	2.08 mL	1.16 mL	0.33 mL
Distilled water	1.05 mL	1.94 mL	
SDS 20%	25 µL	25 µL	10 µL
APS 20%	15 µL	15 µL	10 µL
TEMED	5 µL	5 µL	5 µL

Samples were run in Tris-glycine buffer (Tris 25 mM, glycine 20 mM and SDS 0.5%) at 10 mA voltage during stacking, and voltage was raised to 20 mA once the samples reached the running gel (if the number of gels was more than 1, amperage was increased). This was done with a Mini-PROTEAN Tetra Cell (BioRad).

V.3 Protein transference to a PVDF membrane and protein detection

After resolving proteins on gel, they were transferred to a PVDF membrane (Immobilon-FL, 0.45 µM) and were then transferred and run in transfer buffer (48 mM Tris, 39 mM glycine and 20% methanol) for 1 h and 15 min at 100 volts (V) by the Mini Trans-Blot Cell system (BioRad). The membrane was blocked to avoid non-specific unions of antibodies with 5% BSA in PBS or with Sea Blocking buffer (Thermo Scientfic 37527) for 1 h at room temperature (RT) or o/n at 4ºC.

To detect specific proteins, the primary antibody was diluted in blocking solution and incubated with the membrane for 2 h at RT (Table 7). Next the membrane was washed 3 times with PBS that contained 0.1% Tween-20 for 5 min. The secondary antibody diluted in blocking solution was also added and incubated for 1 h at RT (Table 8). Afterwards the membrane was washed once more (the last wash was done only with PBS).

To develop the signal, the Odyssey ® Imaging System (from LI-COR Company) was used. By this technology, two longitudinal waves were detected at the same time, which allowed the simultaneous detection of two proteins of a similar size.

Table 7. Primary antibodies used

Detected antigen	Species	Code	Company
ACTIN	Rabbit IgG	A2066	Sigma
COI	Mouse IgG2	459600	Invitrogen
DAPIT	Rabbit	17716-1-AP	Proteintech
NDUFA9	Mouse IgG	ab14713	Abcam
OPA1	Mouse IgG	612606	BD Bioscience
TOM20	Rabbit IgG	sc-11415	Santa Cruz
UQCRC1	Mouse IgG1	Ab110252	Abcam
UQCRC2	Rabbit	17716-1-AP	Proteintech

Table 8. Secondary antibodies used

Detected antigen	Conjugation	Code	Company
Mouse IgG (H+L)	DyLightTM 800	610-145-121	Rockland
Mouse IgG (H+L)	Alexa Fluor 680	A21057	Life Technologies
Rabbit IgG (H+L)	DyLightTM 800	610-145-122	Rockland
Rabbit IgG (H+L)	Alexa Fluor 680	A210766	Life Technologies
Rat IgG(H+L)	IRDye800	926-32219	LI-COR
Rat IgG(H+L)	Alexa Fluor 680	A21096	Life Technologies

VI. ANALYSIS OF MITOCHONDRIAL COMPLEXES AND SUPERCOMPLEXES

VI.1 Mitochondria extraction from cells and tissues

Mitochondria isolation was done following the protocol of J.A. Enríquez's laboratory (Fernández-Vizarra, López-Pérez and Enriquez, 2002).

Mitochondria from cells

To isolate mitochondria from cells, 10 plates of 10 mm were required. Cells were trypsinised and then pelleted. The pellet was washed with PBS prior to extraction. At this point, the pellet can be stored at -80ºC or directly extracted. In the next step, hypotonic medium (sucrose 83 mM, MOPS 10 mM, pH 7.2) was added to resuspend the pellet (seven volumes of the pellet volume). After 2 min on ice, the pellet was placed into a glass tissue potter and homogenised in a stirrer (Heidolph RZR 2041). Afterwards, the same volume was added to the hypertonic medium (250 mM sucrose, 30 mM MOPS pH 7.2). Then it was centrifuged at 1,000g for 5 min at 4ºC. The supernatant was collected in several 1.5mL phials and centrifuged at 13,000g for 5 min at 4ºC. Next pellets were collected and washed

with medium A (320 mM sucrose, 10 mM Tris, 1mM EDTA, pH 7.4) several times and placed in a single phial. Finally, samples were quantified by the Bradford method (see Section III.1) and stored at -80ºC in 50 mM Bis-Tris, 1M aminocaproic acid at a concentration of 10 ug/uL.

Mitochondria from tissues

Instead of using a hypo/hypertonic medium, the mitochondria from tissues were homogenised directly in medium A, except when extracting mitochondria from the heart, when fatty acid-free BSA was added.

VI.2 Mitochondria samples preparation

Fresh or defrosted mitochondria were lysed with digitonin, a soft detergent at a detergent:protein ratio of 4:1 (g/g). Each 10-µL (100 µg of protein) aliquot was treated with 4 µL of 10% digitonin. The mix was incubated for 5 min on ice and centrifuged at 13,000g for 30 minutes at 4ºC. The supernatant was then collected and applied to 3 µL of loading buffer (5% Coomassie Blue G-250 in 1M aminocaproic acid).

VI.3 Blue-Native PAGE gel

Blue-Native Gel (BN) electrophoresis should be carried out to visualise mitochondrial complexes (Schägger, 1995; Wittig, Braun and Schägger, 2006). A gradient gel is required to resolve high-molecular-weight complexes (**Table 9**). Using the gradient, resolving gel was prepared in 1.5 mm-thick glass plates with the gradient former connected to a peristaltic pump.

Table 9. BN gel composition

Resolving gel component	Acrylamide solution, 3%	Acrylamide solution, 13%
A/BA 48:1.5	0.305 mL	0.866 mL
Buffer 3x *	1.667 mL	1.111 mL
Distilled water	3 mL	0.713 mL
Glycerol 85%	-	0.643 mL
APS 20%	20 µL	7 µL
TEMED	4 µL	3 µL

*** Buffer 3x: Bis-Tris 150 mM, aminocaproic acid 1.5 M, pH 7**

See Section III.2 for the stacking gel composition

VI.4 BN-PAGE electrophoresis

Mitochondria samples, already digitonised and containing the loading buffer, were loaded onto gels and run in a Mini-PROTEAN Tetra Cell apparatus (BioRad). Different buffers were used to run cathode A (50 mM tricine, 7.5 mM imidazole, 0.02% Coomassie blue G-250, pH 7), cathode B (50 mM tricine, 7.5 mM imidazole, pH 7), and anode (25 mM imidazole, pH 7). The first run was at 150V for 40 min using cathode A, with an extra 1 h at 300V with cathode B (the anode buffer was the same throughout the process).

To transfer the mitochondria complexes to a membrane, the same protein transfer procedure was followed (see Section III.3).

VII. MITOCHONDRIAL ANALYSIS

VII.1 Subcellular fractionation

Mitochondria isolation was done as previously described (see Section Methods IV.1). Fresh mitochondria were treated with trypsin to digest he proteins in the OMM, as previously described (Perales-Clemente *et al.*, 2011).

VII.2 ATP synthesis

An ATP synthesis measurement was taken in fresh mitochondria. ATP was detected by the luciferin/luciferase fluorimetric method that follows this reaction:

Luciferase + luciferin + ATP → luciferase-luciferil-AMP + PPi

Luciferase-luciferil-AMP + O_2 → luciferase + oxyluciferin + AMP+ CO_2 +*hv*

The produced light was proportional to the amount of ATP, with maximal emission in 560 nm (Vives-Bauza, Yang and Manfredi, 2007).

Using flat-bottomed white plates (96-well Costar Assay Plates), 160 µL of buffer A (50 mM KCl, 25 mM Tris-HCl, 2 mM EDTA, 0.1% BSA, 10 mM KPO_4, 0.1 mM $MgCl_2$, pH 7.4) were added. Next a standard ATP curve was done to relate the amount of light and the ATP concentration by adding 10 µL at varying ATP concentrations (from 0 to 10 mM). To calculate ATP production in the experimental samples, 50 µg of mitochondria were added (in the 160 µL of buffer A) to each well. Later substrates were added (a 5 µL mix of 6 mM DP5 + 5 µL pyruvate/glutamate/malate, depending on the substrate to be evaluated, + 5 µL ADP). Three replicates were needed for each sample measurement. Finally, 20 µL were

added (0.5 M Tris-acetate, 0.4 mM luciferin, 10 ug/mL luciferase, pH 7.75). After mixing well, the plate was measured in a luminometer (Tubo Sirius, Berthold) for 5 min every 20 sec.

During the analysis, a regression line was done by correlating the ATP concentration and luminescence. Later ATP production was determined as the nmols of ATP produced in 1 minute per protein amount.

VII.3 Ultrastructural mitochondrial morphology analysis by transmission electron microscopy

Apex hearts from mice were collected and fixed in 2.5% glutaraldehyde, 4% formaldehyde in 0.1 M HEPES buffer for 5 h at 4ºC. After several washes with 0.4 M HEPES buffer, samples were postfixed with 1% osmium tetroxide and 3% potassium ferrocyadine in distilled water for 1 h at RT. Then samples were washed in distilled water 3 times for 10 minutes each time. Next they were dehydrated with different percentages of acetone and were embedded in a resin (Spurr Low-Viscosity Embedding).

After solidification, blocks were cut in 60-nm sections, mounted on a copper grid and lead citrate-stained. Samples were evaluated by JEOL 10-10 electron microscopy with different objectives.

VII.4 Metabolic test in mice

Glucose tolerance test (GTT)

The main objective of the GTT experiment was to determine the capacity of the organism to clear glucose from blood (Harlass *et al.*, 1991). To carry this out, male mice were subjected to starvation conditions for 6 h before the test started (from 8 a.m. to 2 p.m.). Glucose was administered via intra-peritoneal injection. The amount of glucose used in this experiment was 1.8 g of glucose per kg of mouse weight. Next a small incision was made at the end of the mouse tail to obtain a sufficient amount of blood required to measure the glucose concentration. Blood glucose levels were measured prior to glucose administration at 15, 30, 60, 90 and 120 minutes using specific strips (Lite Blood Glucose Test Strips from FreeStyle).

Insulin tolerance test (ITT)

The ITT measures glucose levels by monitoring the response to insulin administration. ITT was carried out in mice that had fasted for 2 h (from 12 p.m. to 2 p.m.). Insulin was then administered by injection at a concentration of 0.75 U/mL. As well as in GTT, blood glucose levels were measured with specific strips at 15, 30, 60 and 90 min after insulin administration.

VII.5 Mitochondrial swelling assay

In isolated mitochondria, swelling occurs due to the large cytosolic amount of proteins and other solutes. This event occurs *in vitro* after opening the mPTP, which is why it is commonly used as a measure of mPTP opening.

Fresh mitochondria were used, 25 µg per sample in 100 µL of mPTP buffer (200 mM sucrose, 10 mM HEPES, 5 mM KH_2PO_4, 10 µM EGTA, pH 7.3). In 96-well glass plates, each sample was placed in a well and then measured by a spectrophotometer. A volume of 750 µM calcium chloride ($CaCl_2$) was added to trigger mitochondrial swelling. Measurements were taken every 15 secs for 6 min in a spectrophotometer at A540. A 1 µM concentration of cyclosporine A (CsA) was added to half the wells as a negative control to avoid mitochondrial pore opening.

VII.6 Immunoprecipitation of and resolving ATP synthase proteins

To isolate proteins from the ATP synthase complex, the ATP synthase Immunocapture kit from Abcam (ab109715) was used with some modifications. At least 1 mg of mitochondria at a concentration of 5.5 mg/mL in PBS was needed. This mixture was solubilised with 1% n-Dodecyl-D-Maltoside (DDM), a non-ionic detergent, to disrupt the external membrane. This mitochondrial suspension was kept on ice for 30 min before centrifuging at 13,000g for 30 minutes at 4ºC. The supernatant was finally collected.

During centrifugation, agarose beads that contained specific immunocapture antibodies for the ATP synthase complex were prepared. They were cleaned with PBS and placed in a new phial (all the working steps with beads were done with blue tips cutting the end). The previously collected supernatant was added to beads, incubated at 4ºC and left on a rotating wheel o/n.

The following day, samples were centrifuged at minimum velocity to allow beads to lower. Beads were resuspended again in PBS with protease inhibitors and 0.05% DDM, and were

placed in a 15-mL phial. Washing was done at 4ºC by leaving the phial on the rotating wheel for 15 min. This last step was repeated 3 times, and in the last repetition beads were transferred to a 1.5-mL phial. To elute proteins from beads, sample buffer (50 mM Tris-HCl, 20% SDS, 10% glycerol, 1% β-mercaptoethanol, 0.02% bromophenol blue, pH 6.8) was added with no medium. The sample buffer was collected and stored at -80ºC.

To resolve the proteins obtained from the immunocapture, a big gradient gel (10-15%) was done using the former gradient (Table 10) in a big glass. Runs were done with the same buffer as SDS-PAGE electrophoresis (Section III.2)

Table 10. Big gradient gel composition

Resolving gel component	Acrylamide solution, 10%	Acrylamide solution, 15%
A/BA 29:1	4 ml	3.5 mL
Separated buffer 4x *	3 ml	1.75 mL
Distilled water	4.9 ml	1.75 mL
APS 20%	15 µL	10 µL
TEMED	5.76 µL	3.36 µL

*** Separated buffer 4x: Tis-HCl 1.5 M, SDS 0.4%, EDTA 8 mM pH 8.8**

Stacking gel component	
A/BA 29:1	1.2 mL
Concentrated buffer 4x *	2 mL
Distilled water	4.7 mL
APS 20%	37 µL
TEMED	20 µL

*** Concentrated buffer 4x: Tis-HCl 0.5 M, SDS 0.4%, EDTA 8 mM pH 6.8**

Then to stain proteins, silver staining (PlusOne Silver Staining Kit form GE Healthcare Life Science) was done.

Results

I. PROTEINS ASSOCIATED WITH H^+- ATP SYNTHASE

I.1 Establishment of the mice DAPIT and MP68 knockout colonies

DAPIT knockout mice

DAPIT is a subunit of mitochondrial H^+-ATP synthase, which has been identified very recently and whose role in the complex remains unclear. To study its expression pattern and role *in vivo*, a versatile knock-in mouse was established, which can be used as both lacZ reporter and conditional knock out from the European Mouse Mutant Archive (EMMA), ID EM:07834.

Following *in vitro* fertilisation, the obtained animals were crossed with C57BL/6 mice to verify the germinal transmission of the transgenic cassette (Fig. 15A). Next, the sequences between FRT sites, including neomycin resistance and LacZ genes were deleted by crossing the positive descendants with Rosa26:FLP mice, a transgenic mouse line that expresses the flipase gene (Fig. 15B). This was done to avoid interfering with gene expression levels. In this way, floxed mice were obtained with the codified exons of interest between loxP sites. Lastly, in order to obtain the knockout (KO) mice of interest, floxed mice were crossed with a Sox2:Cre line to delete the codified exons (Fig. 15C).

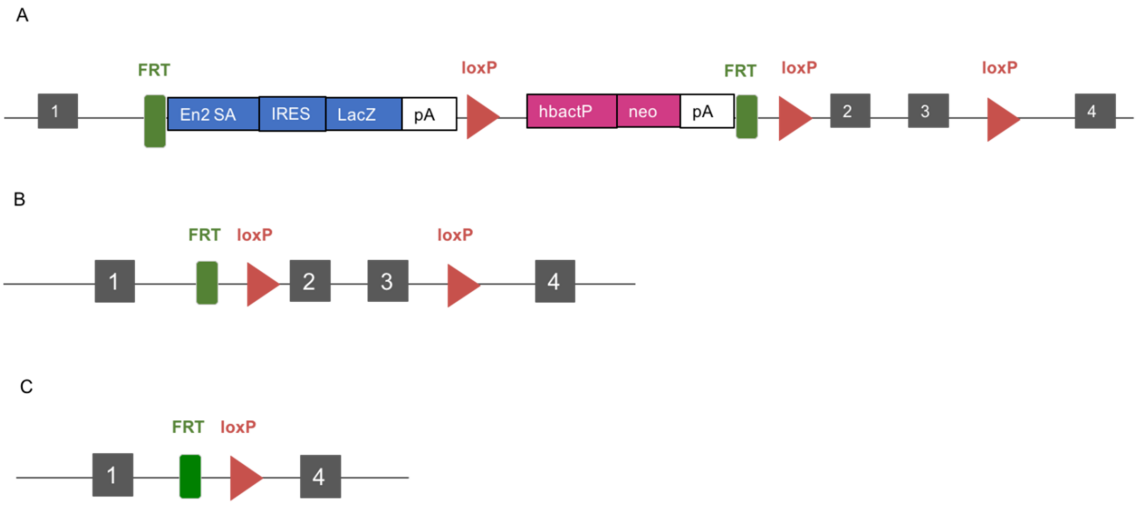

Figure 15. Schematic representation of the different transgenic lines of proteins DAPIT and MP68. A. Original construct of the transgenic Dapit mouse. **B.** Representation of an allelic construct after crossing transgenic Dapit with a flipase mouse. Neo-LacZ cassette deletion occurred. **C.** Construct was obtained after the crossing with a Cre protein expression mouse line. The exons between LoxP sites were deleted.

MP68 knockout mice

To obtain the MP68 knockout mouse, the same strategy was employed as that for the DAPIT knockout with specific primers to the genotype (Fig. 15). In this case, ES cells were obtained from the European Mouse Mutant Cell Repository (EuMMCR). The transgenic ES for the 2010107E04Rik gene (*Mp68*) was used in the JM8A1.N3 cell line. ES cells were used to obtain a C57BL/6 chimera, which was crossed several times until the germinal transmission of the transgene was observed. To obtain the KO mice, floxed mice were crossed with a Sox2:Cre to generate total KO mice.

Previously to the establishment of mouse colonies, mitochondria isolated from fibroblast in culture were used to study the function of the ATPase associated proteins DAPIT and MP68. When we analysed the ATPase complex by staining with ATP beta antibody, the monomeric form of the ATPase was detected, but no multimeric forms were observed (Fig.16). This excludes the use of cells to analyse all the possible conformations of ATPase and highlights the importance of using an in vivo model to analyse ATPase supercomplexes. For this reason, the remaining experiments were performed with tissue-isolated mitochondria.

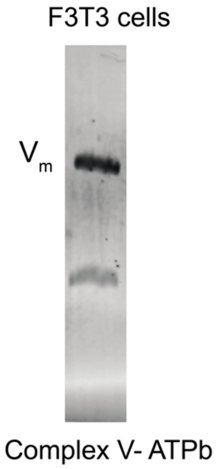

Figure 16. Blue native of cell mitochondria to analyse the ATPase organization by using ATP beta antibody.

I.2 Characterisation of DAPIT KO mice

The mice that harboured the original construct (Fig. 15A) constitutively expressed the β-galactosidase gene under the endogenous *Dapit* promoter. This allowed us to investigate the *Dapit* expression pattern during embryonic development by staining with X-gal. For this purpose, E9.5 and E12.5 embryos were chosen. In the E9.5 embryo, the signal was detected in heart. At E12.5, this signal became stronger and extended to other tissues from the ventral embryo part (Fig. 17).

Figure 17. X-galactosidase staining of the whole embryo. A. Mouse embryo in the E9.5 developmental stage staining to detect LacZ expression to follow *Dapit* gene expression. **B** and **C**. The mouse embryo that expresses LacZ in the ventral area, and more specifically in heart. Bars, 200 µm (A), and 1 mm (B, C).

LacZ staining was then analysed in the E12.5 embryo sections. The signal was detected mainly in the heart and the neural system, including retina ganglion neurons (Fig. 18).

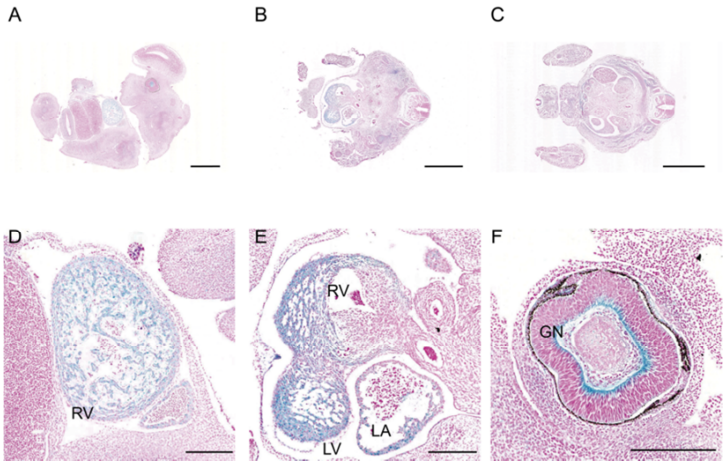

Figure 18. X-galactosidase staining in the E12.5 embryo. X-galactosidase staining (blue) represents the areas in which the *Dapit* gene is expressed in this stage. **A.** Longitudinal plane of the E12.5 embryo showing LacZ expression in blue. **B and C**. Transversal plane of the E12.5 embryo showing LacZ expression in blue. **D.** Longitudinal section of X-galactosidase staining of the embryonic heart. **E.** Transversal section of X-galactosidase staining of the embryonic heart. **F.** Transversal image of the eye embryo (RV: right ventricle, LV: left ventricle, LA: left atrium, GN: ganglion neuron. Scale A-C 1mm, D-F 250 um).

To determine whether the expression levels were maintained during development, adult organs were also analysed (Fig. 19). In addition to heart, lacZ staining was also detected in the liver, kidney, brain, skeletal muscle and spleen.

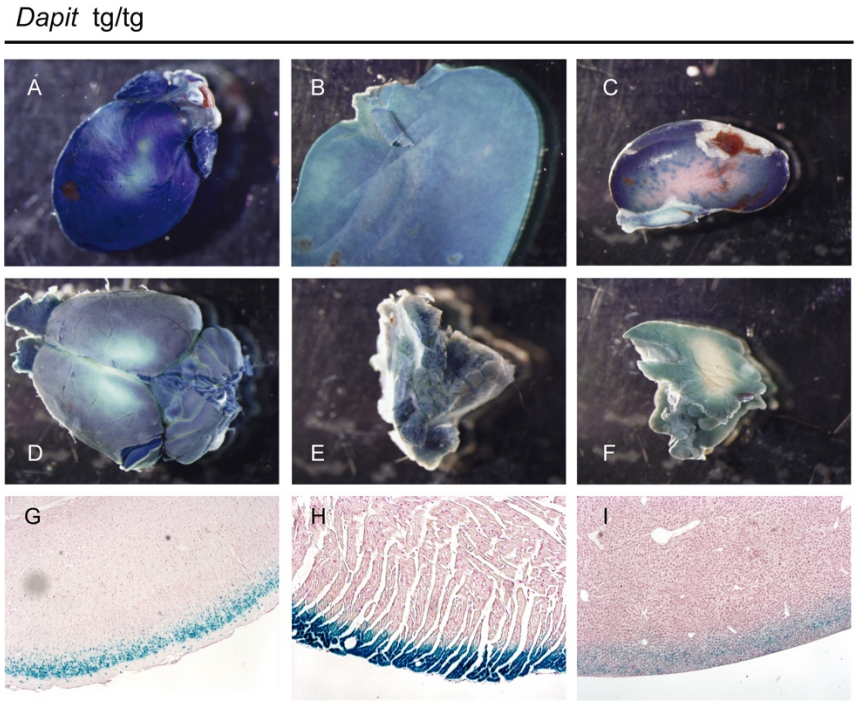

Figure 19. X-galactosidase staining of the adult organs of the *Dapit* transgenic mice (*Dapit* tg/tg). **A-F.** Whole mount X-galactosidase staining **A.** heart, **B.** liver, **C.** kidney **D.** brain, **E.** muscle, **F.** spleen. **G-H.** Cut organs after X-galactosidase staining. **G.** Brain slide after X-galactosidase staining. **H.** Heart slide after X-galactosidase staining. **I.** Liver slide after X-galactosidase staining.

I.3 Characterisation of mitochondria and OXPHOS function in DAPIT knockout.

As DAPIT expression was detected at a high level in the heart in different developmental stages, DAPIT function was studied primarily in this tissue. To confirm the absence of the DAPIT protein in the total KO mice, mitochondrial protein from heart was analysed and resolved under denaturalising conditions by SDS gel. However, the available commercial antibody did not detect any signal at the expected location (Fig. 20A).

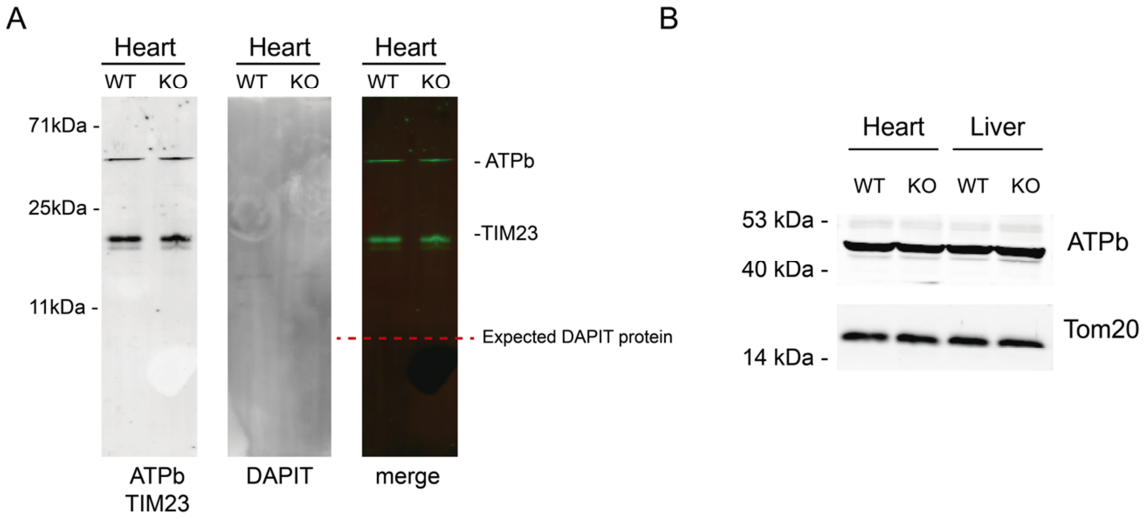

Figure 20. The SDS gel of tissue mitochondria. Mitochondria from wild-type (WT) and KO heart, liver, spleen and brain were analysed by Western blot. **A**. Using the DAPIT antibody, no signal was detected at the expected size of 7kDa, which corresponds to the DAPIT protein. **B.** Detection of the ATPb subunit to calculate the amount of the ATPase complex in mitochondria. Tom20 was used to check the quantity of total mitochondria in each sample.

A reduction in the total quantity of the ATPase complex in the DAPIT knockdown cell has been reported (Ohsakaya *et al.*, 2011). To analyse this, the WT and KO heart and liver mitochondria were analysed by Western blot (Fig. 20B). No reduction in ATPase was observed in the KO mitochondria compared with the WT, which indicates that lack of DAPIT protein did not alter the amount of ATPase in the investigated tissues. This observation contrasts with previous reports which have shown that the H^+-ATP synthase complex in DAPIT knockdown cells reduces (Ohsakaya *et al.*, 2011).

Next the DAPIT commercial antibody was tested under native conditions. Complex V was labelled in the WT sample, but not in the DAPIT KO sample, which revealed an efficient deletion of the Dapit allele and the absence of the protein product (Fig. 21). Therefore, the commercial antibody only detected DAPIT in its folded form.

Figure 21. The blue native of the mitochondria from the WT and DAPIT KO heart mice. Western blotting revealed the absence of the DAPIT protein in the KO mice. Vdac was used as the loading control.

To analyse the effect of DAPIT loss of function on the different mETC complexes, the mitochondria from the DAPIT KO mice were analysed by BN (Fig. 22). No differences were observed in the organisation of complexes I, III and IV between the WT and KO heart mitochondria.

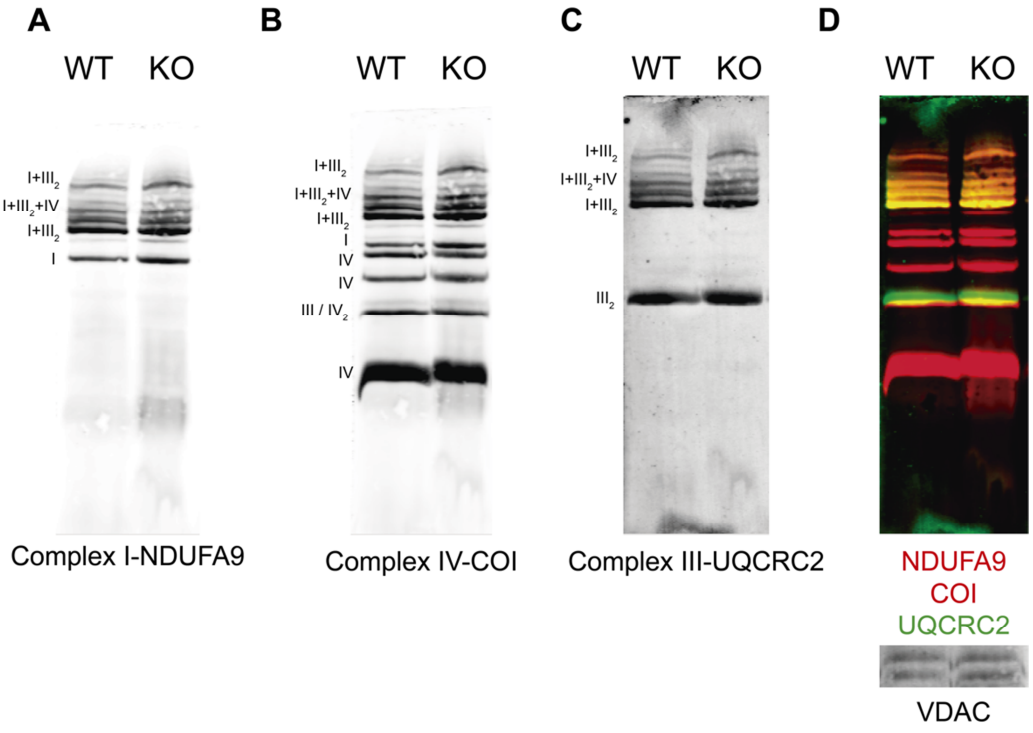

Figure 22. Analysis of the complexes of the heart mitochondria of the DAPIT WT and knockout by BN. Different complexes of digitonise mitochondria were analysed. **A.** The BN of the WT and KO mitochondria analysed with a specific complex I antibody that detects the Ndufa9 subunit. **B.** The previous membrane incubated with a specific antibody of complex IV that detected subunit CoI. **C.** Analysis of complex III by the UQCRC2 antibody in the previous membrane. **D.** Merging of previous antibody signals.

These results are not heart-specific as they were confirmed in the liver mitochondria (Fig. 23).

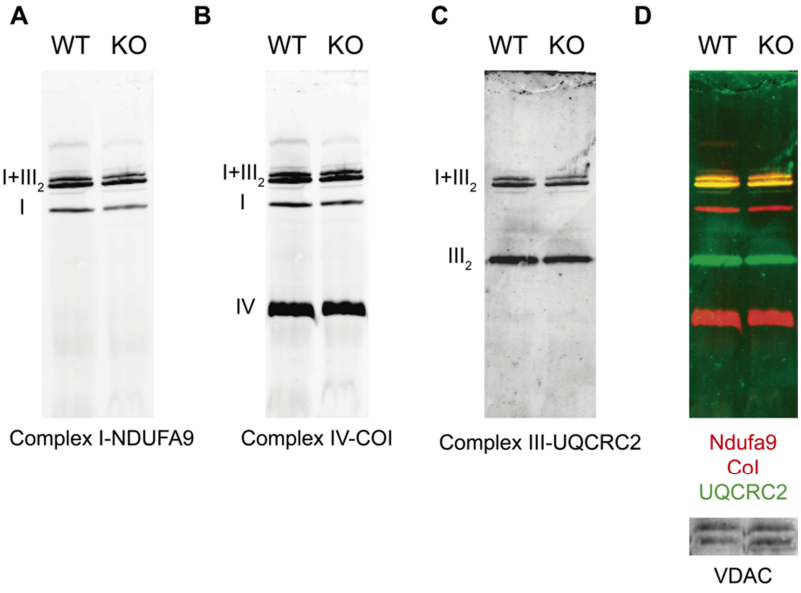

Figure 23. Analysis of the complexes of the liver mitochondria of the DAPIT WT and knockout by BN. Different complexes of digitonised mitochondria were analysed. **A.** The BN of the WT and KO mitochondria analysed with a specific complex I antibody that detected the Ndufa9 subunit. **B.** The previous membrane incubated with a specific antibody of complex IV that detected subunit CoI. **C.** Analysis of complex III by an UQCRC2 antibody in the previous membrane. **D.** Merging of previous antibody signals.

Next ATPase organisation was analysed. In the WT mice, DAPIT co-migrated with the monomeric form of ATPase (Fig. 24). In the DAPIT knockout mitochondria, this complex migrated slightly more than in the WT, which suggests that the complex could have a reduced mass (Fig. 24A). As DAPIT has been described as a supernumerary subunit of ATPase, one possible explanation could be that its absence results in an observed reduced size of complex V. Other explanation could be the change in the conformation of ATPase complex that alter the migration pattern under native conditions.

A change in ATPase organisation was observed in the DAPIT KO mice (Fig. 24B). In the WT mice, a high-molecular-weight band was observed that corresponded to ATPase in its dimeric form, but it was not observed in the DAPIT KO mice. This result indicates that DAPIT is necessary for ATPase dimer formation.

An additional lower-molecular-weight band was observed (Fig. 24A). This band was also stained with the anti-beta subunit antibody located in the ATPase F_1 domain. The molecular weight of this band was estimated to be between 400 and 500 kDa. This ruled out the possibility that this band corresponded to the F_1 domain, whose weight was estimated as 350 kDa.

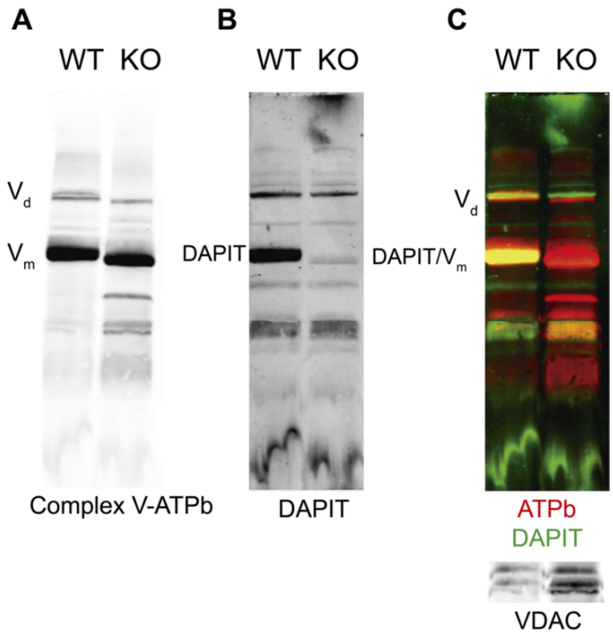

Figure 24. Analysis of Complex V of the heart mitochondria of the DAPIT WT and KO by BN. A. ATPase complex detection. B. DAPIT detection in the WT and KO heart mice mitochondria. C. Merging of the signal detected with the DAPIT and ATP subunit beta antibodies.

A similar result was detected in the DAPIT knockout mice liver. However, the ATPase dimers and the F_1 domain were not so clearly detected, which made it difficult to analyse this phenotype in the liver mitochondria (Fig. 25).

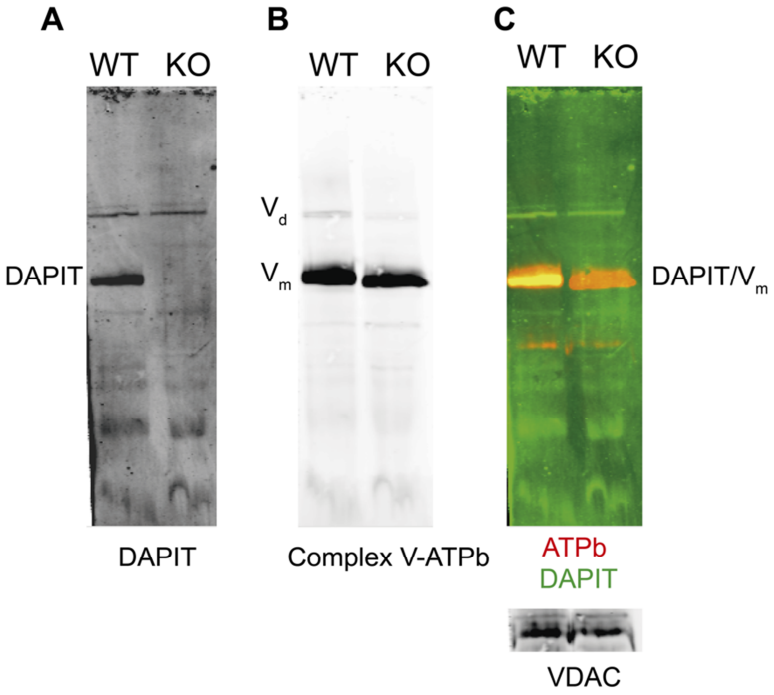

Figure 25. Analysis of Complex V of the liver mitochondria of the DAPIT WT and knockout by BN. A. DAPIT detection in the WT and KO heart mice mitochondria. **B.** ATPase complexes detection. **C.** Merging of the signal detected with the DAPIT and ATP subunit beta antibodies.

Further antibodies were used to confirm the identity of the ATPase subcomplex detected in the DAPIT KO mitochondria (Fig. 26). The alpha subunit, which is present in the F_1 domain of ATPase, was detected in that band (Fig. 26B). However, the ATP5I protein, which pertains to subunit F_0, was not detected in the studied subcomplex (Fig. 26D).

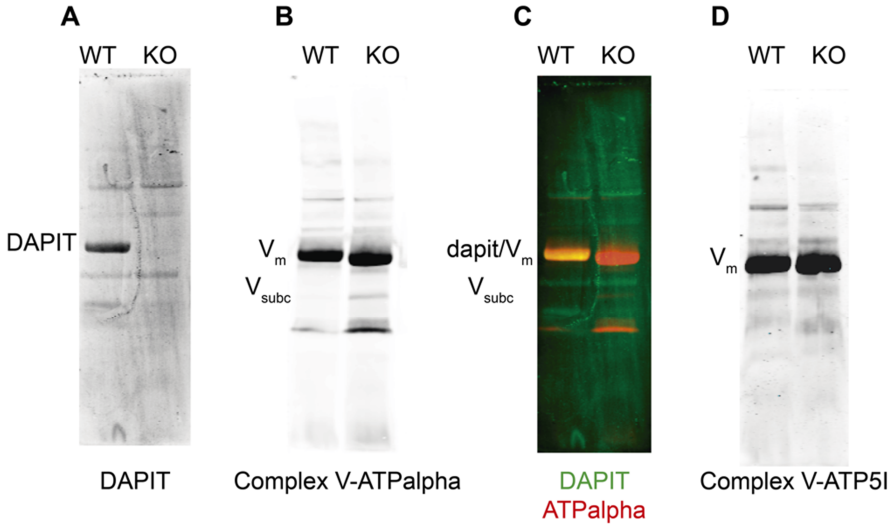

Figure 26. Analysis of the heart mitochondria complexes by BN. A. DAPIT protein detection in the heart mitochondria. **B.** Analysis of the ATPase complexes using an ATP alpha antibody. **C.** Merging of previous antibody signals. **D**. Another BN gel to analyse the ATP complex by an ATP5I antibody.

Then, the functionality of the ATPase subcomplex observed in DAPIT KO was evaluated by *in gel activity*. It was demonstrated that at least hydrolytic capacity remained in that subcomplex (Fig. 27).

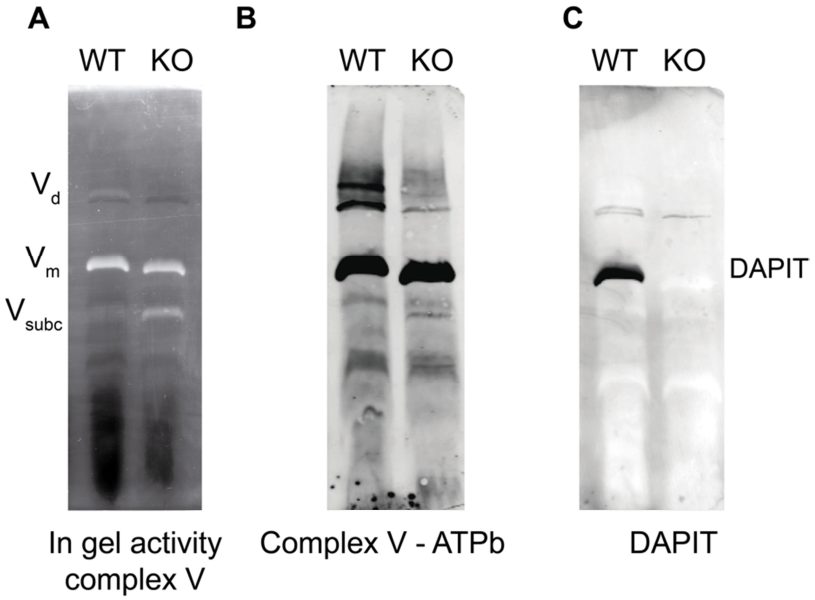

Figure 27. Functional analysis of the ATPase subcomplex in the DAPIT KO heart mitochondria. A. In the gel activity of complex V using ATP as a substrate of the reaction. **B.** Western blot detection of the ATPb subunit in a parallel running gel. **C.** The previous membrane detected the DAPIT protein.

To exclude the possibility that these results were caused by the specific detergent concentration, a digitonin/protein proportion effect was evaluated. The ATPase subcomplex was detected independently of the amount of detergent used, which indicates that it is not a technical artifact, but is present in cells instead (Fig. 28).

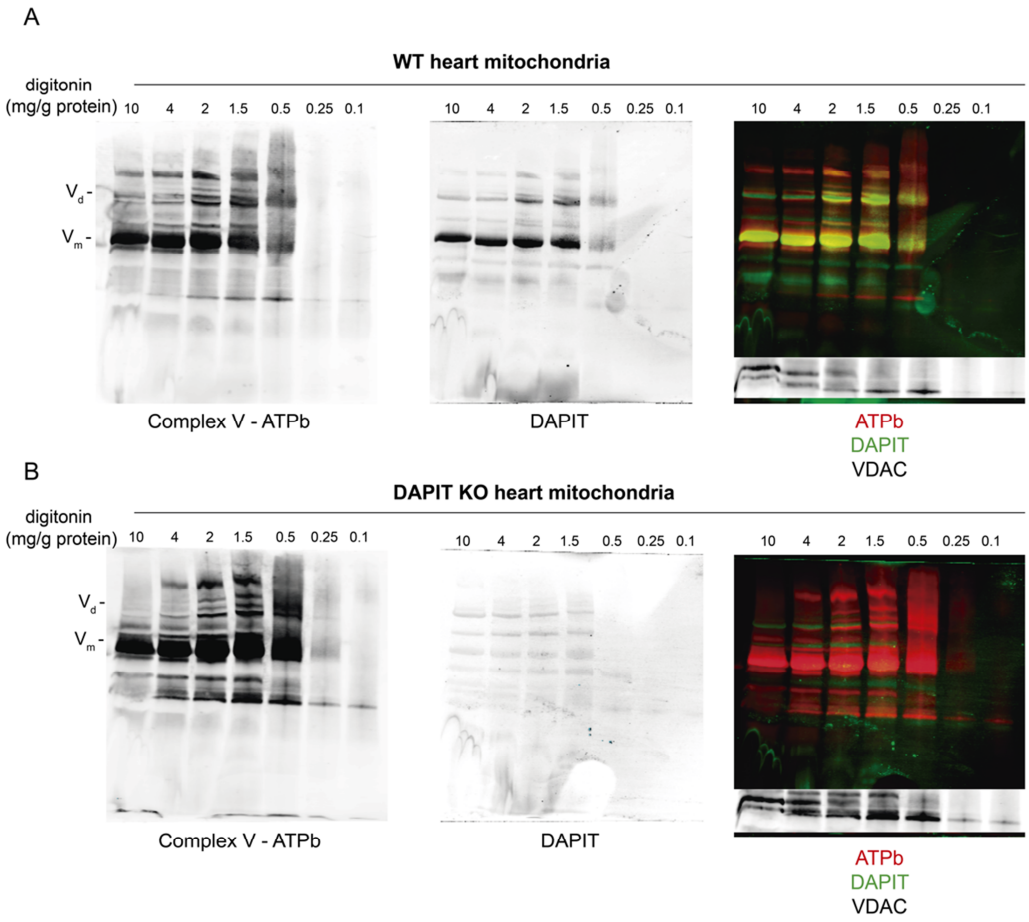

Figure 28. Digitonine curve analysis in BN gel. A. BN analysis of the heart mitochondria solubilised with different concentrations of digitonine. ATPase and the DAPIT protein were detected by antibodies. **B**. The same analysis using the DAPIT KO mitochondria.

Thus DAPIT, apart from being implicated in the dimerisation of ATPase, is necessary for ATPase monomers stability. In the absence of DAPIT, a 400-500 KDa subcomplex that contained the alpha and beta, but not the e, subunit was dissociated. All these results strongly suggest that it could correspond to the subcomplex identified in the Rho0 cells composed of at least subunits α, β, and γ_1 from F_1, and subunit c from F_O (Nijtmans *et al.*, 1995).

The relationship between the different ATPase peripheral subunits is not clear. To better understand this, the ATPase structure in Rho0 cells was analysed. These cells have no

mtDNA, so the mitochondrial proteins coded by it are absent. Specifically, they lack subunits ATP6 and ATP8. The ATPase structure was altered in Rho0 cells given the absence of these subunits, and the size of the complex reduced. More importantly, the ATPase dimers were not found. Surprisingly, DAPIT was not detected in the ATPase of Rho0 cells (Fig. 29). Since Dapit is coded by the nuclear genome, this result indicates that DAPIT is bound to the rest of ATPase by the proteins coded by the mitochondrial genome. Moreover, the absence of DAPIT may be one of the reasons why the Rho0 ATPase complex is unable to form dimers.

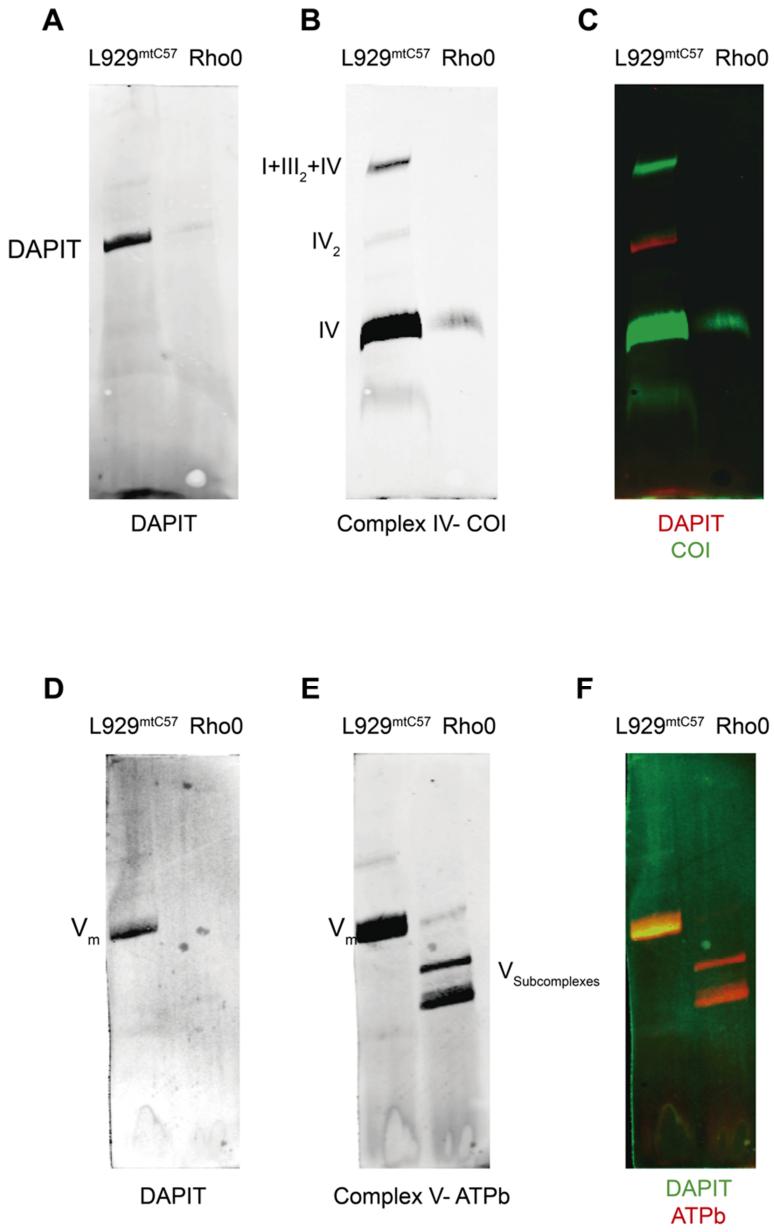

Figure 29. The Rho0 mitochondria analysis by BN gel. A-C. In Rho0 cells, the CoI subunit is not present in this cell because it is codified by mtDNA. DAPIT is not detected, nor associated with the ATPase complex. **D-F.** In the Rho0 cells without the DAPIT protein, ATPase complex organisation differs and several subcomplexes appear.

In order to analyse how the absence of DAPIT affected the rest of the ATPase complex, ATPase was immunoprecipitated from the tissue mitochondria. After resolving its subunits in gradient gel and staining proteins with silver, no differences were detected in the other ATPase subunits (Fig. 31). Only a small difference was detected at the bottom of the gel, which could correspond to the DAPIT peptide that was absent in the KO ATPase complex.

Taken together, these results indicate that while other subunits are necessary for DAPIT assembly in ATPase, DAPIT does not affect the assembly of these subunits.

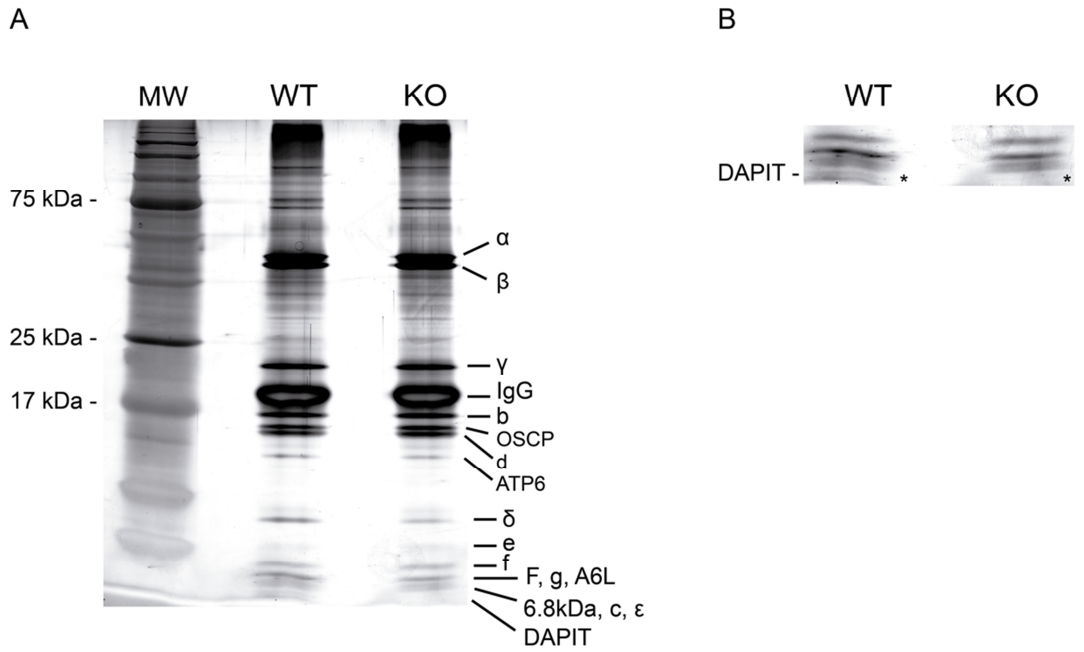

Figure 30. Immunoprecipitation of the ATPase complex. A. The proteins that form the ATPase complex were isolated and resolved in a gradient acrylamide gel and stained with silver. In the WT and KO ATPase, the main proteins were identified and a difference was observed only in the band that contained the small-sized proteins due to the absence of DAPIT in the KO mitochondria. **B.** Zoom of the part of the gel where the DAPIT protein is. (* is located, indicating the presence and absence of the DAPIT protein).

The results reported here indicated that ATPase was the only mitochondrial complex affected by the absence of DAPIT. The functionality of this complex was tested in the mitochondria isolated from heart and liver. ATP production was evaluated by adding different substrates, including glutamate/malate and succinate, to promote the electron transfer from complex I or II, respectively (Fig. 31). No differences in ATP synthesis were observed between the WT and DAPIT KO mitochondria. This result indicates that ATPase dimer formation is not essential for ATP production by mitochondrial ATPase.

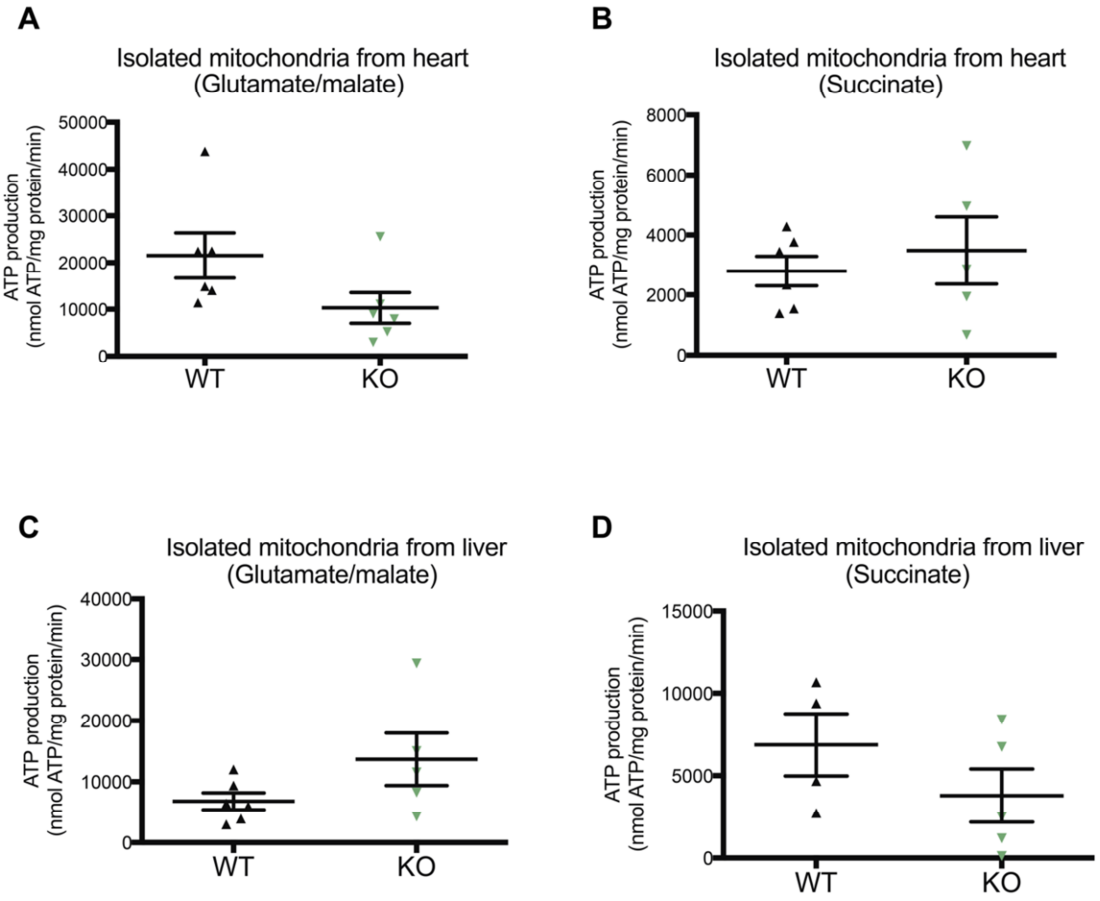

Figure 31. ATP synthesis in the tissue mitochondria. Analysis of ATP production in the heart mitochondria with glutamate/malate (**A**) or succinate (**B**) as a substrate. Analysis of ATP production in the liver mitochondria with glutamate/malate (**C**) or succinate (**D**) as a substrate. (A-D represents the ATP production value and SEM) (A p-value=0.0841, B p-value=0.5651, C p-value=0.1339 and D p-value=0.2520 all by a two-tailed *t*-test).

All these results show that eliminating the DAPIT protein is a very specific way of inhibiting ATPase dimer formation without it affecting ATP production or other subunits of ATPase.

It has been suggested that ATPase dimers are implicated in mPTP opening (Giorgio *et al.*, 2013). To test this hypothesis, the aperture process was analysed in the isolated mitochondria. Addition of calcium to the medium with the heart mitochondria triggered pore aperture by altering mitochondrial morphology. This was detected by a change in the optic density of the medium, which can be evaluated by absorbance measurements. Taking into account the specificity of the signal, demonstrated by mPTP opening inhibition through cyclosporine A, no differences were observed between the WT and DAPIT KO mitochondria (Fig. 32). This result indicates that the disappearance of the ATPase dimers does not affect mPTP opening, and reveals that the ATPase dimers do not form the mitochondrial pore.

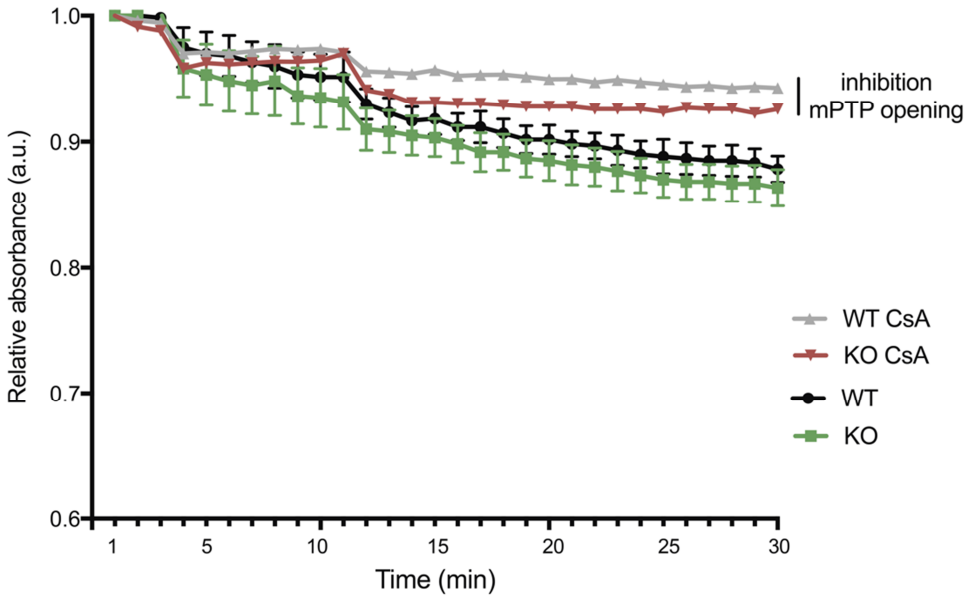

Figure 32. Representation of absorbance variation with time after mPTP opening. Calcium was added to trigger mPTP opening in presence or absence of CsA that acts as opening inhibitor.

I.4 Characterisation of DAPIT knockout mouse adult fibroblasts

Next the phenotype of the immortalised mouse adult fibroblasts obtained from the WT and KO mice was analysed. After confirming lack of DAPIT by BN (Fig. 33A), ATP synthesis was measured in these cells, and no significant differences were detected (Fig. 33B). After treatment with different drugs, which allowed the basal and maxima respiratory capacity to be studied, no changes in the OCR were observed among the other parameters (Fig. 33C). Moreover, lack of DAPIT, associated with ATPase, did not bring about any change in the mitochondrial membrane potential (Fig. 33D). Altogether, these results support that DAPIT plays no major energetic role.

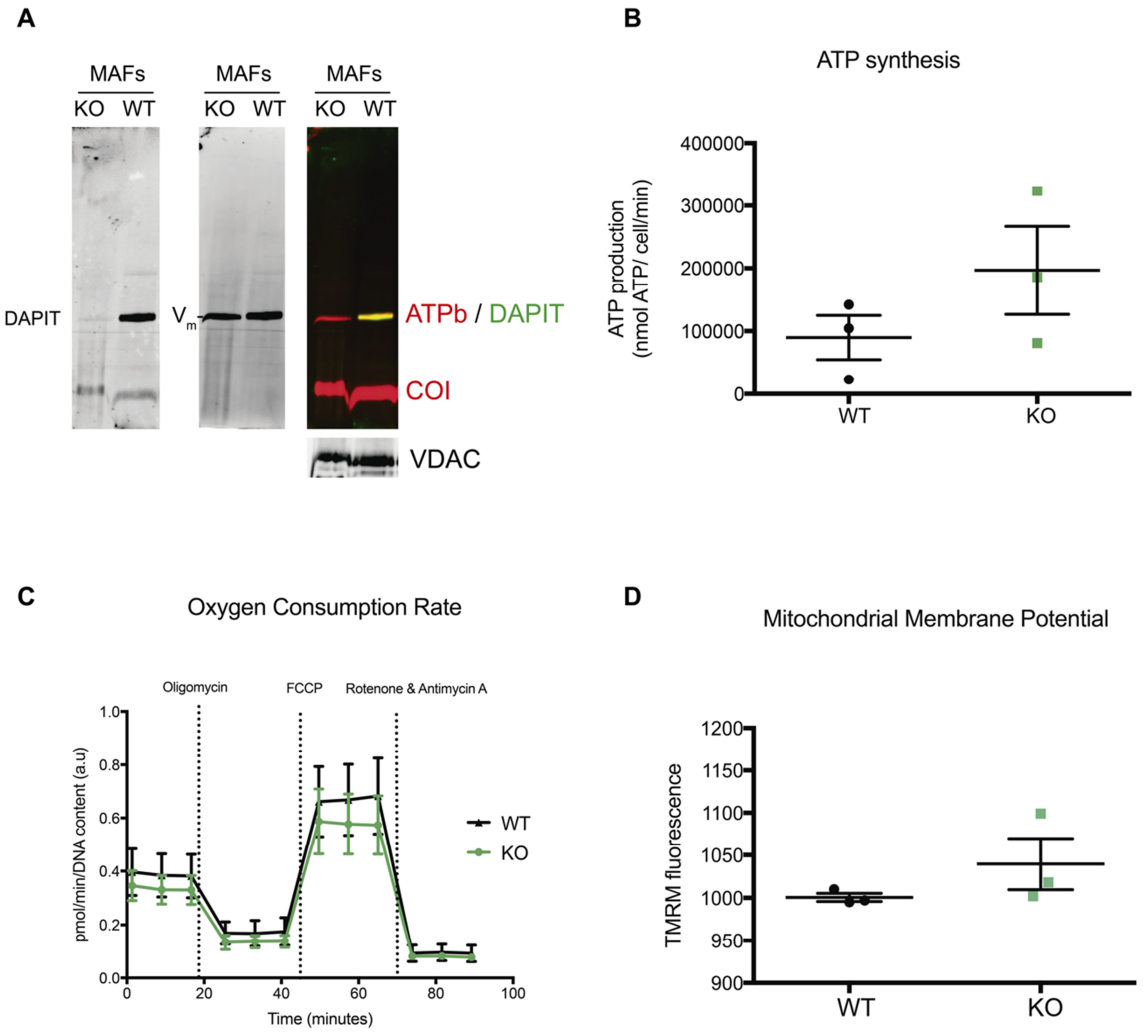

Figure 33. Characterisation of mouse adult fibroblasts (MAFs). Different measurements were taken in one clone of WT MAFs and in another clone of KO MAFs. **A**. BN of the WT and KO MAFs that detected DAPIT, ATPb and VDAC proteins. **B.** Measuring ATP production in the WT and KO MAFs. The ATP production and SEM values are represented (p-value 0.244 by a two-tailed *t*-test). **C.** Time profile of the OCR of the WT and KO MAFs after oligomycin, FCCP, rotenone and antimycin A treatment. **D**. Detection of the mitochondrial membrane potential in the WT and KO MAFs. The value membrane potential and SEM are represented (p-value 0.2687 by a two-tailed *t*-test).

I.5 Role of DAPIT in mitochondria morphology

As ATPase dimers are located on the edge of cristae, their morphology was analysed in our mouse model in which ATPase dimers were absent. The cristae morphology was analysed by transmission electron microscopy (TEM) in the WT and KO mouse hearts. Slightly thinner mitochondrial cristae were detected in the KO mitochondria than in the WT hearts (Fig. 34).

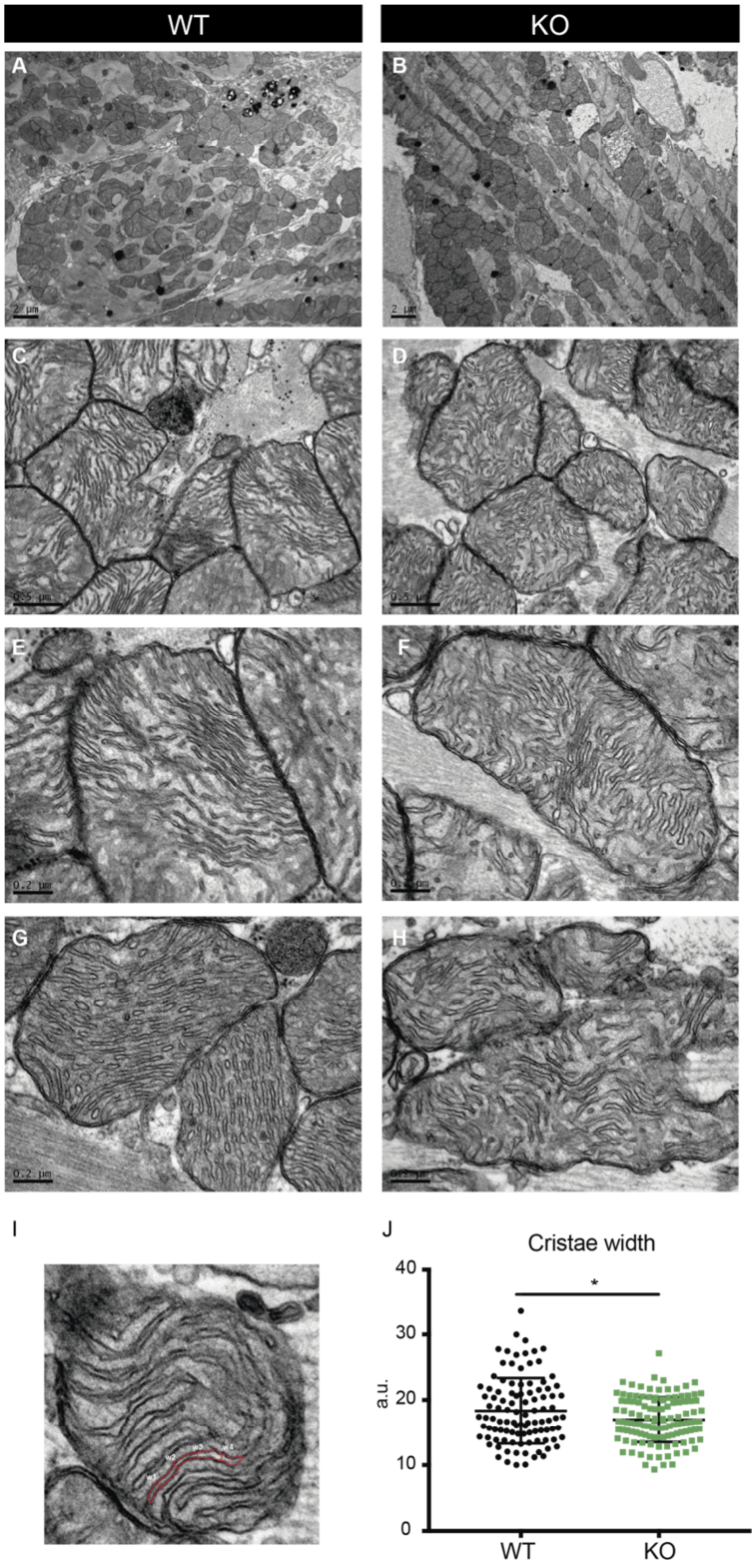

Figure 34. Mitochondria transmission electron microscopy analysis. A and **B.** Heart mitochondria images from the WT and KO mice, respectively, at the 5000x magnification. **C** and **D**. Heart mitochondria images from the WT and KO mice, respectively at the 40000x zoom. **E** and **F**. Heart mitochondria images from the WT and KO mice, respectively, at the 80000x zoom. **G** and **H**. Heart mitochondria images from the WT and KO mice, respectively, at the 80000x zoom. **I.** Representation of how cristae width was measured. A mean of four measurements (w1, w2, w3 and w4) was taken to refer to the width of each crista. **J.** Quantification of cristae width in the WT and KO mitochondria (* p-value = 0.0192 by a two-tailed *t*-test, each dot represents one crista; two animals per group were analysed) (bars A-B 2 µm, C-D 0.5 µm and E-H 0.2 µm).

I.6 Characterisation of the DAPIT knockout mice phenotype

The WT and DAPIT KO mice looked similar when grown under standard conditions, and were fed chow diet (Fig. 35A-B). To test if some differences appeared under extreme conditions, animals were placed on a high-fat diet (HFD). However this diet, which contained a higher percentage of fat (60 kcal/g) did not show any difference (Fig. 35C).

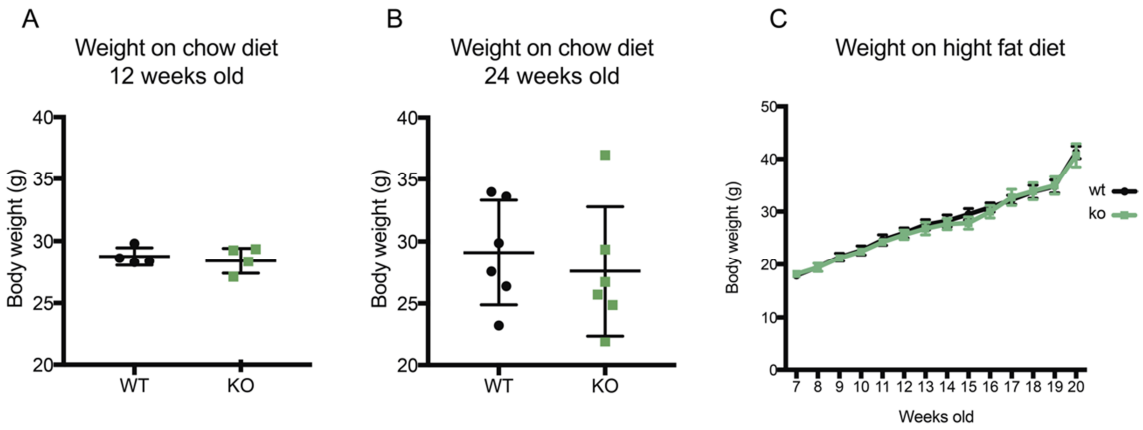

Figure 35. Weight of mice. A. Weight of the 12-week-old mice on the chow diet (p-value = 0.5805 by a two-tailed *t*-test). **B.** Weight of the 24-week-old mice on the chow diet (p-value = 0.5917 by a two-tailed *t*-test). A and B, each dot represents the weight of one mouse. **C.** Weight evolution of the high-fat diet**.** The weight of each group of animals was represented weekly (n=4).

DAPIT was initially identified as an upregulated protein in diabetes mellitus (Kontro *et al.*, 2012). To test its role in glucose metabolism, a glucose tolerance test was performed in the 12-week-old mice. Blood glucose levels were measured before and after glucose intraperitoneal administration (Fig. 36A), and a non-statistically significant tendency was observed for higher glucose levels in the KO *vs.* the WT group, although a tendency was found in all the seven experiments run (Fig. 36B).

To ensure that glucose regulation was not affected at any age range, the same experiment was repeated by comparing the 12- and the 25-week-old mice (Fig. 37). Once again, glucose levels were slightly higher in the KO than in the WT mice in both the 12- and 25-week-old mice. An age effect on glucose levels was detected as the glucose in the younger mice's blood was rapidly cleared.

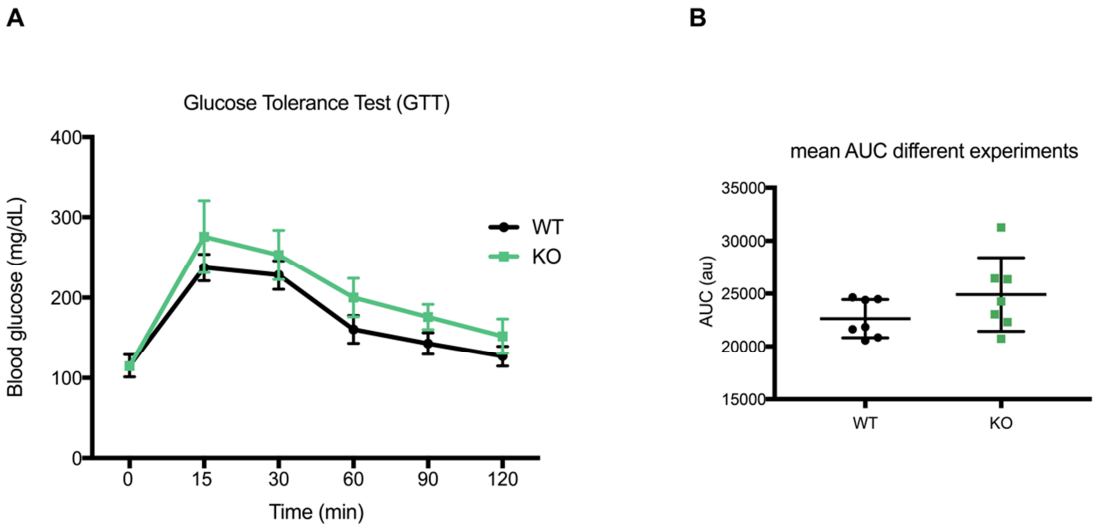

Figure 36. Glucose tolerance test. A. Blood glucose levels were measured in the WT (black line) and KO (green line) mice in 15- or 30-min intervals after glucose administration (n=5 mice, p-value = 0.2056 for the area under the curve (AUC) by a two-tailed *t*-test). A representative plot of the seven experiments is shown. B. The mean of several AUCs from seven different experiments (p-value = 0.1493 by a two-tailed *t*-test).

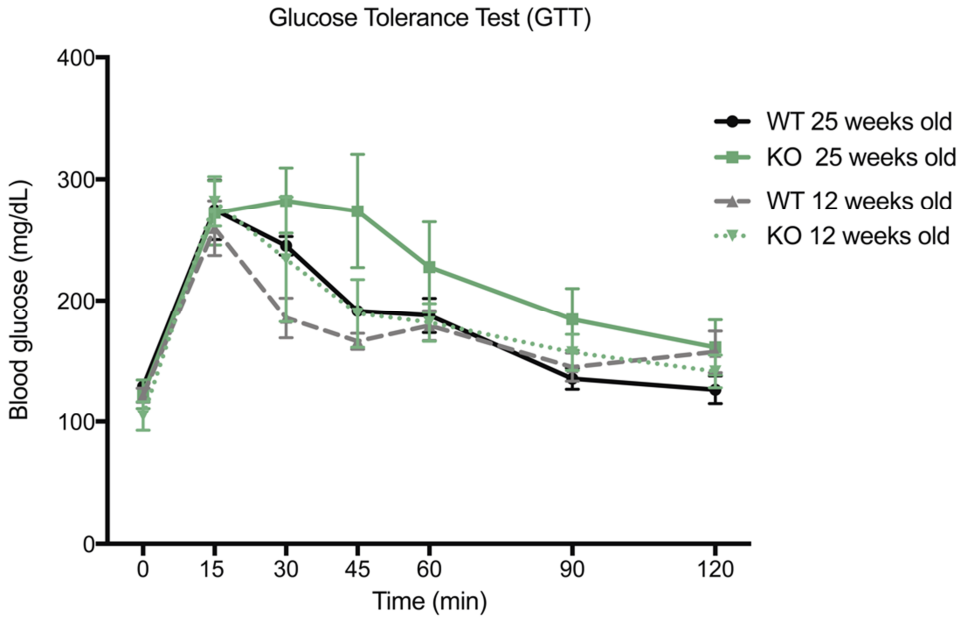

Figure 37. Glucose tolerance test in mice of different ages. Blood glucose levels were measured in the WT (black line) and KO (green line) mice, aged 12- and 25-weeks old in 15- or 30-min intervals after glucose administration (p-value = 0.5130 for the area under the curve when comparing the 12-week-old WT and the 12-week-old KO mice by a two-tailed *t*-test; p-value = 0.1658 for the area under the curve when comparing the 25-week-old WT and the 25-week-old mice KO by a two-tailed *t*-test; n=5).

Next glucose clearance in response to insulin was analysed, but no differences between the WT and KO conditions were observed (Fig. 38).

Taken together, these results indicate that DAPIT does not play a major role in diabetes and glucose metabolism.

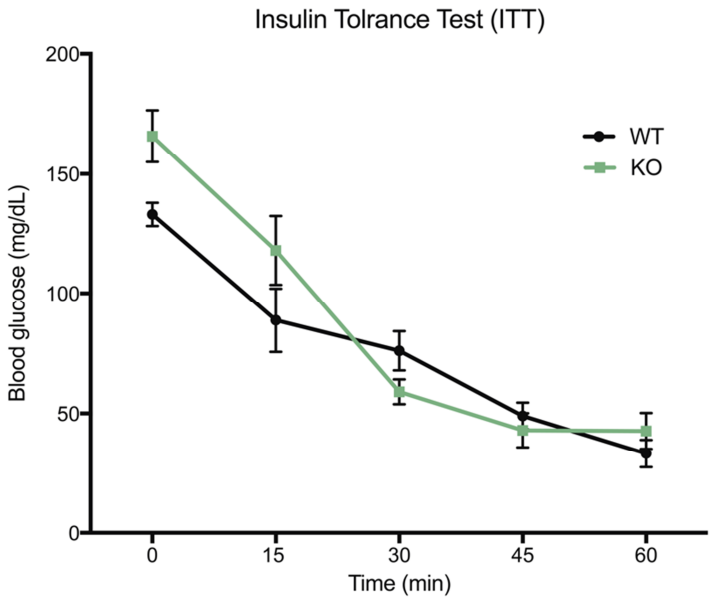

Figure 38. Insulin tolerance test. Blood glucose levels were measured in the 12-week-old WT (black line) and KO (green line) mice in 15-min intervals after insulin administration (n=4 mice, p-value = 0.2056 for the area under the curve by a two-tailed *t*-test). A representative plot of the three experiments is shown.

DAPIT is expressed at very high levels in the heart. To evaluate whether DAPIT affects organ function, an echocardiography was done on both the WT and KO mice (Fig. 39). Diverse parameters were evaluated, such as blood velocity in the mitral valve, and the E/A ratio, which represent the ratio between the top velocity flow in the early diastole and in the late diastole, to evaluate the function of the heart's left ventricle. Ventricle capacity was measured as the left ventricle volume in the diastole, the left ventricle mass or heart rate. Finally, the ejection fraction (EF) and fractional shortening (FS) values were calculated. No differences were observed in these parameters between the WT and DAPIT KO hearts.

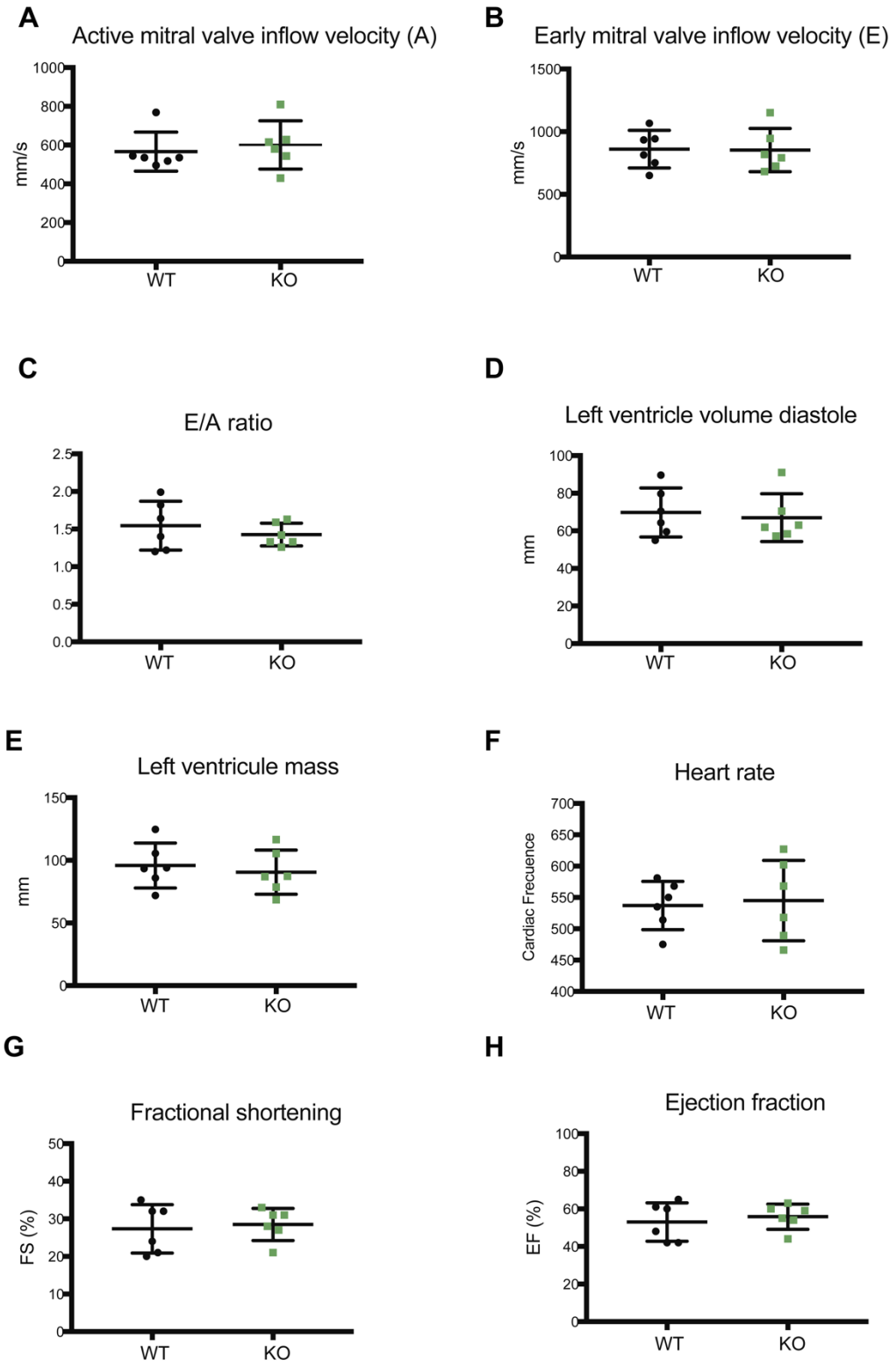

Figure 39. Echocardiography values representation. The echocardiography values of the WT and KO mice are represented. **A**. Late mitral valve velocity (p-value = 0.6050 by a two-tailed *t*-test). **B.** Early mitral valve velocity (p-value = 0.9375 by a two-tailed *t*-test). **C**. E/A ratio to evaluate the left ventricle function (p-value = 0.4377 by a two-tailed *t*-test). **D**. Left ventricle volume in the diastole (p-value = 0.7180 by a two-tailed *t*-test). **E**. Left ventricle mass (p-value = 0.6141 by a two-tailed *t*-test). **F**. Cardiac frequency or heart rate (p-value = 0.8030 by a two-tailed *t*-test). **G**. Fractional shortening value to measure the fraction of diastolic dimension lost in the systole (p-value = 0.7193 by a two-tailed *t*-test). **H**. Ejection fraction value to evaluate the portion of blood ejected from the ventricle with each heartbeat (p-value = 0.5826 by a two-tailed *t*-test) (n= 6 mice per group, each dot represents a different mouse).

In the same echocardiographs, it was possible to detect some insufficiencies. They were divided into mitral insufficiency (when the mitral valve is unable to perfectly close, blood goes backwards from left ventricle), pulmonary insufficiency (the pulmonary valve does not work properly and blood goes back from the pulmonary artery to the right ventricle), tricuspide insufficiency (the tricuspide valve does not work properly and blood returns from the right ventricle to the atrium), and aortic insufficiency (blood goes back from the aorta to the left ventricle when the aortic valve does not close properly).

More types and amounts of valvular insufficiencies were detected in the KO mice compared to the WT mice (Fig. 40) (χ^2 = 7.1106, p-value=0.007665).

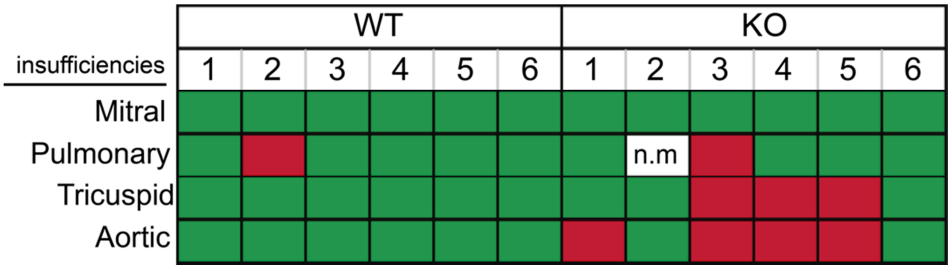

Figure 40. Representation of the number of valve insufficiencies in the WT and DAPIT KO mice. Six mice of each genotype were analysed. Green squares represent absence of insufficiency, and red ones indicate that one insufficiency type was detected (n.m: it was impossible to measure this parameter in this specific mouse). The difference was statistically significant in a chi-square test (χ^2 = 7.1106, p-value=0.007665).

By way of example, aortic insufficiency was seen in the DAPIT KO mouse (Fig. 41). In the WT mouse (Fig. 41A), blood went from the left ventricle to the aorta, which was showed as positive velocity. A different situation was observed in the DAPIT KO mouse (Fig. 41B) as it was possible to distinguish negative velocity in the diastole, which indicates retrograde flux and aortic insufficiency.

A

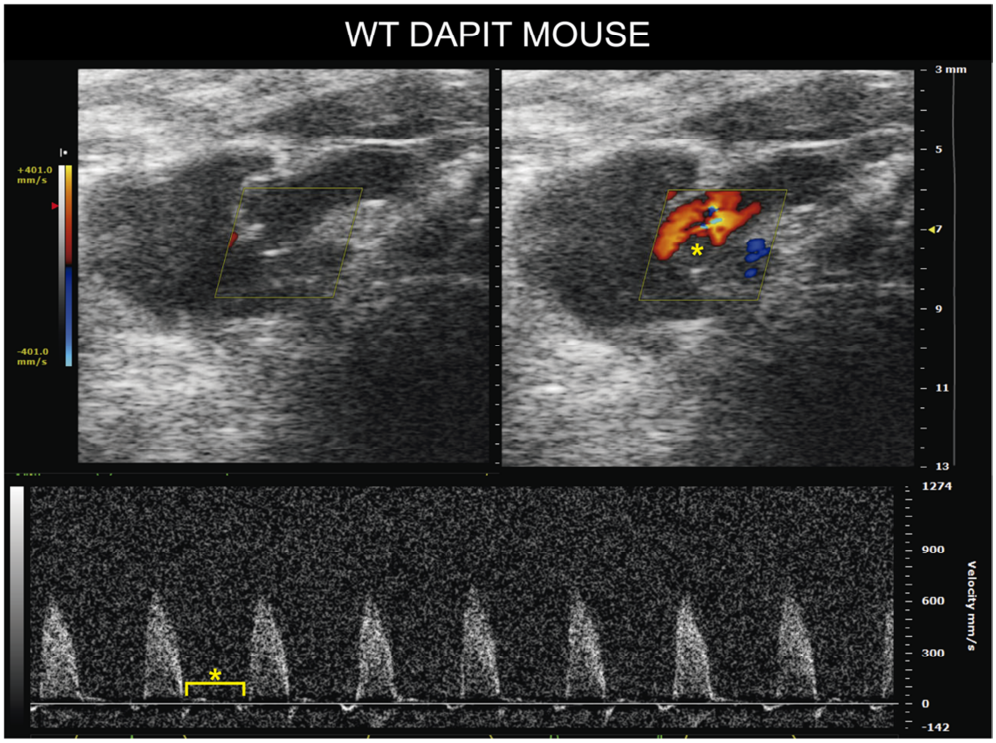

B

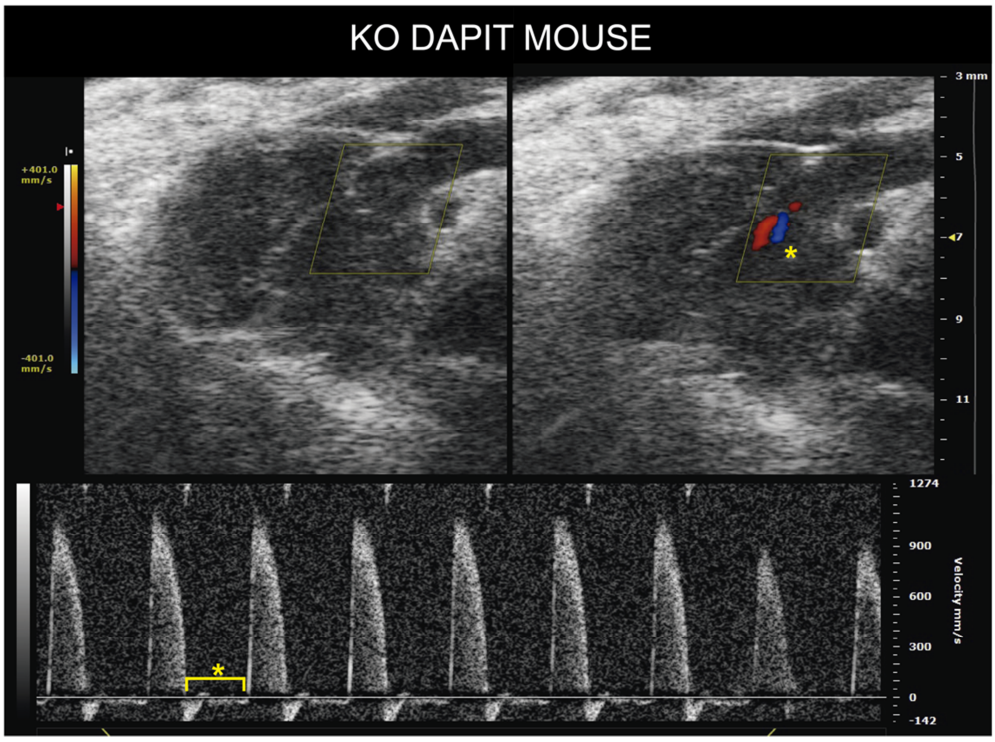

Figure 41. Representative echocardiography image of aortic insufficiency. A. An analysis of blood velocity in a representative WT mouse**. B.** An equal analysis done in the DAPIT KO mouse (a yellow star indicates differences in blood direction and velocity terms).

Other insufficiencies as tricuspid (Fig. 42) and pulmonary insufficiency (Fig. 43) were observed in DAPIT KO mice.

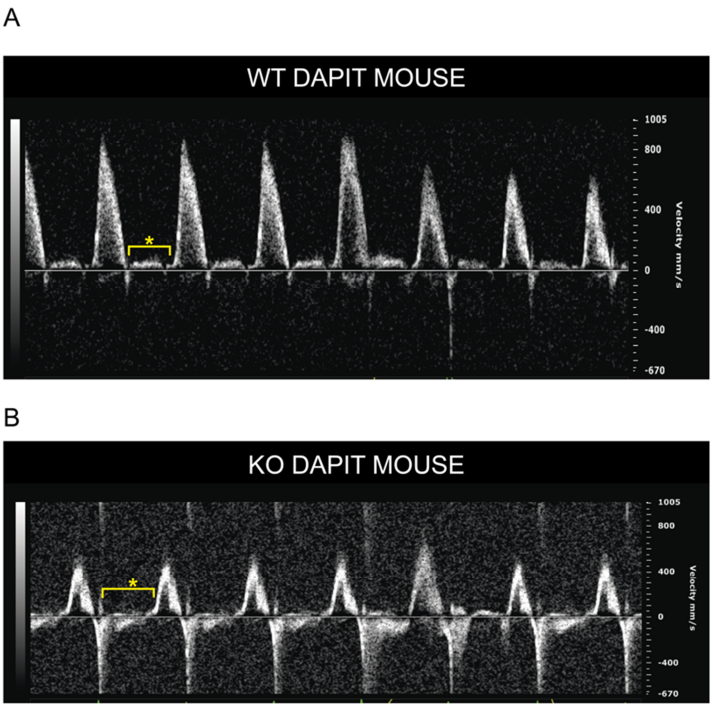

Figure 42. Representative echocardiography image of tricuspid insufficiency. A. An analysis of blood velocity in a representative WT mouse**. B.** An equal analysis done in the DAPIT KO mouse (a yellow star indicates differences in blood direction and velocity terms).

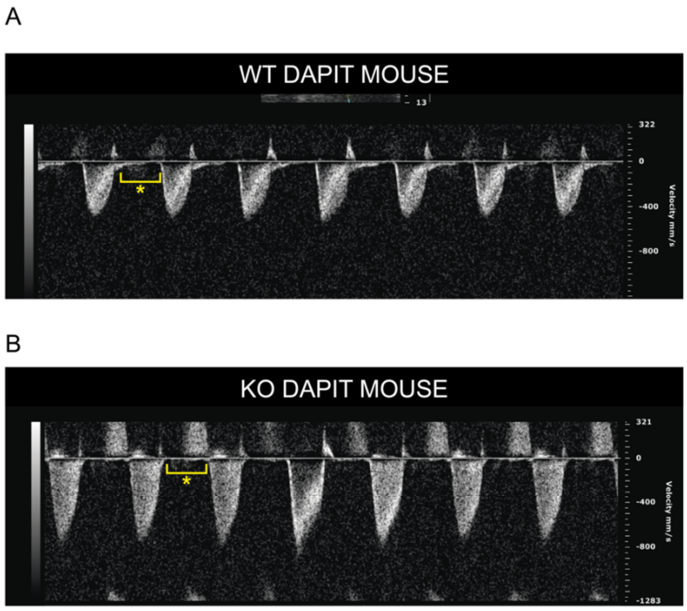

Figure 43. Representative echocardiography image of pulmonary insufficiency. A. An analysis of blood velocity in a representative WT mouse**. B.** An equal analysis done in the DAPIT KO mouse (a yellow star indicates differences in blood direction and velocity terms).

To analyse in more detail the heart functionality, a magnetic resonance imaging (MRI) was performed in WT and DAPIT KO mice. Different parameters were calculated (Fig. 44) showing a weak disffuntion in DAPIT KO hearts, as shown by reduced strock volume (Fig. 44A) and higher volume in the ventricles at the end of the systole (fig. 44C-D). All of these parameters together indicate a worse heart contraction in DAPIT KO compared with WT mice.

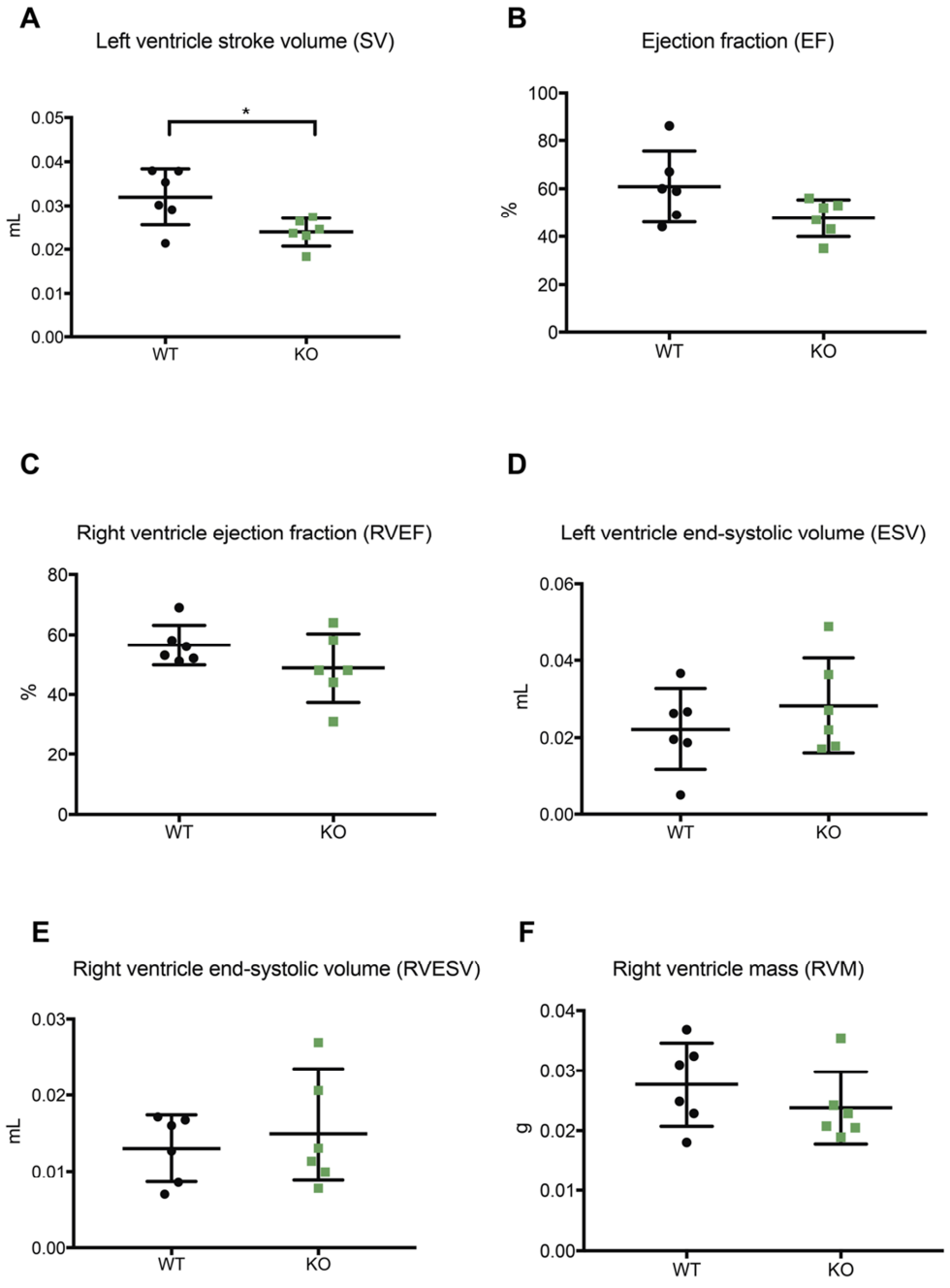

Figure 44. Parameters calculated by analysis of magnetic resonance imaging. A. Left ventricle stroke volume (p-value = 0.0205 by a two-tailed t-test). **B**. Ejection fraction (p-value = 0.0826 by a two-tailed t-test). **C**. Right ventricle ejection fraction (RVEF) (p-value = 0.1869 by a two-tailed t-test). **D**. Left ventricle end-systolic volume (ESV) (p-value = 0.3826 by a two-tailed *t*-test). **E**. Right ventricle nd-systolic volume (RVESV) (p-value = 0.5923 by a two-tailed *t*-test). **F.** Right ventricle mass (RVM) (p-value = 0.3242 by a two-tailed *t*-test).

These results can be visualised representing the volume of both right and left ventricles during a pumping cycle. A lower diastolic volume and a higher systolic volume can be observed in the KO. This supports the previous data showing impaired contraction of the heart in the absence of DAPIT.

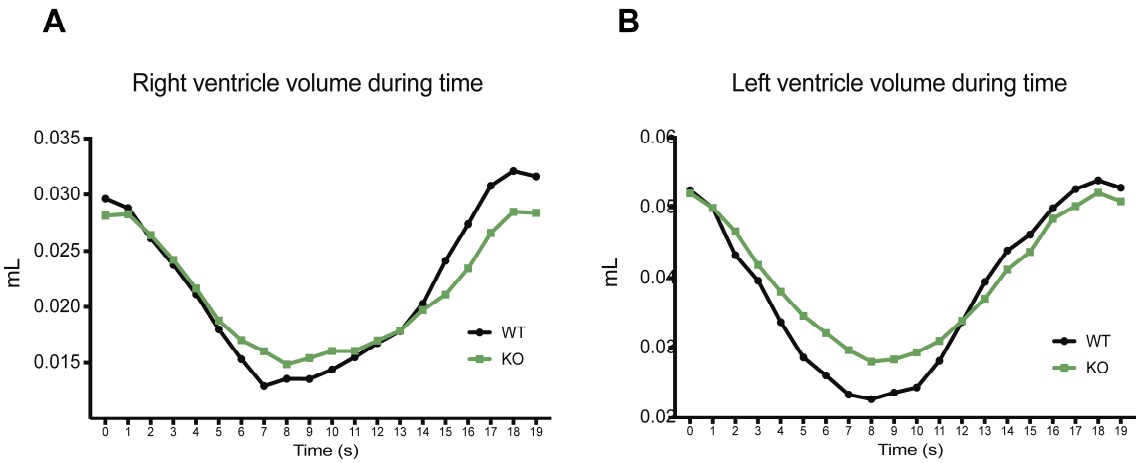

Figure 45. Representation of end-systolic volume in right (A) and left (B) ventricle calculated used magnetic resonance imaging. The graph star to represent the ventricle volumen after systole.

I.7 Characterisation of mitochondria in MP68 knockout.

The MP68 function was studied primarily in heart and liver tissues. To confirm the absence of MP68 in the total KO mice, a mitochondrial protein was analysed under native conditions. An analysis of the KO heart mitochondria using a specific antibody confirmed that MP68 was lacking in the KO mice (Fig. 46).

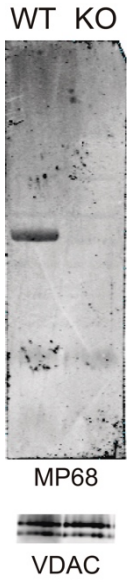

Figure 46. BN to analyse the heart mitochondria. MP68 was not detected in KO heart mitochondria. VDAC protein was used as loading control.

Then the status of mitochondrial complexes I, III and IV was evaluated (Fig. 47), where lack of MP68 did not affect the organisation of these complexes.

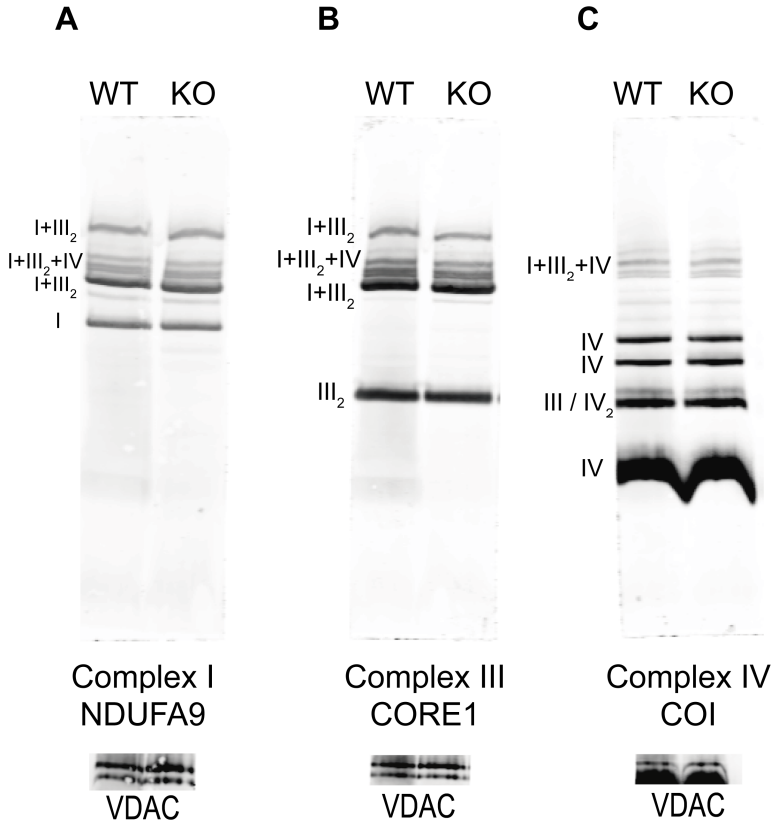

Figure 47. Analysis of the heart mitochondria complexes of the MP68 WT and KO by BN. Different complexes of the digitonised mitochondria were analysed. **A.** The BN of the WT and KO mitochondria analysed with a specific complex I antibody that detects the Ndufa9 subunit. **B.** The BN of the WT and KO mitochondria analysed with a specific antibody of complex IV that recognises subunit CoI. **C.** Analysis of complex III by the UQCRC2 antibody. **D.** Analysis of complex V by the ATPb antibody.

The heart mitochondria from one WT and two different KO mice were analysed (Fig. 48). It can see the band that corresponds to MP68 is present in the WT, but not in the KO mice (Fig. 48A). In the same samples, the change observed in complex V is very interesting. This complex, detected by ATPb, presents a distinctive organisation in the WT and KO mitochondria. Interestly, it was observed that the relation between complex V in the form of monomers and dimers is bigger in KO mitochondria thant in the WT ones (Fig. 48B).

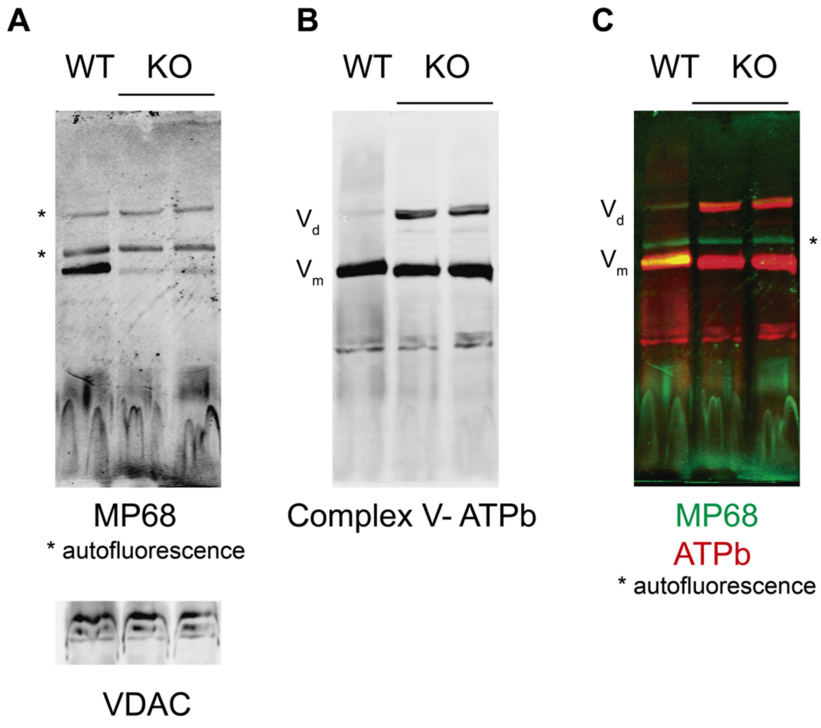

Figure 48. Analysis of the heart mitochondria complexes of the MP68 WT and KO by BN. **A.** The BN of the WT and KO mitochondria analysed with a specific MP68 antibody, and VDAC as the loading control. **B.** The previous membrane incubated with specific antibody ATPb that detects complex V. **C**. Merging of previous antibody signals.

Interestingly, the monomeric form migrated slightly more in MP68 KO (Fig. 48B) samples, as occurs in the DAPIT KO ones.

The liver mitochondria were also analysed (Fig. 49), and the same phenotype was observed with both the absence of MP68 in KO and the differential organisation of complex V.

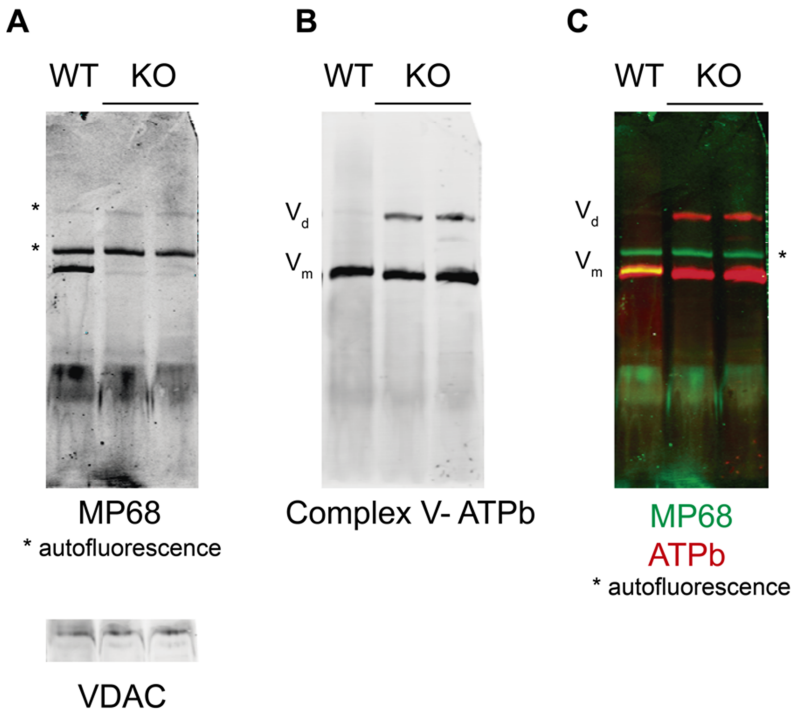

Figure 49. Analysis of the liver mitochondria complexes of the MP68 WT and KO by BN. A. The BN of the WT and KO mitochondria analysed with a specific MP68 antibody, and VDAC as the loading control**. B**. The previous membrane incubated with a specific antibody ATPb that detects complex V. **C**. Merging of previous antibody signals.

The different organisation of ATPase was confirmed by using a specific antibody for another subunit of ATPase, ATPalpha (Fig. 50).

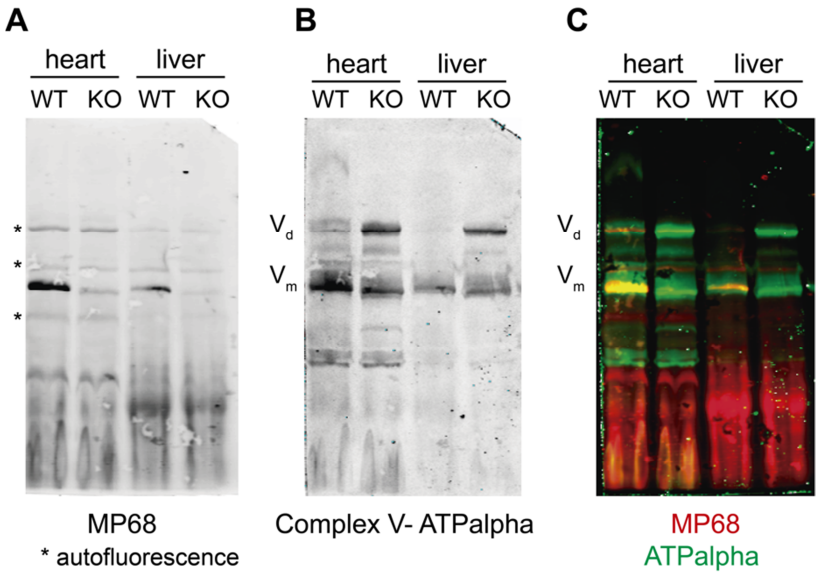

Figure 50. Analysis of the heart and liver mitochondria complexes of the MP68 WT and KO by BN. A. The BN of the WT and KO mitochondria analysed with a specific MP68 antibody. **B.** The previous membrane incubated with a specific antibody ATPalpha that detects complex V. **C.** Merging of previous antibody signals.

Another ATPase subunit, ATP5I, was described as being essential for dimerisation (Arselin *et al.*, 2003). This protein was detected in the monomeric and dimer form os ATPase of both WT and MP68 KO mitochondria (Fig. 51).

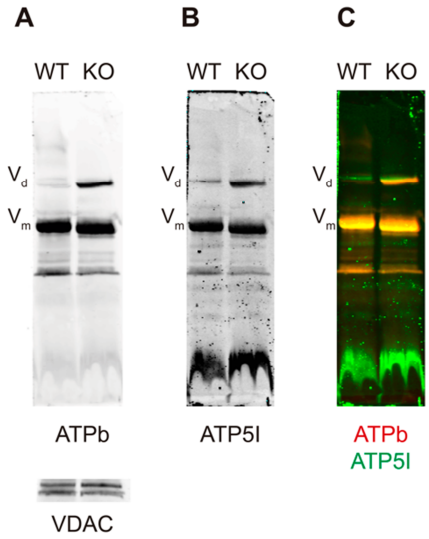

Figure 51. Analysis of the heart mitochondria complexes of the MP68 WT and KO by BN. A. The BN of the WT and KO mitochondria analysed with a specific ATPb antibody, and VDAC as the loading control. **B**. The previous membrane incubated with a specific antibody ATP5I that detects complex V. **C.** Merging of previous antibody signals.

In order to see if the amount of used detergent affected the detection of ATPase organisation, the digitonin/protein ratio was progressively increased, and was visualised by BN gel (Fig. 52). It was possible to confirm the phenotype of the increased amounts of ATPase dimers independently on the amount of detergent.

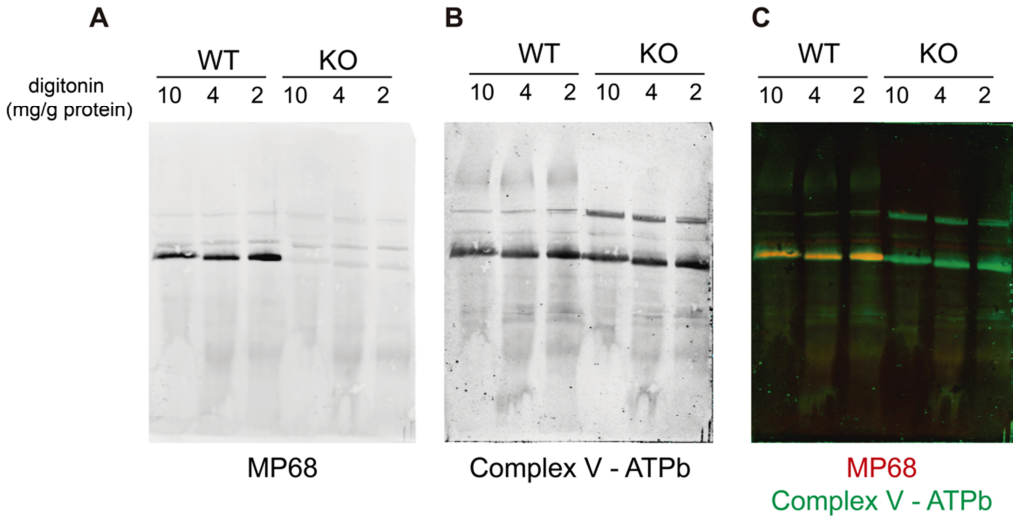

Figure 52. Blue Native analysis of the heart mitochondria solubilised at different digitonine concentrations. A. MP68 was detected in the liver mitochondria. **B.** Complex V was detected by the ATPb antibody. **C.** Merging of both signals.

All these results together confirm that lack of MP68 affects ATPase organisation by promoting its dimerisation.

The relationship between mtDNA codified subunits of ATPase and DAPIT was previously described in this thesis. Now, the link between MP68 and these subunits is studied using also Rho0 cells. In these cells, the particular pattern of ATPase as well as the absence of MP68 in Rho0 cells was observed (Fig. 53). These results indicate that the presence of M68 in the ATPase complex depends on the presence of ATP6 and ATP8.

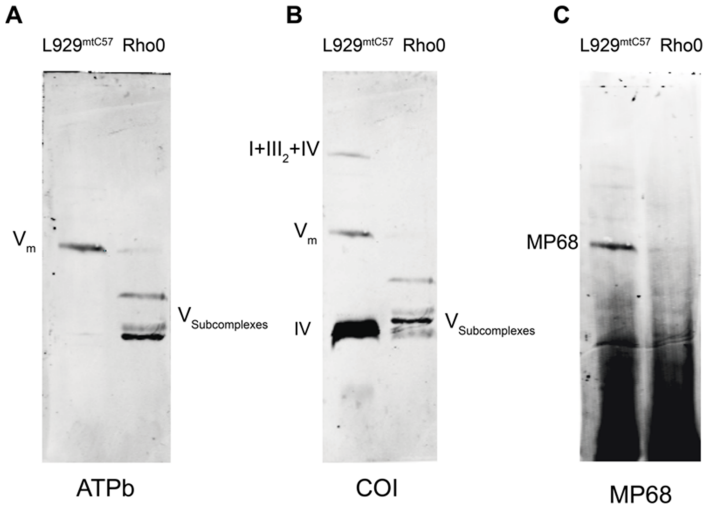

Figure 53. The Rho0 mitochondria analysis by BN gel. A. In Rho0 cells, ATPase complex organisation differs and several subcomplexes appear usin ATPb antibody **.B.** mtDNA encoded suunit detected by using COI antibody. **C**. MP68 is not detected in Rho0 cells, nor associated with the ATPase complex

DAPIT and MP68 have been described to be of a similar small size, to form the IMD domain and to interact with one other. To understand how lack of MP68 could affect the interaction of DAPIT with the rest of ATPase, DAPIT was analysed in the MP68 KO hearts. While MP68 was not detected in the MP68 KO mitochondria, DAPIT was present in both the ATPase monomer and the dimers of the KO and WT mitochondria (Fig. 54). This means that MP68 is not necessary to make DAPIT form part of ATPase.

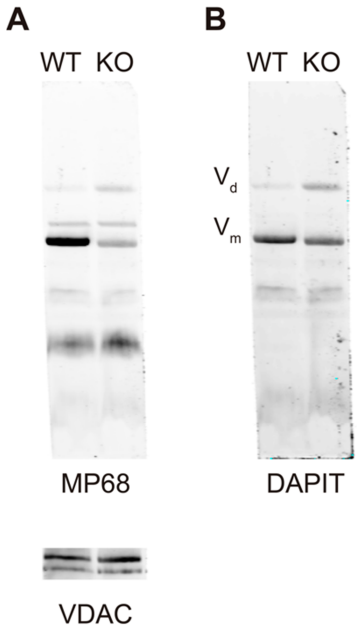

Figure 54. BN to analyse the DAPIT protein in the MP68 KO heart mitochondria. A. MP68 protein detection in the MP68 WT and KO heart mitochondria. **B**. DAPIT detection in MP68 WT and KO heart mitochondria.

To analyse the opposite, if DAPIT is necessary to correctly place of MP68 in ATPase complex, the presence of MP68 was analysed in absence of DAPIT (Fig. 55). In this situation no changes were observed, MP68 was located in ATPase complex even in absence of DAPIT in both heart a liver mitochondria.

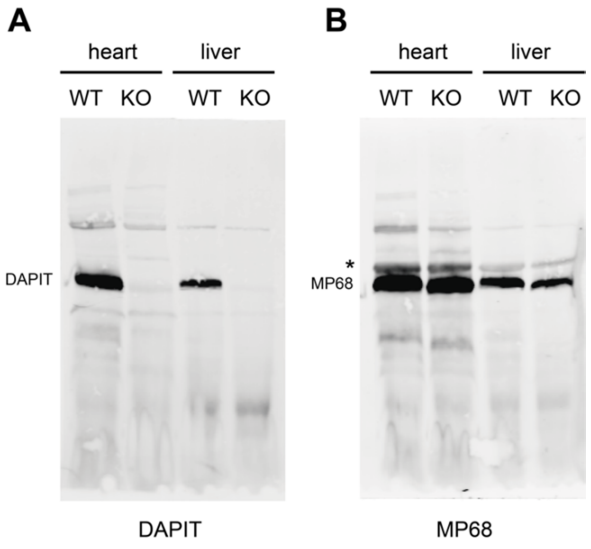

Figure 55. BN to analyse MP68 in the DAPIT KO heart mitochondria. A. DAPIT detection in the DAPIT WT and KO heart mitochondria. **B**. MP68 detection in the the DAPIT WT and KO heart mitochondria (* autofluorescence).

II. DELTARHODOPSIN

II.1 Deltarhodopsin expression in mammalian cells

To target the HtdR protein in the mitochondria of mammalian cells, the HtdR sequence was cloned by adding a mitochondrial target signal (MTS) to the N-terminal domain, based on subunit 8 of complex IV, and an HA-tag to the C-terminal domain (Fig. 56A). Stable HtdR expression was performed by viral infection in the mammalian control cells, L929mtC57. At the total protein level two bands of about 28kDa in weight in HtdR-expressing cells were observed (Fig. 56B). The higher band corresponded to the total protein that was expressed, and the lower band correspond to HtdR without the MTS. This is the first evidence to demonstrate that HtdR is able to enter mitochondria. Next in order to observe the importing efficiency to mitochondria, the proportion of HtdR in both the cytoplasm and mitochondria was checked. Although the cytosol contained a portion of HtdR (Fig. 56C), the largest amount of the HtdR protein was located in mitochondria.

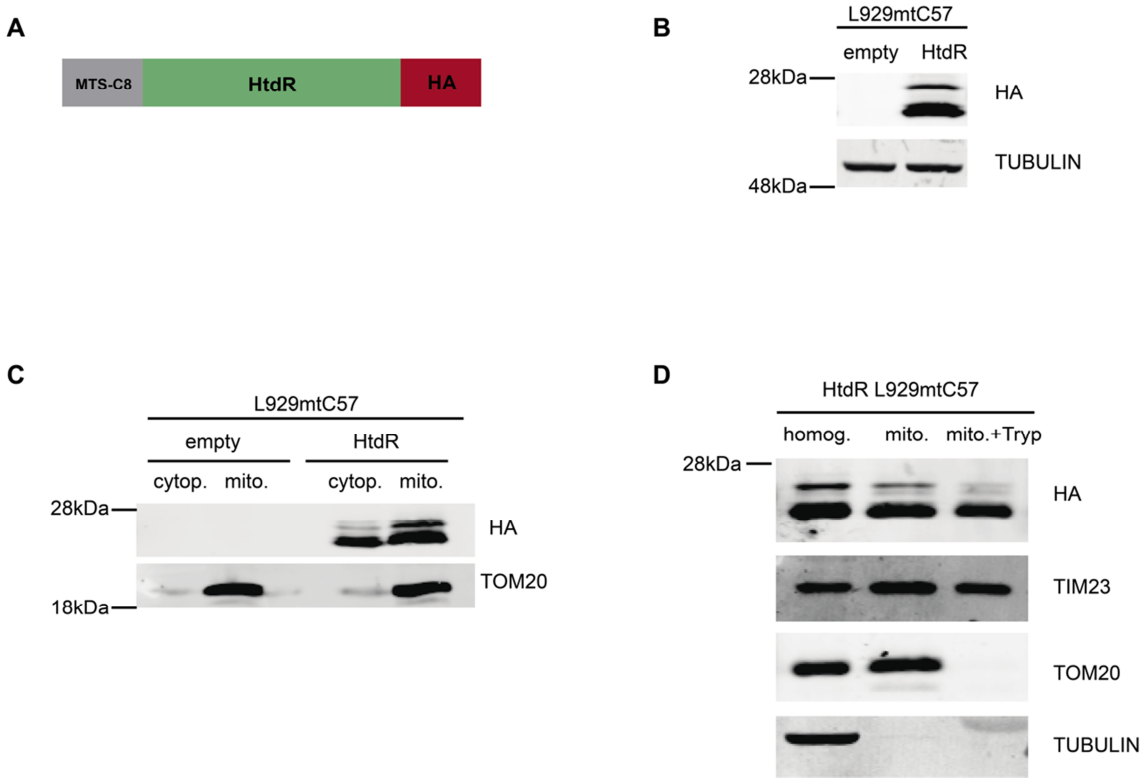

Figure 56. Deltarhodopsin (HtdR) expression in mammalian cells. A. Scheme of the HtdR construct, including MTS-C8 as the mitochondrial target signal (MTS), and HA tag. **B.** Immunodetection with the HA and tubulin antibodies of the total protein from the empty and HtdR-expressing cells. **C.** Immunodetection with the HA and Tom20 antibodies of the cytoplasm and mitochondria protein from the empty and HtdR-expressing cells. **D.** Immunodetection of mitochondrial proteins of the HtdR-expressing cells after treatment with trypsin with the HA, Tom20 and Tim23 antibodies.

To be functional, HtdR has to reach the inner mitochondrial membrane and be inserted into the right orientation. There the H+ gradient is generated and converted into chemical energy by ATP synthase. To test HtdR submitochondrial localisation, a protection assay was run. Following trypsin treatment, only IMM proteins Tim23 and HtdR remained undigested, while OMM protein Tom20 was digested. (Fig. 56D). This demonstrates that HtdR is targeted to the IMM, where it should be located to generate a proton gradient.

Next HtdR location was checked by immunofluorescence (Fig. 57). We observed partial co-localisation with the CoI mitochondrial protein. This effect was due to the higher expression levels of the protein and its accumulation in the ER.

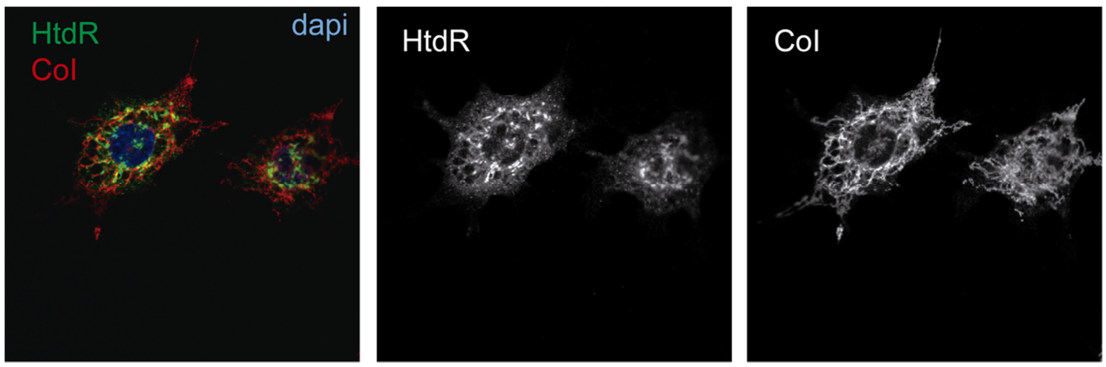

Figure 57. Immunofluoresce of the HtdR-expressing cells. Detection of HtdR with the HA antibody and mitochondria morphology with the CoI antibody.

In order to improve mitochondrial expression, new proteins with different MTS were synthesised, including those from subunit 8 of cytochrome c oxidase (C8) and subunit 9 of ATPase (M9), and with sequence Kir2.1, an ER exporting signal (Fig. 58A).

From the analysis of the total protein from the cells that expressed the different constructs, it was concluded that HtdR expression existed in all cases. Comparisong of the size of the different constructs, confirmed that the small band corresponded to HtdR after the MTS was removed, while the bigger band corresponded to HtdR with the MTS (Fig. 58B). The removal of the MTS further supports the notion that most HtdR is targeted to mitochondria. The C8-HtdR construct displayed the best performance in terms of expression level and efficiency of import judging by the cleavage of the MTS. It was, therefore, chosen for the following studies.

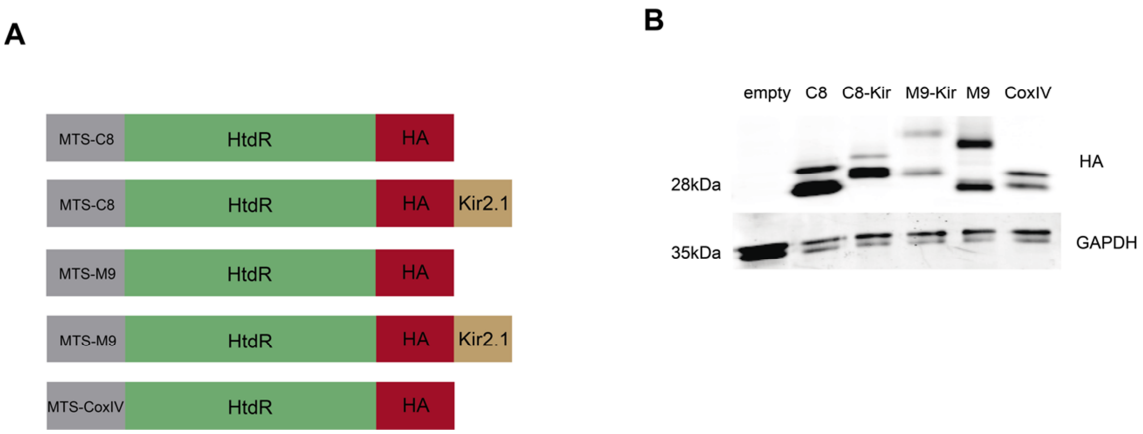

Figure 58. Deltarhodopsin with different mitochondrial target signals. A. Scheme of the HtdR construct with different mitochondrial target signals. B. Immunodetection of HtdR with different sequences that act as the MTS with the HA antibody.

II.2 Cell growth without functional OXPHOS

To test the functionality and efficiency of HtdR, cell growth under conditions that force them to rely on mitochondrial ATP production rather than on glycolysis was tested by using different carbon sources and inhibitors.

Unlike glucose, galactose does not allow cells to generate sufficient ATP by glycolysis to survive. However, it provides enough energy if generated by the ETC. Under these conditions, the ETC is the main source of energy (Bayona-Bafaluy, Fernández-Silva and Enríquez, 2002). In order to block the ETC, we used antimycin A (Aa), an inhibitor of complex III. Thus in galactose with Aa, cells cannot use glycolysis or ETC to produce ATP and cells die.

Growth of control and HtdR-expressing cells was evaluated in glucose-enriched medium that contained Aa for 5 days either in the dark or light. As expected, both the control (Fig. 59A) and HtdR-expressing cells (Fig. 59B) grew normally because they generated enough energy by glycolysis. Neither HtdR nor the used lighting conditions had any apparent toxic effect.

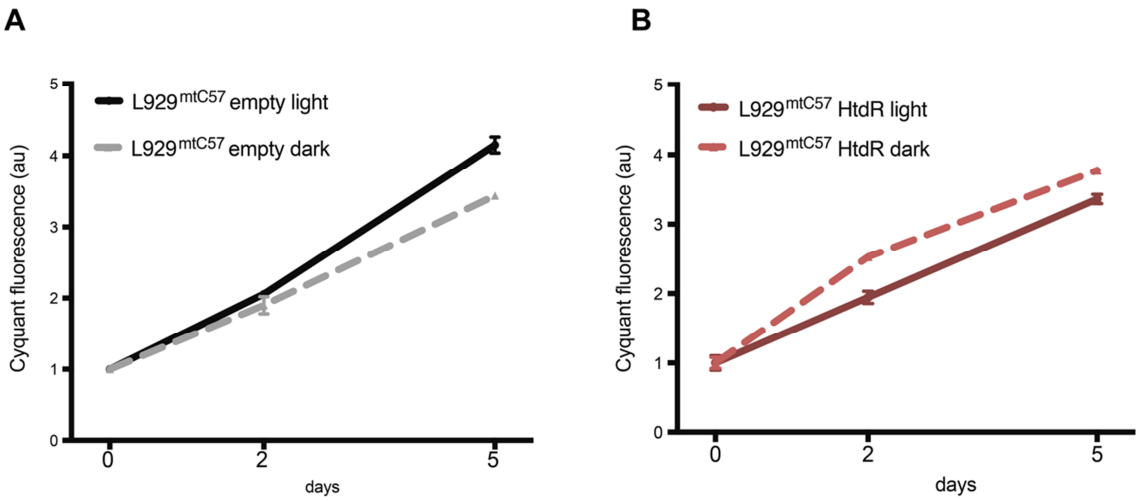

Figure 59. Growth curve of the cells in the glucose-enriched medium. A. Growth curve of empty vector expressing cells in glucose medium in the presence (black continuous line) and absence of light (grey discontinuous line). B. Growth curve of the HtdR cells in glucose medium in the presence (red continuous line) and absence of light (red discontinuous line).

When cells were shifted to galactose, the control cells were unable to survive in the presence of Aa either in the dark or light (Fig. 60A). On the contrary, the cells that expressed the HtdR protein survived in galactose plus Aa, but only if they were illuminated (Fig. 60B). This indicates that under light conditions HtDR generates sufficient p.m.f. to allow ATP synthesis by mitochondrial ATPase because, in this way, it rescues cells from death (Fig. 59B). The possibility that HtdR itself promotes cell survival by a different mechanism was ruled out by the fact that cells died in the absence of light. These results demonstrate for the first time that mammalian cells can convert light energy into electrochemical energy, which is used later by ATPase to produce ATP that can support cell growth.

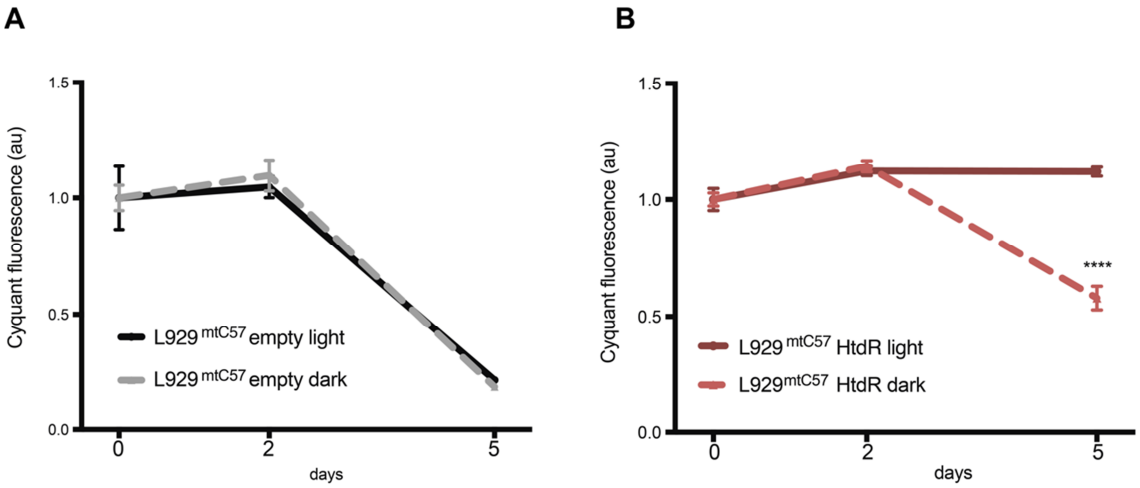

Figure 60. Growth curve of the cells in the galactose-enriched medium. A. Growth curve of the control cells in galactose medium in the presence (black continuous line) and absence of light (grey discontinuous line). **B.** Growth curve of the HtdR cells in galactose medium in the presence (red continuous line) and absence of light (red discontinuous line) (in the last point: **** p-value < 0.0001 by a two-tailed *t*-test).

This cellular tool, in combination with the previously developed cell lines that express genes AOX and/or NDL1, will allow us to split the different function of the OXPHOS system into mammalian cells and to contribute to physiopathology.

Discussion

I. ASSOCIATED PROTEINS WITH ATP SYNTHASE

ATPase conformation is important for determining mitochondrial morphology and cristae formation. For the first time, we report that DAPIT is necessary for dimer formation. In the absence of the DAPIT protein, the capacity to form dimers disappears. The lack of DAPIT does not affect to the lost of other ATPase subunits, indicating that our model is a very usefull tool to anlayse specifically how affects the lost of the ATPase dimers to the cell. Moreover, DAPIT KO ATPase has the same capacity to produce ATP as the WT mitochondria, but without the presence of dimers. This indicates that ATPase function is independly of it dimeric conformation.

ATPase dimers have been proposed to form the mPTP (Giorgio *et al.*, 2013). Because the lack of DAPIT is a specific way to analyse the ATPase dimeres funtion, we presently report that the absence of these dimers does not alter mPTP properties according to mitochondrial swelling measurements. The capacity of mPTP opening following calcium induction remained even in the mitochondrial DAPIT KO. In the future, these results could be verified by more specific experiments, including calcium retention capacity measurements to calculate the calcium amount threshold that triggers mPTP opening.

Interestingly, the ATPase monomers migrate differently under native conditions between WT and DAPIT KO mitochondria. Migration was higher in KO mitochondria than in WT one, indicating a small size or different conformation of ATPase monomer that alters the velocity of migration.

Apart from the absence of ATPase dimers in the DAPIT KO mitochondria, a new subcomplex was detected. We describe this complex as an association of subunits α, β, and γ_1 from F_1, and subunits c from F_O. We defined the identity of this subcomplex based on its size, and also by the presence or absence of different subunits tested by Western blot, which indicates that the alpha and beta subunits are contained in it, but with no e subunit. Interestingly, a similar complex was described in the Rho0 cells. In these cells, without mtDNA, ATPase is unable to form dimers, but is found in a monomeric form and also in other subcomplexes (Nijtmans *et al.*, 1995). One of them, called V*, has a similar weight as the subcomplex detected in the DAPIT KO mitochondria. Proteomic assays would be the best way to fully characterise the identity of this complex. Analysing its protein composition would be the determinant result to ensure how the subcomplex is generated through lack of DAPIT.

DAPIT was not detected in the proteomic analysis of ATPase from the Rho0 cells. This result was explained as a technical limitation (Wittig *et al.*, 2010). Nonetheless, we did not detect DAPIT when using the specific antibody, which could indicate that it is very likely to be absent in the ATPase of these cells. Lack of mtDNA that encodes subunits A6L and ATP8 plays a role as it affects the association of DAPIT with the rest of the ATPase. Interestingly, immunoprecipitation was carried out and demonstrated that the ATPase complex from the DAPIT KO mitochondria presented all its subunits, except DAPIT itself. This evidence led to affirm that the phenotype of absence of dimers observed in Rho0 cells could be caused by the absence of DAPIT. This reveals that DAPIT could be one of the last proteins to link to the ATPase complex, and that its association to ATPase depends on the presence of other subunits. This perfectly matches the fact that DAPIT is absolutely necessary for ATPase dimer formation.

The following model was proposed by considering all these results together (Fig. 61). In the presence of the DAPIT protein, ATPase is found in dimer association (Fig. 61A). However, this link is not possible when DAPIT is absent, and ATPase is found in a monomer form (Fig. 61B) and in addition, the monomeric ATPase is disestablished and generates a subcomplex (Fig. 61C).

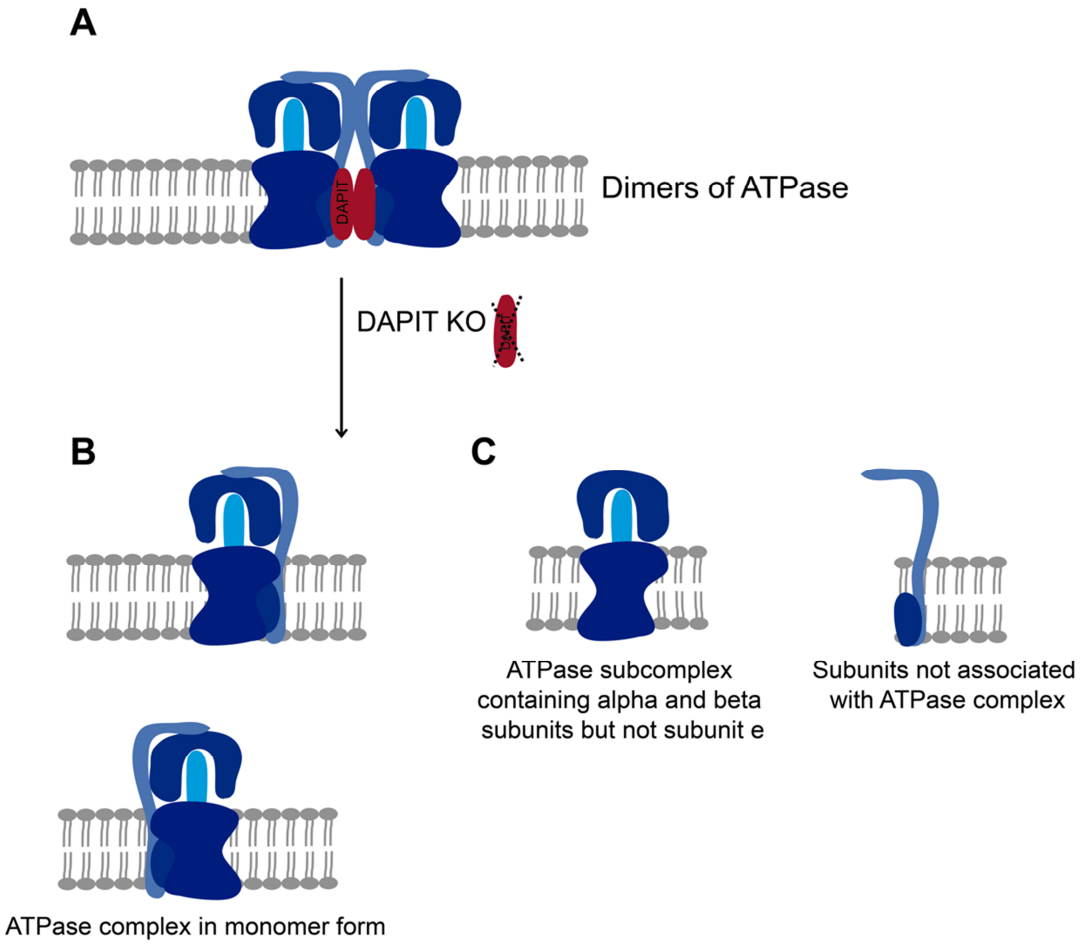

Figure 61. Schematic model showing the consequences of lack of the DAPIT protein. A. ATPase dimers are formed in the presence of DAPIT. **B.** ATPase, in a monomer form, results from lack of DAPIT. **C**. The ATPase subcomplex forms in the absence of DAPIT that contains alpha and beta subunits, but not subunit e.

Recently, a new domain in ATPase has been described, the intermembrane space domain (IMD). The IMD may, or may not, be associated with the rest of ATPase, which determines two compositional states for IMD (Fischer *et al.*, 2017). These two states do not affect the 43º curvature of the IMM determined by ATPase. It has been suggested that the IMD is formed only by DAPIT and MP68. This indicates that DAPIT and MP68 could be essential for determining the ATPase state by acting either together or individually. Furthermore, the absence of these proteins would not affect the inner mitochondrial morphology.

Our results in an *in vivo* model were surprising if we consider previously published results in cells (Ohsakaya *et al.*, 2011; Kontro *et al.*, 2015). It has been reported that low DAPIT levels in cells affects the amount of ATPase in mitochondria. However, this was not the case in the DAPIT KO mice.

DAPIT signifies “diabetes-associated protein in insulin-sensitive tissues” and a role in glucose metabolism has been proposed. The generation of the DAPIT KO mouse colony was valuable to study the role of the DAPIT protein in diabetes, as previously described. DAPIT KO mice were submitted to a glucose tolerance test experiment, in which they did not show any defect in terms of clearing glucose from blood. Moreover, they responded in the same way as the WT mice responded to insulin administration. Taken together, these results suggest that lack of DAPIT does not affect glucose metabolism in the studied contexts. It would be interesting to induce diabetes in DAPIT KO mice, follow its evolution and determine through experimentation whether the DAPIT protein is required for adaptation in these circumstances.

In this thesis, several deficiencies in the cardiac function of DAPIT KO mice were found. A blood return was observed in the valves: pulmonary, aortic, tricuspide or mitral, with more frequency in DAPIT KO than in WT mice. Moreover, MRI revealed a ventricle stroke volume increased in the DAPIT KO hearts that generates impaired contraction of the heart in the DAPIT KO mice. Lack of the DAPIT protein somehow affects heart functionality, but how DAPIT affects this function is still unknown. In line with this, recently, it was published that the lack of DAPIT in zebrafish was associated with the development of dilated cardiomyopathy since the fishes with reduced DAPIT levels develop larger pericardial sac and atrial areas and reduced ventricular fractional shortening than the WT fishes (Nagata *et al.*, 2017). The relationship between DAPIT and cardiac defects was also suggested by a mouse model of congenital myopathy. This cardiomyopathy was caused by the lack of *Klhl31,* a skeletal muscle specific gene, and it was found that *Dapit* gene is one the most upregulated genes (Papizan *et al.*, 2017). Similarly, but in skeletal muscle, DAPIT was observed as the protein that increased most its levels in a pig model of Duchenne muscular dystrophy (Fröhlich *et al.*, 2016).

The DAPIT KO mice are perfectly viable and fertile. These mice are able to live without ATPase dimers, which indicates that ATPase complex organisation is not essential for life. However, it could be relevant in other contexts not explored herein, such as exercise conditions or ageing. Moreover, the DAPIT protein is conserved in metazoan during evolution, which well indicates its relevant role. These suggest that other DAPIT functions remain hidden whose exploration is pending.

Considering the other subunit that forms the IMD, MP68, a mouse model to study the function of this protein was developed. Using this model, a key role in dimer formation regulation was demonstrated. The absence of MP68 promotes the dimerisation of ATPase in both the heart and liver mitochondria.

Moreover, the migration pattern of ATPase under native conditions was also different when comparing the MP68 WT and KO mitochondria. This fact could be explained by not only lack of MP68, but also by the change in ATPase complex morphology that occurred when MP68 was not present in ATPase.

As both proteins form the IMD, and given the faster migration pattern of monomeric ATPase in both mouse models, our results suggest that changes in IMD composition could alter ATPase conformation.

The lack of MP68 does not affect to the localisation of DAPIT in the ATPase complex. Interestingly the opposite was also true; in DAPIT KO mitochondria, MP68 remains in ATPase complex when DAPIT is absent. This fact indicates that our mouse models are very specific and this allows to study the lack of only one of these proteins.

Although both proteins form part of the IMD, the absence of each one leads to an opposite phenotype regarding ATPase dimerisation (Fig. 62). A structural analysis in both mutants could clarify how the absence of these proteins affects the ATPase structure and its dimerisation.

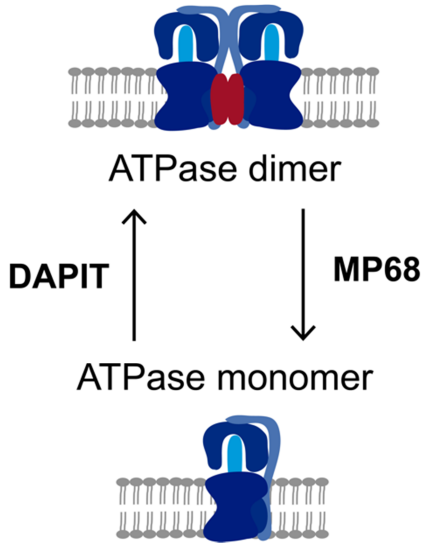

Figure 62. Schematic representation of the role of DAPIT and MP68 in ATP synthase dimerisation.

II. DELTARHODOPSINE

In this work, we demonstrated that light can be used by mammalian cells to obtain energy. This was achieved by the expression of the H^+ proton-pumping protein HtdR in the IMM. This protein uses the energy of photons to translocate protons to the intermembrane space, which is used by ATPase to produce ATP from ADP in the absence of functional glycolysis and the ETC (Fig. 63). This is a proof of concept that mammalian cells can use light as a source of energy.

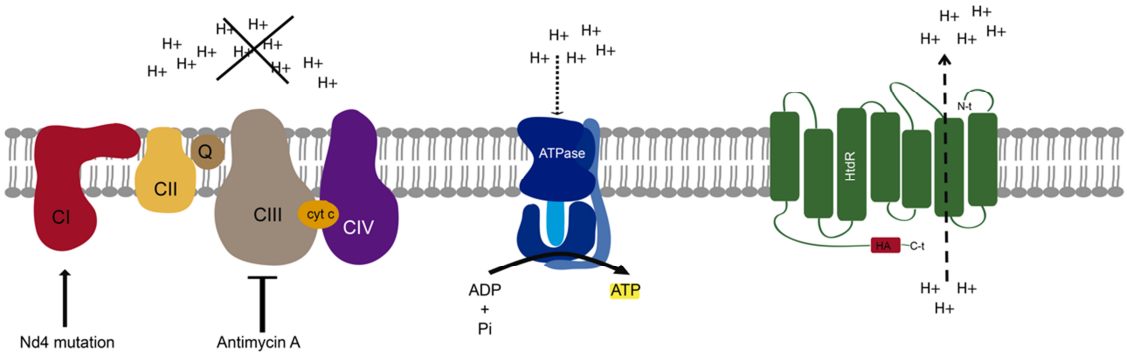

Figure 63. Working model that describes the effect of HtdR expression on mammalian cells under electron transport chain (ETC) dysfunction. ETC inhibition, due to an antimycin effect, is unable to pump protein to the mitochondrial IS. The HtdR is able to restore the proton gradient, which can be used by ATP synthase to produce ATP.

This is also a very interesting tool to characterise ETC deficiencies. There are some mitochondrial mutations in which it is unclear whether the phenotype is caused by lack of energy or by other secondary mutation effects (Kirches, 2011). This tool could be used in the future to determine the mechanisms of these diseases.

The use of cell-based robots that can be controlled by the use of light has been recently reported (Park *et al.*, 2016). However, this device needs glucose media as a source of energy. The possibility of combining this robot with HtdR herein reported could increase the independency of these devices by enabling them to obtain their own energy.

There is increasing evidence that metabolism is not only the way cells obtain energy, but can also play a role in cell specification and cellular differentiation (Chung *et al.*, 2007, 2010; Tormos *et al.*, 2011). Using this tool to manipulate the energy status of the cell can provide new insights into the role of metabolism.

In conclusion, this work represents the proof of concept that mammalian cells can use light energy to grow, and a powerful tool to manipulate metabolism.

Conclusions

1. Absence of DAPIT does not affect the viability of mice

2. DAPIT determines dimerisation of the ATPase complex and lack of DAPIT does not allow the formation of ATPase dimers

3. Absence of DAPIT generates an ATPase subcomplex that probably contains the subunits α, β, and γ_1 from F_1, and the c subunits from F_O

4. The ATPase complex phenotype observed in Rho0 cells could be caused by lack of the DAPIT protein in these cells

5. DAPIT deficit does not affect mPTP opening

6. ATPase dimers are not the mPTP

7. DAPIT deficiency in mice does not affect glucose metabolism

8. Lack of MP68 promotes ATPase dimer formation

9. HtdR-expressing cells can use light energy to grow

Conclusiones

1. La ausencia de DAPIT asociado a la ATPasa no afecta a la viabilidad del ratón.

2. DAPIT determina la dimerización del complejo ATPasa y su ausencia no permite la formación de dímeros de ATPasa.

3. La ausencia de DAPIT genera subcomplejos de ATPasa formados probablemente por las subunidades α, β, y γ_1 del dominio F_1, y las subunidades c del dominio F_O.

4. El fenotipo de organización del complejo ATPasa observado en células Rho0 puede deberse a la ausencia de DAPIT en dichas células.

5. La falta de DAPIT en la célula no afecta a la apertura del mPTP

6. Los dímeros de ATPasa no forman el mPTP.

7. La ausencia de DAPIT en ratones no afecta al metabolismo de la glucosa.

8. La ausencia de MP68 promueve la formación de dímeros de ATPasa.

9. Las células que expresan HtdR son capaces de usar la luz para crecer.

Bibliography

Abrahams, J. P., Leslie, A. G. W., Lutter, R. and Walker, J. E. (1994) 'Structure at 2.8 Â resolution of F1-ATPase from bovine heart mitochondria', *Nature*. Nature Publishing Group, 370(6491), pp. 621–628.

Acín-Pérez, R., Fernández-Silva, P., Peleato, M. L., Pérez-Martos, A. and Enriquez, J. A. (2008) 'Respiratory Active Mitochondrial Supercomplexes', *Molecular Cell*, 32(4), pp. 529–539.

Alavian, K. N., Beutner, G., Lazrove, E., Sacchetti, S., Park, H.-A., Licznerski, P., Li, H., Nabili, P., Hockensmith, K., Graham, M., Porter, G. A. and Jonas, E. A. (2014) 'An uncoupling channel within the c-subunit ring of the F1FO ATP synthase is the mitochondrial permeability transition pore.', *Proceedings of the National Academy of Sciences of the United States of America*.

Alexander, C., Votruba, M., Pesch, U. E. A., Thiselton, D. L., Mayer, S., Moore, A., Rodriguez, M., Kellner, U., Leo-Kottler, B., Auburger, G., Bhattacharya, S. S. and Wissinger, B. (2000) 'OPA1, encoding a dynamin-related GTPase, is mutated in autosomal dominant optic atrophy linked to chromosome 3q28', *Nature Genetics*, 26(2), pp. 211–215.

Allen, R. D., Schroeder, C. C. and Fok, A. K. (1989) 'An Investigation of Mitochondrial Inner Membranes by Rapid-Freeze Deep-Etch Techniques', *The Journal of Cell Biology*, 108, pp. 2233–2240.

Arnold, I., Pfeiffer, K., Neupert, W., Stuart, R. A. and Schägger, H. (1998) 'Yeast mitochondrial F1F0-ATP synthase exists as a dimer: Identification of three dimer-specific subunits', *EMBO Journal*, 17(24), pp. 7170–7178.

Arselin, G., Giraud, M.-F., Dautant, A., Vaillier, J., Brethes, D., Coulary-Salin, B., Schaeffer, J. and Velours, J. (2003) 'The GxxxG motif of the transmembrane domain of subunit e is involved in the dimerization/oligomerization of the yeast ATP synthase complex in the mitochondrial membrane', *European Journal of Biochemistry*, 270(8), pp. 1875–1884.

Azzolin, L., von Stockum, S., Basso, E., Petronilli, V., Forte, M. A. and Bernardi, P. (2010) 'The mitochondrial permeability transition from yeast to mammals', *FEBS Letters*. Federation of European Biochemical Societies, 584(12), pp. 2504–2509.

Baughman, J. M., Nilsson, R., Gohil, V. M., Arlow, D. H., Gauhar, Z. and Mootha, V. K. (2009) 'A computational screen for regulators of oxidative phosphorylation implicates SLIRP in mitochondrial RNA homeostasis.', *PLoS genetics*. Public Library of Science, 5(8), p. e1000590.

Bayona-Bafaluy, M. P., Fernández-Silva, P. and Enríquez, J. A. (2002) 'The thankless task of playing genetics with mammalian mitochondrial DNA: A 30-year review', *Mitochondrion*, 2(1–2), pp. 3–25.

Beutner, G., Eliseev, R. A. and Porter, G. A. (2014) 'Initiation of Electron Transport Chain Activity in the Embryonic Heart Coincides with the Activation of Mitochondrial Complex 1 and the Formation of Supercomplexes', *PLoS ONE*.

Bezawork-Geleta, A., Rohlena, J., Dong, L., Pacak, K. and Neuzil, J. (2017) 'Mitochondrial

Complex II: At the Crossroads', *Trends in Biochemical Sciences*, pp. 312–325.

Boekema, E. J. and Braun, H.-P. (2007) 'Supramolecular structure of the mitochondrial oxidative phosphorylation system', *The Journal of biological chemistry*, 282(1), pp. 1–4.

Bradford, M. M. (1976) 'A rapid and sensitive method for the quantitation of microgram quantities of protein utilizing the principle of protein-dye binding', *Analytical Biochemistry*, 72(1–2), pp. 248–254.

Carew, J. S. and Huang, P. (2002) 'Mitochondrial defects in cancer.', *Molecular cancer*, 1, p. 9.

Carroll, J., Fearnley, I. M. and Walker, J. E. (2006) 'Definition of the mitochondrial proteome by measurement of molecular masses of membrane proteins.', *Proceedings of the National Academy of Sciences of the United States of America*.

Chen, R., Runswick, M. J., Carroll, J., Fearnley, I. M. and Walker, J. E. (2007) 'Association of two proteolipids of unknown function with ATP synthase from bovine heart mitochondria', *FEBS Letters*, 581(17), pp. 3145–3148.

Chen, Y.-C., Taylor, E. B., Dephoure, N., Heo, J.-M., Tonhato, A., Papandreou, I., Nath, N., Denko, N. C., Gygi, S. P. and Rutter, J. (2012) 'Identification of a Protein Mediating Respiratory Supercomplex Stability', *Cell Metabolism*, 15, pp. 348–360.

Chicco, A. J. and Sparagna, G. C. (2007) 'Role of cardiolipin alterations in mitochondrial dysfunction and disease.', *Am. J. Physiol., Cell Physiol.*, 292(1), pp. C33-44.

Chinopoulos, C. (2017) 'ATP synthase complex and the mitochondrial permeability transition pore: poles of attraction', *EMBO reports*, 18(7), pp. 1041–1042.

Chung, S., Arrell, D. K., Faustino, R. S., Terzic, A. and Dzeja, P. P. (2010) 'Glycolytic network restructuring integral to the energetics of embryonic stem cell cardiac differentiation', *Journal of Molecular and Cellular Cardiology*, 48(4), pp. 725–734.

Chung, S., Dzeja, P. P., Faustino, R. S., Perez-Terzic, C., Behfar, A. and Terzic, A. (2007) 'Mitochondrial oxidative metabolism is required for the cardiac differentiation of stem cells', *Nature Clinical Practice Cardiovascular Medicine*. Nature Publishing Group, 4, pp. S60–S67.

Cogliati, S., Calvo, E., Loureiro, M., Guaras, A. M., Nieto-Arellano, R., Garcia-Poyatos, C., Ezkurdia, I., Mercader, N., Vázquez, J. and Enriquez, J. A. (2016) 'Mechanism of super-assembly of respiratory complexes III and IV.', *Nature*. Nature Publishing Group, 539(7630), pp. 579–582.

Cogliati, S., Enriquez, J. A. and Scorrano, L. (2016) 'Mitochondrial Cristae: Where Beauty Meets Functionality', *Trends in Biochemical Sciences*, 41(3), pp. 261–273.

Cogliati, S., Frezza, C., Soriano, M. E., Varanita, T., Quintana-Cabrera, R., Corrado, M., Cipolat, S., Costa, V., Casarin, A., Gomes, L. C., Perales-Clemente, E., Salviati, L., Fernandez-Silva, P., Enriquez, J. A. and Scorrano, L. (2013) 'Mitochondrial cristae shape determines respiratory chain supercomplexes assembly and respiratory efficiency', *Cell*, 155(1), pp. 160–171.

Collinson, I. R., Runs, M. J., Buchanan, S. K., Fearnley, I. M., Skehel, J. M., Van Raaij, M. J.,

Griffiths, D. E. and Walker, J. E. (1994) 'F0 Membrane Domain of ATP Synthase from Bovine Heart Mitochondria: Purification, Subunit Composition, and Reconstitution with Fi-ATPase1', *Biochemistry*, 33, pp. 7971–7978.

Daum, B., Walter, A., Horst, A., Osiewacz, H. D. and Kuhlbrandt, W. (2013) 'Age-dependent dissociation of ATP synthase dimers and loss of inner-membrane cristae in mitochondria', *Proceedings of the National Academy of Sciences*, 110(38), pp. 15301–15306.

Delettre, C., Lenaers, G., Griffoin, J.-M., Gigarel, N., Lorenzo, C., Belenguer, P., Pelloquin, L., Grosgeorge, J., Turc-Carel, C., Perret, E., Astarie-Dequeker, C., Lasquellec, L., Arnaud, B., Ducommun, B., Kaplan, J. and Hamel, C. P. (2000) 'Nuclear gene OPA1, encoding a mitochondrial dynamin-related protein, is mutated in dominant optic atrophy', *Nature Genetics*, 26(2), pp. 207–210.

Demongeot, J., Glade, N., Hansen, O. and Moreira, A. (2007) 'An open issue: The inner mitochondrial membrane (IMM) as a free boundary problem', *Biochimie*. Elsevier Masson, 89(9), pp. 1049–1057.

Dudkina, N. V, Eubel, H., Keegstra, W., Boekema, E. J. and Braun, H.-P. (2005) 'Structure of a mitochondrial supercomplex formed by respiratory-chain complexes I and III.', *Proceedings of the National Academy of Sciences of the United States of America*, 102(9), pp. 3225–9.

Duvezin-Caubet, S., Jagasia, R., Wagener, J., Hofmann, S., Trifunovic, A., Hansson, A., Chomyn, A., Bauer, M. F., Attardi, G., Larsson, N. G., Neupert, W. and Reichert, A. S. (2006) 'Proteolytic processing of OPA1 links mitochondrial dysfunction to alterations in mitochondrial morphology', *Journal of Biological Chemistry*, 281(49), pp. 37972–37979.

Elmore, S. (2007) 'Apoptosis: A Review of Programmed Cell Death', *Toxicologic Pathology*, pp. 495–516.

Enríquez, J. A. (2016) 'Supramolecular Organization of Respiratory Complexes', *Annual review of physiology*, 78(533–61).

Eskes, R., Antonsson, B., Osen-Sand, A., Montessuit, S., Richter, C., Sadoul, R., Mazzei, G., Nichols, A. and Martinou, J. C. (1998) 'Bax-induced cytochrome C release from mitochondria is independent of the permeability transition pore but highly dependent on Mg2+ ions', *Journal of Cell Biology*.

Esparza-Moltó, P. B., Nuevo-Tapioles, C. and Cuezva, J. M. (2017) 'Regulation of the H+-ATP synthase by IF1: a role in mitohormesis', *Cellular and Molecular Life Sciences*. Springer International Publishing, 74(12), pp. 2151–2166.

Eubel, H., Heinemeyer, J. and Braun, H. (2004) 'Identification and Characterization of Respirasomes in Potato mitochondria', *Plant Physiology*, 134(April), pp. 1450–1459.

Fernández-Vizarra, E., López-Pérez, M. J. and Enriquez, J. A. (2002) 'Isolation of biogenetically competent mitochondria from mammalian tissues and cultured cells', *Methods*, 26(4), pp. 292–297.

Fiedorczuk, K., Letts, J. A., Degliesposti, G., Kaszuba, K., Skehel, M. and Sazanov, L. A. (2016) 'Atomic structure of the entire mammalian mitochondrial complex I', *Nature*. Nature Publishing Group, 538(7625), pp. 406–410.

Fischer, N., Beilsten-Edmands, V., Chorev, D. S., Hauer, F., Jiko, C., Shimada, S., Shinzawa-Itoh, K., Robinson, C. V, Stark, H. and Gerle, C. (2017) 'Structure and function of the intermembrane space domain of mammalian F o F 1 ATP synthase'.

Folmes, C. D. L., Dzeja, P. P., Nelson, T. J. and Terzic, A. (2012) 'Mitochondria in control of cell fate', *Circulation Research*, 110(4), pp. 526–529.

Folmes, C. D. L. and Terzic, A. (2016) 'Energy metabolism in the acquisition and maintenance of stemness', *Seminars in Cell and Developmental Biology*. Elsevier Ltd, 52, pp. 68–75.

Fröhlich, T., Kemter, E., Flenkenthaler, F., Klymiuk, N., Otte, K. A., Blutke, A., Krause, S., Walter, M. C., Wanke, R., Wolf, E. and Arnold, G. J. (2016) 'Progressive muscle proteome changes in a clinically relevant pig model of Duchenne muscular dystrophy', *Nature Publishing Group*. Nature Publishing Group, (August), pp. 1–14.

Fujikawa, M., Ohsakaya, S., Sugawara, K. and Yoshida, M. (2014) 'Population of ATP synthase molecules in mitochondria is limited by available 6.8-kDa proteolipid protein (MLQ)', *Genes to Cells*.

García-Bermúdez, J., Cuezva, J. M. and Bernardi, P. (2016) *The ATPase Inhibitory Factor 1 (IF1): A master regulator of energy metabolism and of cell survival.*, *Biochimica et biophysica acta*. Elsevier B.V.

Garlich, J., Strecker, V., Wittig, I. and Stuart, R. a (2017) 'Mutational Analysis of the QRRQ Motif in the Yeast Hig1-type 2 Protein, Rcf1, Reveals a Regulatory Role for the Cytochrome c Oxidase Complex', *Journal of Biological Chemistry*, 292(13), p. jbc.M116.758045.

Giorgi, C., Missiroli, S., Patergnani, S., Duszynski, J., Wieckowski, M. R. and Pinton, P. (2015) 'Mitochondria-Associated Membranes: Composition, Molecular Mechanisms, and Physiopathological Implications', *Antioxidants & Redox Signaling*. Mary Ann Liebert, Inc. 140 Huguenot Street, 3rd Floor New Rochelle, NY 10801 USA , 22(12), pp. 995–1019.

Giorgio, V., von Stockum, S., Antoniel, M., Fabbro, A., Fogolari, F., Forte, M., Glick, G. D., Petronilli, V., Zoratti, M., Szabó, I., Lippe, G. and Bernardi, P. (2013) 'Dimers of mitochondrial ATP synthase form the permeability transition pore.', *Proceedings of the National Academy of Sciences of the United States of America*, 110(15), pp. 5887–92.

Giraud, M. F., Paumard, P., Soubannier, V., Vaillier, J., Arselin, G., Salin, B., Schaeffer, J., Brèthes, D., Di Rago, J. P. and Velours, J. (2002) 'Is there a relationship between the supramolecular organization of the mitochondrial ATP synthase and the formation of cristae?', *Biochimica et Biophysica Acta - Bioenergetics*, 1555(1–3), pp. 174–180.

Gogol, E. P., Lücken, U. and Capaldi, R. A. (1987) 'The stalk connecting the F1 and F0 domains of ATP synthase visualized by electron microscopy of unstained specimens',

FEBS Letters, 219(2), pp. 274–278.

Gohil, V. M., Hayes, P., Matsuyama, S., Schägger, H., Schlame, M. and Greenberg, M. L. (2004) 'Cardiolipin biosynthesis and mitochondrial respiratory chain function are interdependent', *Journal of Biological Chemistry*, 279(41), pp. 42612–42618.

Grote, M. and O'Malley, M. A. (2011) 'Enlightening the life sciences: The history of halobacterial and microbial rhodopsin research', *FEMS Microbiology Reviews*, pp. 1082–1099.

Gu, J., Wu, M., Guo, R., Yan, K., Lei, J., Gao, N. and Yang, M. (2016) 'The architecture of the mammalian respirasome', *Nature*, 537(7622), pp. 1–16.

Guglielmi, G., Falk, H. J. and De Renzis, S. (2016) 'Optogenetic Control of Protein Function: From Intracellular Processes to Tissue Morphogenesis', *Trends in Cell Biology*, pp. 864–874.

Habersetzer, J., Larrieu, I., Priault, M., Salin, B., Rossignol, R., Brèthes, D. and Paumard, P. (2013) 'Human F1F0 ATP synthase, mitochondrial ultrastructure and OXPHOS impairment: a (super-)complex matter?', *PloS one*. Public Library of Science, 8(10), p. e75429.

Hackenbrock, C. R., Chazotte, B. and Gupte, S. S. (1986) 'The random collision model and a critical assessment of diffusion and collision in mitochondrial electron transport', *Journal of Bioenergetics and Biomembranes*, 18(5), pp. 331–368.

Hägerhäll, C. (1997) 'Succinate: Quinone oxidoreductases. Variations on a conserved theme', *Biochimica et Biophysica Acta - Bioenergetics*, pp. 107–141.

Hahn, A., Parey, K., Bublitz, M., Mills, D. J., Zickermann, V., Vonck, J., Kühlbrandt, W. and Meier, T. (2016) 'Structure of a Complete ATP Synthase Dimer Reveals the Molecular Basis of Inner Mitochondrial Membrane Morphology', *Molecular Cell*, 63(3), pp. 445–456.

Halestrap, A. P. (2009) 'What is the mitochondrial permeability transition pore?', *Journal of Molecular and Cellular Cardiology*, 46, pp. 821–831.

Hara, K. Y., Wada, T., Kino, K., Asahi, T. and Sawamura, N. (2013) 'Construction of photoenergetic mitochondria in cultured mammalian cells.', *Scientific reports*, 3, p. 1635.

Harlass, F. E., McClure, G. B., Read, J. A. and Brady, K. (1991) 'Use of a standard preparatory diet for the oral glucose tolerance test. {Is} it necessary?', *The Journal of Reproductive Medicine*, 36(2), pp. 147–150.

Hatefi, Y., Haavik, A. G., Fowler, L. R. and Griffiths, D. (1962) 'Studies on the Electron Transfer System XLII. Reconstitution of the electron transfer system.', *The Journal of biological chemistry*, 237(8).

Hayashi, S., Tenzen, T. and McMahon, A. P. (2003) 'Maternal inheritance of Cre activity in aSox2Cre deleter strain', *genesis*, 37(2), pp. 51–53.

He, J., Carroll, J., Ding, S., Fearnley, I. M. and Walker, J. E. (2017) 'Permeability transition in human mitochondria persists in the absence of peripheral stalk subunits of ATP synthase.', *Proceedings of the National Academy of Sciences of the United States of*

America, 114(34), pp. 9086–9091.

He, J., Ford, H. C., Carroll, J., Ding, S., Fearnley, I. M. and Walker, J. E. (2017) 'Persistence of the mitochondrial permeability transition in the absence of subunit c of human ATP synthase', *Proceedings of the National Academy of Sciences*, 114(13), pp. 3409–3414.

Holt, I. J., Harding, A. E. and Morgan-Hughes, J. A. (1988) 'Deletions of muscle mitochondrial DNA in patients with mitochondrial myopathies', *Nature*. Nature Publishing Group, 331(6158), pp. 717–719.

Hom, J. R., Quintanilla, R. A., Hoffman, D. L., de Mesy Bentley, K. L., Molkentin, J. D., Sheu, S. S. and Porter, G. A. (2011) 'The permeability transition pore controls cardiac mitochondrial maturation and myocyte differentiation', *Developmental Cell*.

Hunter, D. R. and Haworth, R. A. (1979) 'The Ca2+-induced membrane transition in mitochondria. I. The protective mechanisms.', *Archives of biochemistry and biophysics*, 195(2), pp. 453–9.

Idevall-Hagren, O., Dickson, E. J., Hille, B., Toomre, D. K. and De Camilli, P. (2012) 'Optogenetic control of phosphoinositide metabolism', *Proceedings of the National Academy of Sciences*, 109(35), pp. E2316–E2323.

Inglés-Prieto, Á., Reichhart, E., Muellner, M. K., Nowak, M., Nijman, S. M. B., Grusch, M. and Janovjak, H. (2015) 'Light-assisted small-molecule screening against protein kinases', *Nature Chemical Biology*, 11(12), pp. 952–954.

Iwata, S. (1998) 'Complete Structure of the 11-Subunit Bovine Mitochondrial Cytochrome bc1 Complex', *Science*, 281(5373), pp. 64–71.

J.E.Walker, I.M.Fearnley, N.J.Gay, B.W.Gibson, F.D.Northrop, S.J.Powell, M.J.Runswick, M.Saraste and V.L.J.Tybulewicz (1985) 'Primary structure and subunit stoichiometry of F1-ATPase from bovine mitochondria', *Journal of Molecular Biology*. Academic Press, 184(4), pp. 677–701.

Kamo, N., Hashiba, T., Kikukawa, T., Araiso, T., Ihara, K. and Nara, T. (2006) 'A light-driven proton pump from Haloterrigena turkmenica: Functional expression in Escherichia coli membrane and coupling with a H+ co-transporter', *Biochemical and Biophysical Research Communications*, 341(2), pp. 285–290.

Keilin, D. and Hartree, E. F. (1947) 'Activity of the cytochrome system in heart muscle preparations', *Biochemical Journal*, 41(4), pp. 500–502.

Kennedy, M. J., Hughes, R. M., Peteya, L. A., Schwartz, J. W., Ehlers, M. D. and Tucker, C. L. (2010) 'Rapid blue-light-mediated induction of protein interactions in living cells.', *Nature methods*. NIH Public Access, 7(12), pp. 973–5.

Kirches, E. (2011) 'LHON: Mitochondrial Mutations and More', *Current Genomics*, 12, pp. 44–54.

Kontro, H., Cannino, G., Rustin, P., Dufour, E. and Kainulainen, H. (2015) 'DAPIT over-expression modulates glucose metabolism and cell behaviour in HEK293T Cells', *PLoS ONE*, 10(7).

Kontro, H., Hulmi, J. J., Rahkila, P. and Kainulainen, H. (2012) 'Cellular and tissue expression of DAPIT, a phylogenetically conserved peptide', *European Journal of Histochemistry*, 56(2), pp. 111–116.

Krause, F., Reifschneider, N. H., Goto, S. and Dencher, N. A. (2005) 'Active oligomeric ATP synthases in mammalian mitochondria', *Biochemical and Biophysical Research Communications*, 329(2), pp. 583–590.

Kroemer, G. and Reed, J. C. (2000) 'Mitochondrial control of cell death', *Nature Medicine*. Nature Publishing Group, 6(5), pp. 513–519.

Kwong, J. Q. and Molkentin, J. D. (2015) 'Physiological and Pathological Roles of the Mitochondrial Permeability Transition Pore in the Heart', *Cell Metabolism*, 21, pp. 206–214.

Lanyi, J. K. (1998) 'Understanding structure and function in the light-driven proton pump bacteriorhodopsin.', *Journal of structural biology*, 124(2–3), pp. 164–78.

Lapuente-Brun, E., Moreno-Loshuertos, R., Acín-Pérez, R., Latorre-Pellicer, A., Colás, C., Balsa, E., Perales-Clemente, E., Quirós, P. M., Calvo, E., Rodríguez-Hernández, M. a, Navas, P., Cruz, R., Carracedo, Á., López-Otín, C., Pérez-Martos, A., Fernández-Silva, P., Fernández-Vizarra, E. and Enríquez, J. A. (2013) 'Supercomplex assembly determines electron flux in the mitochondrial electron transport chain.', *Science*, 340(6140), pp. 1567–70.

Lee, J., Ding, S. J., Walpole, T. B., Holding, A. N., Montgomery, M. G., Fearnley, I. M. and Walker, J. E. (2015) 'Organization of subunits in the membrane domain of the bovine F-ATPase revealed by covalent cross-linking', *Journal of Biological Chemistry*, 290(21), pp. 13308–13320.

Lenaz, G. and Genova, M. L. (2007) 'Kinetics of integrated electron transfer in the mitochondrial respiratory chain: random collisions vs. solid state electron channeling.', *American journal of physiology. Cell physiology*, 292(4), pp. C1221-39.

Letts, J. A., Fiedorczuk, K. and Sazanov, L. A. (2016) 'The architecture of respiratory supercomplexes', *Nature*, 537(7622), pp. 644–648.

Levskaya, A., Weiner, O. D., Lim, W. A. and Voigt, C. A. (2009) 'Spatiotemporal control of cell signalling using a light-switchable protein interaction', *Nature*, 461(7266), pp. 997–1001.

MacVicar, T. and Langer, T. (2016) 'OPA1 processing in cell death and disease – the long and short of it', *Journal of Cell Science*, 129(12), pp. 2297–2306.

McKenzie, M., Lazarou, M., Thorburn, D. R. and Ryan, M. T. (2006) 'Mitochondrial Respiratory Chain Supercomplexes Are Destabilized in Barth Syndrome Patients', *Journal of Molecular Biology*, 361(3), pp. 462–469.

Menendez-Montes, I., Escobar, B., Palacios, B., Gómez, M. J., Izquierdo-Garcia, J. L., Flores, L., Jiménez-Borreguero, L. J., Aragones, J., Ruiz-Cabello, J., Torres, M. and Martin-Puig, S. (2016) 'Myocardial VHL-HIF Signaling Controls an Embryonic Metabolic Switch Essential for Cardiac Maturation', *Developmental Cell*, 39(6), pp. 724–739.

Meyer, B., Wittig, I., Trifilieff, E., Karas, M. and Schägger, H. (2007) 'Identification of two proteins associated with mammalian ATP synthase.', *Molecular & cellular proteomics : MCP*, 6(10), pp. 1690–1699.

Mileykovskaya, E. and Dowhan, W. (2014) 'Cardiolipin-dependent formation of mitochondrial respiratory supercomplexes', *Chemistry and Physics of Lipids*, 179, pp. 42–48.

Nagata, Y., Yamagishi, M., Konno, T., Nakanishi, C., Asano, Y., Ito, S., Nakajima, Y., Seguchi, O., Fujino, N., Kawashiri, M., Takashima, S., Kitakaze, M. and Hayashi, K. (2017) 'Heat Failure Phenotypes Induced by Knockdown of DAPIT in Zebrafish: A New Insight into Mechanism of Dilated Cardiomyopathy', *Scientific Reports*. Nature Publishing Group, 7(1), p. 17417.

Nass, M. M. K. and Nass, S. (1963) 'INTRAMITOCHONDRIAL FIBERS WITH DNA CHARACTERISTICS', *The Journal of Cell Biology*, 19(3).

Nijtmans, L. G., Klement, P., Houstek, J. and van den Bogert, C. (1995) 'Assembly of mitochondrial ATP synthase in cultured human cells: implications for mitochondrial diseases', *Biochim Biophys Acta*, 1272(3), pp. 190–198.

Nůsková, H., Mráček, T., Mikulová, T., Vrbacký, M., Kovářová, N., Kovalčíková, J., Pecina, P. and Houštěk, J. (2015) 'Mitochondrial ATP synthasome: Expression and structural interaction of its components', *Biochemical and Biophysical Research Communications*, 464(3), pp. 787–793.

Ohsakaya, S., Fujikawa, M., Hisabori, T. and Yoshida, M. (2011) 'Knockdown of DAPIT (Diabetes-associated Protein in Insulin-sensitive Tissue) results in loss of ATP synthase in mitochondria', *Journal of Biological Chemistry*.

Päivärinne, H. and Kainulainen, H. (2001) 'DAPIT, a novel protein down-regulated in insulin-sensitive tissues in streptozotocin-induced diabetes', *Acta Diabetologica*, 38(2), pp. 83–86.

Palade, G. E. (1952) 'The fine structure of mitochondria', *The Anatomical Record*. Wiley Subscription Services, Inc., A Wiley Company, 114(3), pp. 427–451.

Palade, G. E. (1953) 'AN ELECTRON MICROSCOPE STUDY OF THE MITOCHONDRIAL STRUCTURE', *Journal of Histochemistry & Cytochemistry*, 1(4), pp. 188–211.

Papizan, J. B., Garry, G. A., Brezprozvannaya, S., McAnally, J. R., Bassel-Duby, R., Liu, N. and Olson, E. N. (2017) 'Deficiency in Kelch protein Klhl31 causes congenital myopathy in mice', *The Journal of Clinical Investigation*. American Society for Clinical Investigation, 127(10), pp. 3730–3740.

Park, S.-J., Gazzola, M., Park, K. S., Park, S., Di Santo, V., Blevins, E. L., Lind, J. U., Campbell, P. H., Dauth, S., Capulli, A. K., Pasqualini, F. S., Ahn, S., Cho, A., Yuan, H., Maoz, B. M., Vijaykumar, R., Choi, J.-W., Deisseroth, K., Lauder, G. V., Mahadevan, L. and Parker, K. K. (2016) 'Phototactic guidance of a tissue-engineered soft-robotic ray', *Science*, 353(6295), pp. 158–162.

Paumard, P., Vaillier, J., Coulary, B., Schaeffer, J., Soubannier, V., Mueller, D. M., Brèthes, D., di Rago, J.-P. P. and Velours, J. (2002) 'The ATP synthase is involved in generating

mitochondrial cristae morphology.', *The EMBO journal*. EMBO Press, 21(3), pp. 221–30.

Perales-Clemente, E., Bayona-Bafaluy, M. P., Pérez-Martos, A., Barrientos, A., Fernández-Silva, P. and Enriquez, J. A. (2008) 'Restoration of electron transport without proton pumping in mammalian mitochondria.', *Proceedings of the National Academy of Sciences of the United States of America*, 105(48), pp. 18735–9.

Perales-Clemente, E., Fernández-Silva, P., Acín-Pérez, R., Pérez-Martos, A. and Enríquez, J. A. (2011) 'Allotopic expression of mitochondrial-encoded genes in mammals: Achieved goal, undemonstrated mechanism or impossible task?', *Nucleic Acids Research*, 39(1), pp. 225–234.

Petros, J. A., Baumann, A. K., Ruiz-Pesini, E., Amin, M. B., Sun, C. Q., Hall, J., Lim, S., Issa, M. M., Flanders, W. D., Hosseini, S. H., Marshall, F. F. and Wallace, D. C. (2005) 'mtDNA mutations increase tumorigenicity in prostate cancer.', *Proceedings of the National Academy of Sciences of the United States of America*. National Academy of Sciences, 102(3), pp. 719–24.

Pfeiffer, K., Gohil, V., Stuart, R. A., Hunte, C., Brandt, U., Greenberg, M. L. and Schägger, H. (2003) 'Cardiolipin Stabilizes Respiratory Chain Supercomplexes', *Journal of Biological Chemistry*. in Press, 278(52), pp. 52873–52880.

Racker, E. (1963) 'A mitochondrial factor conferring oligomycin sensitivity on soluble mitochondrial ATPase', *Biochemical and Biophysical Research Communications*, 10(6), pp. 435–439.

Rak, M., Tetaud, E., Godard, F., Sagot, I., Salin, B., Duvezin-Caubet, S., Slonimski, P. P., Rytka, J. and Di Rago, J. P. (2007) 'Yeast cells lacking the mitochondrial gene encoding the ATP synthase subunit 6 exhibit a selective loss of complex IV and unusual mitochondrial morphology', *Journal of Biological Chemistry*, 282(15), pp. 10853–10864.

Rasola, A. and Bernardi, P. (2007) 'The mitochondrial permeability transition pore and its involvement in cell death and in disease pathogenesis', *Apoptosis*, pp. 815–833.

Rexroth, S., Meyer Zu Tittingdorf, J. M. W., Schwassmann, H. J., Krause, F., Seelert, H. and Dencher, N. A. (2004) 'Dimeric H+-ATP synthase in the chloroplast of Chlamydomonas reinhardtii.', *Biochimica et biophysica acta*, 1658(3), pp. 202–11.

Rich, P. R. (2017) 'Mitochondrial cytochrome c oxidase: catalysis, coupling and controversies', *Biochemical Society Transactions*, 45(3), pp. 813–829.

Rieger, B., Junge, W. and Busch, K. B. (2014) 'Lateral pH gradient between OXPHOS complex IV and F(0)F(1) ATP-synthase in folded mitochondrial membranes.', *Nature communications*. Nature Publishing Group, 5, p. 3103.

Sagan, L. (1967) 'On the origin of mitosing cells', *Journal of Theoretical Biology*. Academic Press, 14(3), p. 225–IN6.

Schägger, H. (1995) 'Native electrophoresis for isolation of mitochondrial oxidative phosphorylation protein complexes', *Methods in Enzymology*, 260(C), pp. 190–202.

Schägger, H. and Pfeiffer, K. (2000) 'Supercomplexes in the respiratory chains of yeast and mammalian mitochondria.', *The EMBO journal*, 19(8), pp. 1777–1783.

Schatz, G., Haslbrunner, E. and Tuppy, H. (1964) 'Deoxyribonucleic acid associated with yeast mitochondria', *Biochemical and Biophysical Research Communications*. Academic Press, 15(2), pp. 127–132.

Scheffler, I. E. (1999) *Mitochondria*. Wiley-Liss.

Scherr, M., Battmer, K., Blömer, U., Ganser, A. and Grez, M. (2001) 'Quantitative Determination of Lentiviral Vector Particle Numbers by Real-Time PCR', *Short Technical Reports*, 31, pp. 520–516.

Schwartz, R. and Dayhoff, M. (1978) 'Origins of prokaryotes, eukaryotes, mitochondria, and chloroplasts', *Science*, 199(4327).

Sjostrand, F. S. (1953) 'Electron Microscopy of Mitochondria and Cytoplasmic Double Membranes', *Nature*. Nature Publishing Group, 171(4340), pp. 30–31.

Slater, E. C. (2003) 'Keilin, cytochrome, and the respiratory chain', *Journal of Biological Chemistry*, 278(19), pp. 16455–16461.

Sousa, J. S., Mills, D. J., Vonck, J. and Kühlbrandt, W. (2016) 'Functional asymmetry and electron flow in the bovine respirasome', *eLife*, 5, pp. 1–17.

Spannagel, C., Vaillier, J., Arselin, G., Graves, P. V and Velours, J. (1997) 'The subunit f of mitochondrial yeast ATP synthase--characterization of the protein and disruption of the structural gene ATP17', *European journal of biochemistry / FEBS*, 247(3), pp. 1111–1117.

Von Stockum, S., Giorgio, V., Trevisan, E., Lippe, G., Glick, G. D., Forte, M. A., Da-R, C., Checchetto, V., Mazzotta, G., Costa, R., Szab, I. and Bernardi, P. (2015) 'F-ATPase of drosophila melanogaster forms 53-picosiemen (53-pS) channels responsible for mitochondrial Ca<inf>2+</inf>-induced Ca<inf>2+</inf> release', *Journal of Biological Chemistry*, 290(8), pp. 4537–4544.

Symersky, J., Osowski, D., Walters, D. E. and Mueller, D. M. (2012) 'Oligomycin frames a common drug-binding site in the ATP synthase', *Proceedings of the National Academy of Sciences*, 109(35), pp. 13961–13965.

Symersky, J., Pagadala, V., Osowski, D., Krah, A., Meier, T., Faraldo-Gómez, J. D. and Mueller, D. M. (2012) 'Structure of the c10 ring of the yeast mitochondrial ATP synthase in the open conformation', *Nature Structural & Molecular Biology*, 19(5), pp. 485–491.

Teixeira, F. K., Sanchez, C. G., Hurd, T. R., Seifert, J. R. K., Czech, B., Preall, J. B., Hannon, G. J. and Lehmann, R. (2015) 'ATP synthase promotes germ cell differentiation independent of oxidative phosphorylation', *Nature Cell Biology*.

Terzi, E., Boyot, P., Van Dorsselaer, A., Luu, B. and Trifilieff, E. (1990) 'Isolation and amino acid sequence of a novel 6.8-kDa mitochondrial proteolipid from beef heart. Use of FAB-MS for molecular mass determination', *FEBS Letters*, 260(1), pp. 122–126.

Tormos, K., Anso, E., Hamanaka, R., Eisenbart, J., Joseph, J., Kalyanaraman, B. and Chandel, N. (2011) 'Mitochondrial Complex III ROS Regulate Adipocyte Differentiation', *Cell*

Metabolism, 14(4), pp. 537–544.

Trifunovic, A., Wredenberg, A., Falkenberg, M., Spelbrink, J. N., Rovio, A. T., Bruder, C. E., Bohlooly-Y, M., Gidlöf, S., Oldfors, A., Wibom, R., Törnell, J., Jacobs, H. T. and Larsson, N.-G. (2004) 'Premature ageing in mice expressing defective mitochondrial DNA polymerase', *Nature*, 429(6990), pp. 417–423.

Vance, J. E. (2014) 'MAM (mitochondria-associated membranes) in mammalian cells: Lipids and beyond', *BBA - Molecular and Cell Biology of Lipids*, 1841, pp. 595–609.

Vives-Bauza, C., Yang, L. and Manfredi, G. (2007) 'Assay of Mitochondrial ATP Synthesis in Animal Cells and Tissues', *Methods in Cell Biology*, pp. 155–171.

Walker, J. E. (2013) 'The ATP synthase: the understood, the uncertain and the unknown.', *Biochemical Society transactions*. Portland Press Limited, 41(1), pp. 1–16.

Wallace, D. C. (2005) 'A mitochondrial paradigm of metabolic and degenerative diseases, aging, and cancer: a dawn for evolutionary medicine.', *Annual review of genetics*, 39, pp. 359–407.

Wallace, D. C., Fan, W. and Procaccio, V. (2010) 'Mitochondrial Energetics and Therapeutics', *Annual Review of Pathology: Mechanisms of Disease*, 5(1), pp. 297–348.

Wallace, D. C., Singh, G., Lott, M. T., Hodge, J. A., Schurr, T. G., Lezza, A. M., Elsas, L. J. and Nikoskelainen, E. K. (1988) 'Mitochondrial DNA mutation associated with Leber's hereditary optic neuropathy.', *Science (New York, N.Y.)*, 242(4884), pp. 1427–30.

Wittig, I., Braun, H.-P. and Schägger, H. (2006) 'Blue native PAGE.', *Nature protocols*, 1(1), pp. 418–428.

Wittig, I., Meyer, B., Heide, H., Steger, M., Bleier, L., Wumaier, Z., Karas, M. and Schägger, H. (2010) 'Assembly and oligomerization of human ATP synthase lacking mitochondrial subunits a and A6L', *Biochimica et Biophysica Acta - Bioenergetics*, 1797(6–7), pp. 1004–1011.

Wittig, I. and Schägger, H. (2005) 'Advantages and limitations of clear-native PAGE', *Proteomics*, 5(17), pp. 4338–4346.

Wu, M., Gu, J., Guo, R., Huang, Y. and Yang, M. (2016) 'Structure of Mammalian Respiratory Supercomplex I1III2IV1', *Cell*. Elsevier, 167(6), p. 1598–1609.e10.

Wu, Y. I., Frey, D., Lungu, O. I., Jaehrig, A., Schlichting, I., Kuhlman, B. and Hahn, K. M. (2009) 'A genetically encoded photoactivatable Rac controls the motility of living cells', *Nature*. Nature Publishing Group, 461(7260), pp. 104–108.

Xia, D., Esser, L., Yu, L. and Yu, C.-A. (2007) 'Structural basis for the mechanism of electron bifurcation at the quinol oxidation site of the cytochrome bc 1 complex', *Photosynthesis Research*. Kluwer Academic Publishers, 92(1), pp. 17–34.

Xu, Y., Condell, M., Plesken, H., Edelman-Novemsky, I., Ma, J., Ren, M. and Schlame, M. (2006) 'A Drosophila model of Barth syndrome.', *Proceedings of the National Academy of Sciences of the United States of America*, 103(31), pp. 11584–8.

Yazawa, M., Sadaghiani, A. M., Hsueh, B. and Dolmetsch, R. E. (2009) 'Induction of protein-protein interactions in live cells using light', *Nature Biotechnology*. Nature Publishing

Group, 27(10), pp. 941–945.

Zemelman, B. V, Lee, G. A., Ng, M., Miesenböck, G., Miesenböck, G., Hotta, Y., Matsumoto, H. and Zuker, C. S. (2002) 'Selective photostimulation of genetically chARGed neurons.', *Neuron*. Macmillan, New York, 33(1), pp. 15–22.

Zhang, J., Mizuno, K., Murata, Y., Koide, H., Murakami, M., Ihara, K. and Kouyama, T. (2013) 'Crystal structure of deltarhodopsin-3 from Haloterrigena thermotolerans', *Proteins: Structure, Function and Bioinformatics*, 81(9), pp. 1585–1592.

Zhou, W., Marinelli, F., Nief, C. and Faraldo-Gómez, J. D. (2017) 'Atomistic simulations indicate the c-subunit ring of the F_1F_o ATP synthase is not the mitochondrial permeability transition pore', *eLife*. eLife Sciences Publications Limited, 6, p. e23781.

Zhu, J., Vinothkumar, K. R. and Hirst, J. (2016) 'Structure of mammalian respiratory complex I', *Nature*. Nature Research, 536(7616), pp. 354–358.